



Review

Photoresponsive nanostructure assisted green synthesis of organics and polymers

Maosong Liu^a, Tingyu Peng^a, Henan Li^a, Long Zhao^a, Yuanhua Sang^b, Qunwei Feng^c, Li Xu^d,
Yinhua Jiang^a, Hong Liu^{b,e,*}, Jianming Zhang^{a,**}

^a School of Chemistry and Chemical Engineering, Jiangsu University, Zhenjiang, 212013, China

^b State Key Laboratory of Crystal Materials, Shandong University, Jinan, 250100, China

^c Jiaying Rejdue Environmental Technology Co. Ltd, Jiaying, 314006, China

^d Institute for Energy Research, School of Chemistry and Chemical Engineering, Jiangsu University, Zhenjiang, 212013, China

^e Institute for Advanced Interdisciplinary Research (IAIR), University of Jinan, Jinan 250022, China

ARTICLE INFO

Keywords:

Heterogenous photocatalysis
CO₂ reduction
Photo organic synthesis
Photo polymerization
Nanoparticles

ABSTRACT

Solar light is believed to be the most sustainable and clean energy source. In line with the concept of green chemistry, the use of solar energy has been a formidable impetus toward the development of novel photo-based synthetic technologies to drive various chemical reactions. Photosynthesis is a promising route to achieve a wide array of chemical transformations with distinctive energy and environmental merits which are usually inaccessible with conventional thermal processes. Photoinduced organic synthesis, as one important branch of photosynthesis, has attracted increasingly attentions to meet the growing-up environmental and energy concerns. Highly photoresponsive nanoparticles (NPs), such as semiconductors, can generate photoexcited charge carriers, *i.e.* electron-hole pairs, upon photon absorption, which can favor a vast number of reactions, demonstrating unique advantages including the easily recycling and reuse, the use of mild reaction conditions and the generation of high-purity products devoid of contaminants. This review article highlights recent representative advances in heterogenous photocatalytic organic synthesis, mainly including CO₂ reduction, organic transform and free radical polymerization; in particular, for the first time, the achievements on photoresponsive NP initiated free radical polymerizations are summarized here. We conclude this review by proposing several interesting research directions and future challenges with the hope that it can serve as a good reference for researchers in nanomaterials and catalysis.

1. Introduction

Today, synthetic organic chemistry constitutes a crucial part of human endeavors in chemical science, which offers us materials in huge diversity, such as fuels, biomolecules and plastics. Typically, to obtain desired chemicals with high production yield or drive synthesis at high reaction rate, harsh reaction / operation conditions, *e.g.* high temperature and / or pressure, are usually necessary in many synthetic processes, which usually are driven by fossil energy. The over-consumption of the fossil fuels has caused excessive emission of carbon dioxide (CO₂) and other toxic byproducts, which produce serious pollutants to the environment. The increasing environmental and sustainable-development requirements have thus impelled chemists to explore advanced “green” and clean routes for organic synthesis [1–4].

The ecosystem on the Earth is initiated and supported by the super power source of the sun, almost without exception. Upon the acceptance of the solar energy by plants and other light-harvesting organisms, chemical transitions are initiated to form new chemicals to make creatures vital and diverse. Such a “green” and clean process, known as the natural photosynthesis, utilizes sunlight and carbon dioxide (CO₂)/water as a sustainable energy source and cheap raw materials, respectively (Fig. 1 left). Inspired by the natural photosynthesis of plants, artificial photochemistry technology has been intensely investigated for chemical synthesis [5–10]. In principal, a photoreaction is triggered by a photon-electron-transfer (PET) process, where upon photon energy absorption electrons at molecule orbitals enter the excited states and become highly active to promote chemical transformations. Compared with its thermal counterpart, photosynthesis demonstrates a distinctive

* Corresponding author at: State Key Laboratory of Crystal Materials, Shandong University, Jinan, 250100, China.

** Corresponding author.

E-mail addresses: hongliu@sdu.edu.cn (H. Liu), zhangjm@ujs.edu.cn (J. Zhang).

<https://doi.org/10.1016/j.apcatb.2019.02.071>

Received 15 October 2018; Received in revised form 31 January 2019; Accepted 25 February 2019

Available online 01 March 2019

0926-3373/ © 2019 Elsevier B.V. All rights reserved.

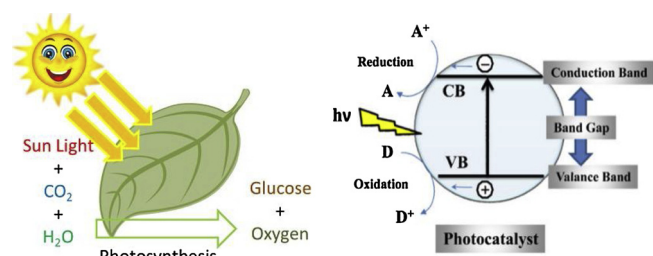


Fig. 1. Schematic illustration of the natural photosynthesis (left) and an artificial heterogeneous photocatalysis using semiconductor NP as catalyst (right) [13]. Reprinted with permission.

advantage to meet the energetic requirements in conducting reactions. Using incident light as energy source, a large variety of chemical reactions can be initiated to selectively catalyze chemical transformations which would be difficult to be activated thermally [5–10]. Solar energy is without contest the greenest and most sustainable energy source currently accessible. Therefore, photochemistry based on solar light is a sustainable, eco-friendly chemical process which has attracted significant attention. Using solar energy to directly convert CO₂ and water into carbon-containing fuels or chemicals is a major topic and frontier in synthetic chemistry. Based on the recognition of the photo-responsive molecules, such as organic dyes or transition metal chromophores, photo-induced organic synthesis from small molecule to polymer scale has been established and rapidly developed for more than a century [5–10]. Nonetheless, many drawbacks still exist in the photo-responsive molecule-initiated synthesis; for example, many of the photo-responsive molecules are toxic and may remain in products as impurities [11,12].

Initiated by the seminal work of Fujishima on 1979 [14], the research of heterogeneous photocatalysis has led to fruitful achievements, and is still in a rapid growth stage. Numerous types of photoresponsive nanoparticles (NPs) have been created and intensely studied [13–21]. As illustrated in Fig. 1 (right), in typical heterogeneous photocatalysis, the absorption of photons excites electrons from valence band (VB) to conduction band (CB) of the semiconductor NP (e.g. TiO₂), leading to the generation of electron-hole pairs (e^-/h^+) or charge carriers. The so-generated electron-hole pairs immigrate to the surface of the NP to interact with electron acceptors and donors adsorbed on NP surface via the PET process, forming extremely active reducing and oxidizing species respectively. The synthesis, therefore, can be proceeded through either oxidative or reductive pathways, or through the combination of both [13,19]. From view point of green chemistry, semiconductor NPs show desirable properties as photoreaction initiators [13,16,18], where the structures and components can be intendedly designed and tuned, using a plethora of known methods, to obtain better charge separation and higher quantum efficiency. More interestingly, compared with the homogeneous photoreactions using small molecules (e.g., dyes), NPs are more chemically stable, environmentally benign as well as less toxic. In addition, as the NPs are insoluble in reaction solution, they can be easily recycled / reused in the successive reactions without remaining in the products, thus leading to a generation of clean products in “one-pot” reactions [13–21].

The pioneer work by Inoue [14] using semiconductor as photocatalyst has opened a revolutionary venue to realize the conversion of CO₂ into simple carbon fuels or organics, e.g. HCOOH, CH₃OH, HCHO and CH₄, upon solar light as the sustainable energy source, revealing a promising route to reduce greenhouse gas and simultaneously produce an array of useful organics in a green fashion and leading to a vast number of publications. Significant achievements have been obtained in the evolution of reaction efficiency as well as the understanding of the reaction mechanism. Some excellent reviews have summarized the state-of-the-art of heterogeneous photocatalytic CO₂ reduction applications [22–28]. For instance, Gong et al. [25] reviewed the main

strategies to improve the surface interaction (adsorption/activation) of CO₂ molecules on semiconductors and the factors dominating the reaction pathways. Jaroniec et al. [26] summarized various 3D hierarchical photocatalysts including nano / microspheres, hetero-structured nanocomposites, yolk/shell structures and hollow structures etc., bearing the advantages of large surface areas, high CO₂ adsorption capabilities and high mass transfer rates for catalysis. Zhang et al. [29,30] reviewed the CO₂ reduction using perovskite oxide nanomaterials, and pointed that perovskite oxides exhibit wider absorption, longer charge carrier lifetime, and favorable band-alignment for CO₂ reduction, which is supposed to be more active than conventional semiconductors. Yu et al. [31] have reviewed the application of graphene (GR) materials in photocatalytic CO₂ reduction, showing that due to the unique properties including excellent conductivity, good optical transmittance, large specific surface area, and superior chemical stability, GR-based catalysts demonstrate good activity. The daily-updated reports enrich the fundamental understanding as well as the development of highly efficient catalysts.

Although abundant scientific results in this domain, currently heterogeneous photocatalytic CO₂ reduction is mainly applied to produce small hydrocarbons. To produce more complex or value-added organics, heterogeneous photocatalytic organic conversion has been developed. Upon the presence of photo-generated active radicals, redox reactions can be conducted to small organic molecules, such as alcohols or alkenes, to produce corresponding derivatives or new chemicals under a mild reaction condition. Some reviews on photocatalytic organic conversion have been published [23,24,40,41,32–39], of which several are more specific on certain reactions. For example, in a review by Yao et al. [37], photocatalytic oxidation reactions, especially, alcohols oxidation, aromatic hydroxylation and alkene oxidation are summarized. Xu and Luque et al. [38,42] reviewed the advances in the selective heterogeneous photocatalytic valorisation of lignin-based compounds. Li et al. [24] surveyed the work on oxidation of amines, carbon-carbon bond formation and carbon-hetero bond formation. Bahnemann and co-workers [23] reviewed the reaction selectivity in photocatalytic organic synthesis, and pointed that the screening of photocatalysts for specific reactions may reach better selectivity. Nonetheless, the fundamental understanding on the exact reaction mechanism is still lacking.

Polymers or macromolecules can also be obtained via a heterogeneous photocatalytic process. Very recently, heterogeneous photocatalytic polymerization technique has demonstrated an evolution to its traditional thermal counterpart to meet the growing demand for easy curing, highly functionalized and well-defined polymer structures as building blocks in nanotechnology, biological and 3D fabrication applications [43,44]. A conventional free radical polymerization process usually works at high temperature, where initial radicals are generated by thermal decomposition of molecule initiators (e.g. organic/inorganic peroxides or diazo compounds) or upon reacting redox-active compounds [45–48]. Despite their remarkable ease of use, their low cost and wide availability, these initiators also show several drawbacks due to their residual presence in the polymer, their lack of sustainability, their odor and potential toxicity. Heterogeneous semiconductor NPs show desirable properties as photoinitiators [13,16,18], since the photogenerated charges can result in the formation of highly active radicals to initiate the reaction. However, compared with the intense focus of CO₂ reduction and organic conversion, the study on heterogeneous photocatalytic polymerization receives less attention, and the review with a systematic summary of the advances in this research domain is missing.

As a complementary to previous excellent reviews, here we have reviewed some up-to-date reports with high novelties from the most prestigious journals. We mainly introduce the application of NP catalyzed photoradical organic synthesis. We start by highlighting the recent advances of semiconductor NPs for photocatalytic CO₂ reduction and move to organic conversion, including alcohols oxidation, aromatic hydroxylation and so on. To differentiate from other review articles as

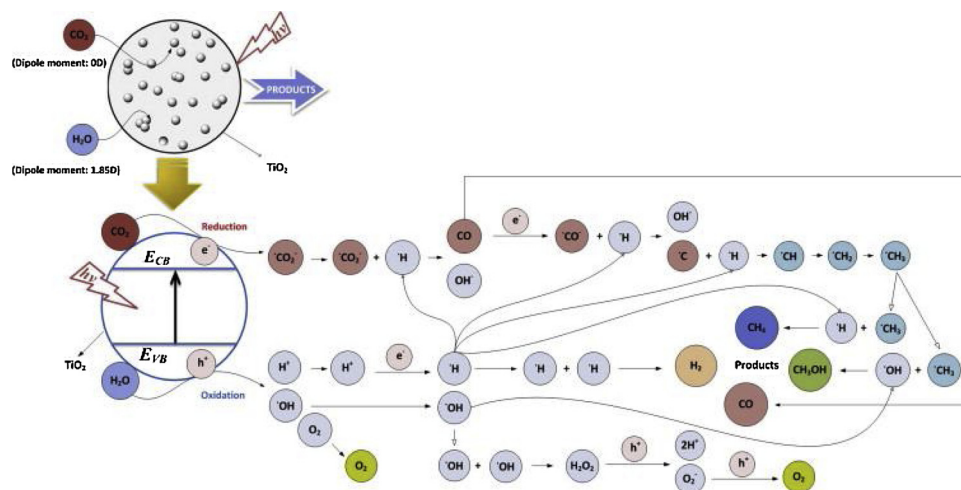


Fig. 2. Proposed mechanism and pathways for the photocatalytic reduction of CO_2 with H_2O vapor to CH_3OH and CH_4 using TiO_2 [49]. Reprinted with permission.

mentioned above, we mainly introduce some very recent state-of-the-art achievements and give a summary of the key parameters affecting the efficiency and/or selectivity of reactions, which are highly diverse yet have been strongly concerned in this field. Then we move to the section of photoinduced free radical polymerization with more detailed information in a relatively longer length, which is systematically summarized for the firstly time; in particular, latest achievements on the use of inorganic NPs for controlled or living radical photopolymerizations are introduced. The fundamental mechanisms underlying the reactions are also briefly addressed. This review concludes with challenges and proposals on how to broaden the utilization of photoresponsive NP in organic transforms, in particular for polymerization, and how to gain more fundamental understanding on the mechanism of photosynthesis. We expect that this review could be a valuable reference for the readers who are interested in photocatalytic synthesis for environmental and clean energy generation.

2. Photoresponsive NP catalyzed organic synthesis

2.1. Photocatalytic conversion of CO_2 to organics

As aforementioned, reports about heterogenous photocatalytic CO_2 reduction have been emerging numerously. Nowadays, to obtain high performance, most of the photocatalysts have been evolved into hetero or hybrid nanostructures, which are mainly composed of several different components with multi-functions or rationally designed architectures. Simple and classic semiconductors, such as TiO_2 or CeO_2 NPs, are seldom used alone for efficient photocatalysis due to their intrinsic drawbacks, e.g. low absorption and quantum yield; however, they are still active for mechanism study and employed as good platforms to fabricate more complex structures. In this section, the content is sequenced on the basis of catalyst type. We start from the most classic TiO_2 by reviewing several latest innovations of simple semiconductor system; afterward we introduce some recent advances of modified semiconductors and nanohybrids. At the end, the parameters affecting reaction efficiency are discussed briefly.

2.1.1. Simple semiconductor catalysts (TiO_2 , CeO_2 and so on)

TiO_2 NPs, as the most intensively investigated photocatalyst, have been widely applied to catalyze the reduction of CO_2 into fuels and hydrocarbons because of their excellent UV light absorption, chemical stability, low cost and easy fabrication etc. [49]. Through precisely programming the microstructures of TiO_2 NPs, such as porosity, oxygen vacancy or crystallite structure, an idea platform can be created to investigate the structure–activity relationship to gain more fundamental

understanding on catalysis. Oxygen vacancies (OVs) have been acknowledged to play a vital role in many photocatalytic reactions [50–52]. The OVs at surface or bulk show distinct functions for catalysis [50–52]. To better understand the effect of OV on catalysis, Yang et al. [53] prepared three different TiO_2 NPs with surface OVs (SOVs) and/or bulk single-electron-trapped OVs (SETOVs) via simple approaches of dehydration or reduction of different Ti precursors. Photocatalytic CO_2 reduction test under Hg lamp irradiation showed that both the bulk SETOVs and SOVs contribute to light absorption enhancement. The SOVs facilitate charge-carrier separation, while the bulk SETOVs work more as the recombination center. For the case of the co-existence of the surface and bulk OVs, the catalytic efficiency to convert CO_2 to CH_4 can be improved by increasing the ratio of surface OVs to bulk SETOVs, indicating a synergistic effect for catalysis. The presence of OV-related defects could not only act as the activation sites for catalysis [53–55], but also can enhance the light absorption of TiO_2 to the visible range [56].

Using KIT-6 SiO_2 as template, Russo et al. [57] synthesized mesoporous TiO_2 NPs with high surface area ($190 \text{ m}^2/\text{g}$ vs. $53 \text{ m}^2/\text{g}$ of P25). CO_2 reduction tests showed that the catalysis upon this mesoporous TiO_2 led to more hydrocarbons, better reaction kinetics and higher stability, due to its superior characteristics than those of the conventional TiO_2 NPs. The larger surface area of mesoporous TiO_2 is highly beneficial to lower adsorbing energy barrier of reactants (CO_2 and H_2O) to TiO_2 . A recent study using mesoporous TiO_2 NP for CO_2 reduction [49] proposed that upon photon absorption, photo-excited electrons reduce the adsorbed CO_2 to an anion radical $\text{CO}_2^{\cdot-}$, while H_2O oxidation is preceded through the interaction with holes, leading to the formation of H^+ and OH^{\cdot} radicals, as demonstrated in Fig. 2. H^+ may accept electrons to form H^{\cdot} , which then reacts with $\text{CO}_2^{\cdot-}$ to form CO , CH^{\cdot} , CH_2^{\cdot} and CH_3^{\cdot} . Subsequently, these alkyl radicals interact with OH^{\cdot} to form CH_3OH as a product with a combination of CH_4 and O_2 [24]. The reaction proceeds mainly by the competitive adsorption of CO_2 and H_2O on the surface of TiO_2 NPs. In addition, UV light intensity, $\text{H}_2\text{O}/\text{CO}_2$ ratio, and structure of NPs all exert important impact on the performance of the catalyst and product yield. The saturation of adsorption center may induce an undesired reverse reaction, where the produced methanol reacts with oxygen (O_2) to generate CO_2 [49]. Kang and co-workers [58] also synthesized ordered mesoporous metal oxides (TiO_2 and SnO_2) with high surface areas ($\sim 100 \text{ m}^2/\text{g}$) for CO_2 photo-reduction. Owing to their high surface area, the mesoporous metal oxides demonstrate 9–10 times higher yields of CH_4 and 2–3 times higher yields of CO than P25.

Rossetti et al. [59] studied the mechanism of photoreduction of CO_2 at high pressure in liquid phase using P25 as photocatalyst in the

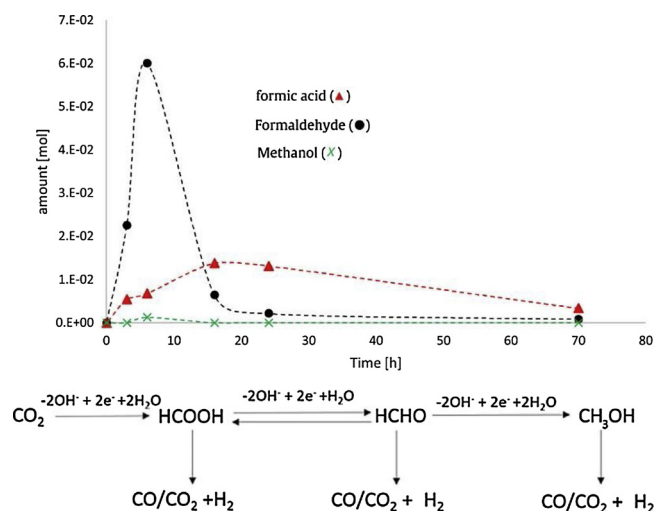


Fig. 3. Amount of liquid phase products with time and the schematic consecutive pathway for CO₂ reduction [59]. Reprinted with permission.

presence of Na₂SO₃ as hole scavenger working at different pH. Using a special reactor which allows improving CO₂ solubility in water at high pressure, products of liquid phase (formic acid, formaldehyde) and gas phase (CH₄) can be successfully produced. Reaction time investigation showed that at the beginning, liquid product of formaldehyde was the main product, followed by the formation of formic acid. Interestingly, as the extension of reaction time, liquid phase products reduce gradually (Fig. 3, upper), while gases, mainly composed of H₂ and CO, start forming and become the major product after the consumption of the Na₂SO₃, which can be ascribed to the photodegradation of the pre-formed organic products (Fig. 3, lower). At this stage, the organic species formed at the beginning, e.g. formaldehyde, may act as alternative hole scavengers. By optimizing reaction condition, such as temperature, pH and reaction time, the productivity of formaldehyde and formic acid can reach as high as 16.537 mol h⁻¹ kg_{cat}⁻¹ and 2.95437 mol h⁻¹ kg_{cat}⁻¹, respectively.

Recent study shows that anatase TiO₂ nanocubes with single crystalline and exposed {100} and {001} facets, synthesized by hydrothermal and calcination approach, display significantly high photoactivity in CO₂ reduction to CH₄ and CH₃OH, because of the synergetic effects of highly ordered crystallization, co-exposure of {100} and {001} and more negative CB position facets (Fig. 4a and b) [60]. CeO₂ NPs have also been broadly used as photocatalyst in CO₂ reduction. A novel CeO₂ homojunction nanomaterial with unique crystallite structures has been fabricated via a crystallographic-oriented growth method by Zhou and co-workers [61], as shown in Fig. 4c–f, where hexahedron prism with exposed {100} facet was anchored on octahedron with exposed surface of {100} facet. The inert CeO₂ octahedron can be activated by prism arms on the surfaces, leading to an increase of its photocatalytic activity for the reduction of CO₂ into CH₄. Three possible factors were proposed to interpret the significantly enhanced performance: first, the prism arms act as fast channels for the transportation of the photogenerated electrons of the homojunction; second, the band alignment of the two exposed facet of {100} and {111} favors the charge separation to the surface of the catalyst; third, high charge carrier mobility due to the different effective mass of electrons of {100} and {111} facets greatly facilitates the charge separation.

2.1.2. Modified semiconductors

In addition to simple metal oxide NPs, compound semiconductors, such as g-C₃N₄, ZnS, CdS and CdSe have also been used for photocatalytic CO₂ reduction [23,24,32–41,62–75]; however, the photoactivity is restricted due to their deficient inferences, such as bandgap limit or high charge recombination rate. Therefore, a great number of

efforts have been conducted to increase the absorption and enhance the quantum efficiency of conventional semiconductors, including doping, dye-sensitizing and forming heterostructures or cocatalysts.

1) Doped semiconductors:

The introduction of dopant, either metals or non-metal elements into semiconductor lattice can effectively suppress the recombination of photogenerated charge carriers, rapidly transfer electrons/holes to the adsorbed reactants, and correct the band gap structure, even by the concomitant red shift of the intrinsic absorption edge. For instance, doping TiO₂ with N, S and Ni²⁺ [76–78] can narrow the band gap and thus increase the visible light absorption. Yu et al. [79] synthesized S-doped g-C₃N₄ with wider absorption range up to 475 nm. Photocatalytic CO₂ reduction test showed that the CH₃OH production yield using S-doped g-C₃N₄ is much bigger than using undoped g-C₃N₄ (1.12 vs. 0.81 μmol g⁻¹). Recently Yu also reported O-doped g-C₃N₄ nanotubes as photocatalyst for CO₂ reduction with improved performance [80]. Besides the modification to band gap and charge separation efficiency, the O-doping to g-C₃N₄ enhances the affinity and uptake capacity to CO₂. TiO₂ NPs doped with Indium (In) exhibits increased surface area and enlarged band gap [81]. The photocatalytic efficiency of In-doped TiO₂ NPs was greatly improved for CO₂ reduction. CO was the main product over pure TiO₂, whereas CH₄ yield was considerably increased using In-doped TiO₂. This enhancement is mainly attributed to the largely increased interfacial transfer efficiency of photogenerated charges, leading to effective charge separation and suppressed recombination of photogenerated charge carriers, owing to the structural change induced by the insert of In into TiO₂ lattice. Ola and Maroto-Valer [82] reported that the Cu doped TiO₂ show visible light absorption with enhancing Cu loading concentration in comparison with pure TiO₂. This change is ascribed to the interaction of Cu⁺ ions with TiO₂ crystal lattice via the replacing Ti⁴⁺ with Cu⁺; moreover, these Cu⁺ species can act as electron traps to suppress the charge recombination and favor the multielectron reactions, thus largely improve the CO₂ reduction efficiency. Other transition metal elements (such as Fe, Co, Pt, Mo and Ni etc.) doped TiO₂ are also found to be effective photocatalysts for reducing CO₂ to CH₄, and other hydrocarbons [81–92].

2) Sensitized semiconductor:

The activity of semiconductor NPs can also be enhanced by sensitizing their surface with photoresponsive molecules, e.g. organic or metal complex dyes, to surface of the semiconductors. In this system, the photogenerated electrons can transfer between sensitizer and CB of semiconductor, and the transfer pathway is determined by the relative positions of the highest occupied molecular orbital and lowest unoccupied molecular orbital (HOMO/LUMO) levels of dyes and CB of semiconductors. In most cases, the dye molecule acts as electron donor and semiconductor as electron acceptor during photocatalysis [93]. The semiconductor with only UV light response, such as TiO₂ or ZnO, can be easily modified into a visible-light responsive one using suitable sensitizers. Metal complex molecules are more stable than organic dyes, and they are thus widely used as sensitizers in photocatalysis. As presented in Fig. 5, Pawan et al. [94] reported a Ru(bpy)₃Cl₂ sensitized TiO₂ nanohybrid (Ru(bpy)₃/TiO₂) as highly selective catalyst for photocatalytic reduction of CO₂ under visible light. In this system, Ru(bpy)₃²⁺ component absorbs visible light and transfer electrons to the CB of TiO₂ for reaction. It is found that the visible light-driven methanol production yield upon Ru(bpy)₃/TiO₂ hybrid catalyst was much higher than that using pure TiO₂ catalyst and Ru(bpy)₃Cl₂ alone. P25 has also been sensitized using Cu complex of Cu(II) tetra(4-carboxylphenyl)porphyrin (CuTCPP) using a hydrothermal approach [95]. CH₄ production in photocatalytic CO₂ reduction using CuTCPP/P25 m (0.5 wt % of CuTCPP) is approximately 46 times higher than that using P25 alone, which is mainly attributed to the

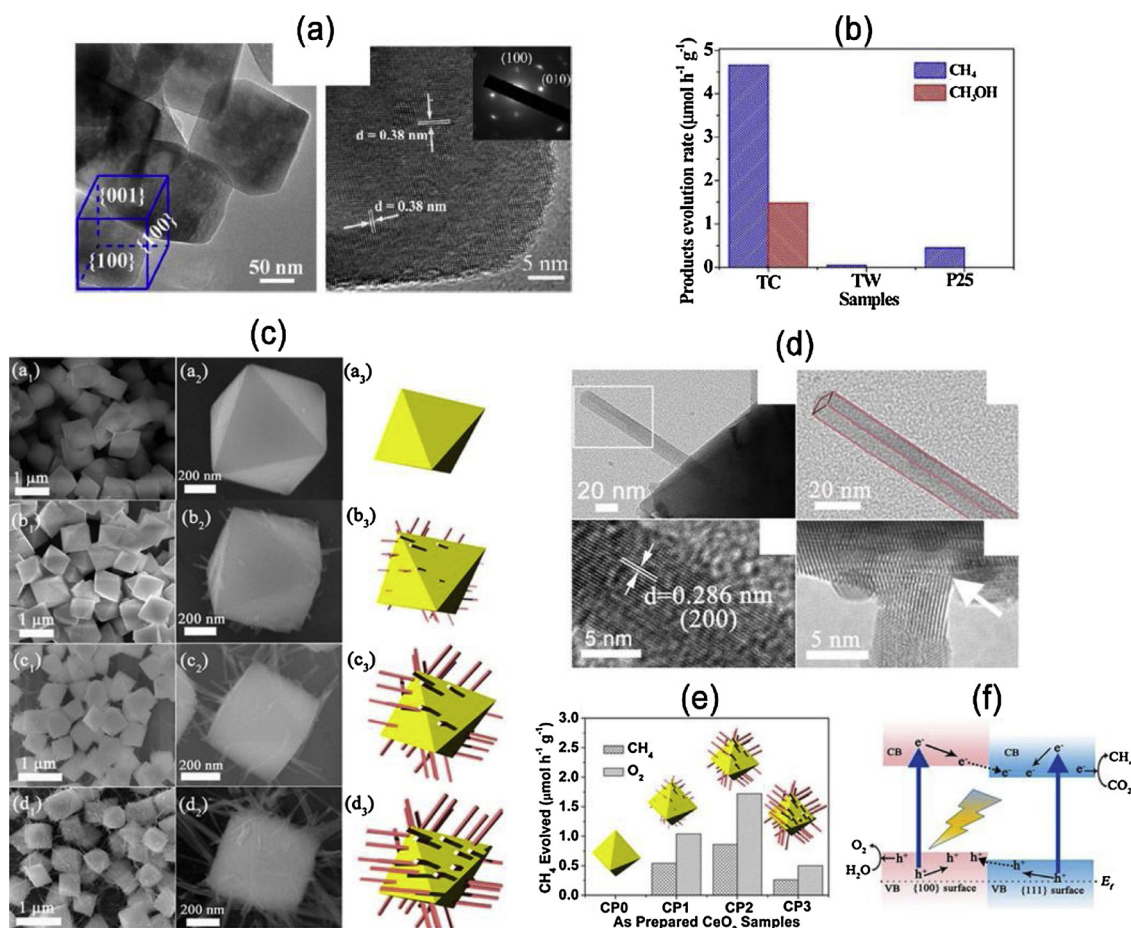


Fig. 4. (a) Transmission electron microscopy (TEM) and high resolution TEM (HR-TEM) images of TiO₂ nanocubes with single crystalline and exposed {100} and {001} facets. (b) Evolution rate of CH₄ and CH₃OH using TiO₂ nanotubes and other TiO₂ catalysts [60]. (c) Scanned electron microscopy (SEM) images of the hexahedron prism-anchored octahedral CeO₂ with different prism length. (d) HR-TEM images of the prism. (e) CH₄ evolution using different CeO₂ catalysts. (f) Proposed PET process for photocatalysis using hexahedron prism-anchored octahedral CeO₂ [61]. Reprinted with permission.

Cu sensitizer, which enhances the absorption of visible light and the rate of charge carrier separation. In another report [33], a comparison study using different sensitizers of Cu(II) phthalocyanines (CuPc) and Cu(II) porphyrins showed that the Cu(II) phthalocyanine (CuPc) (Cu(II) co-ordinated in the middle of the macrocycles) is highly beneficial for the photoactivity, probably due to its favorable reduction potential, indicating the important role of sensitizer

structure on catalytic activity. Currently many attentions have been focused on phthalocyanines containing center metals including Zn (II), Cu(II), Co(II), Ni(II) as sensitizers of semiconductors [96,97].

3) Heterostructures or hybrids:

Without doubt, today almost entirely of efforts in this research domain are concentrated to rationally design semiconductor heterostructures or nanohybrids to improve the reaction efficiency. The

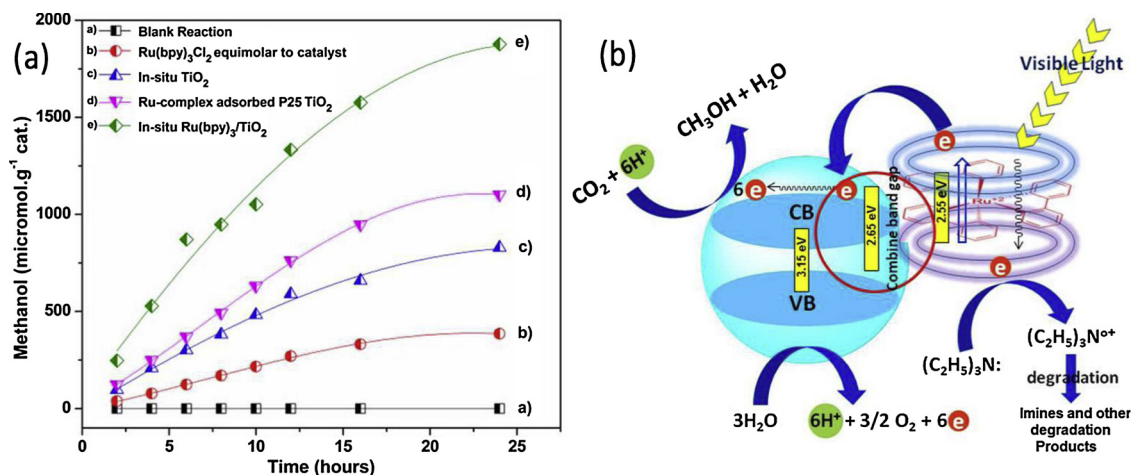


Fig. 5. (a) Methanol production as a function of reaction time upon different photocatalysts. (b) Plausible mechanism of CO₂ reduction on in situ Ru(bpy)₃/TiO₂ nanocomposite [94]. Reprinted with permission.

CO₂-reduction heterostructure catalysts can be generally divided into three categories: noble metal-semiconductor hybrid catalysts, noble metal-free hybrid catalysts, and multi-semiconductor hybrid catalysts, among which most of the attention are focused on the noble metal-semiconductor heterostructures, leading to the huge increase of publications daily. As there have been some excellent reviews about this topic, here we mainly summarize some very recent and most representative work.

a) Noble metal-based hybrid catalyst:

Noble metal NPs, such as Pt [98–104], Pd [105,106], Ag [107–110], Ru [111,112], Au [113] and alloy (or bimetallic) NPs [114–119] have been broadly applied to conjugated with semiconductors to form heterostructures. The synthesis to integrate metal NPs with semiconductor can be generally divided into two methods, which are the *in-situ* growth of metal along with semiconductor, and the coupling of as-synthesized components. Composition, morphology, structure, crystal facets, size, and alloy phase of the noble metal NPs demonstrate profound effect on the activity and selectivity of photocatalytic CO₂ reduction.

Among all noble metals, Pt possesses the unique feature of the highest work function of 5.56 eV, suggesting a very low Fermi level and strong electron-accepting ability. Therefore, Pt nanostructures have been largely applied to decorate semiconductor surface to promote separation of photo charge carriers, thus enhancing catalytic efficiency [28]. Pt NP decorated TiO₂ (Pt/TiO₂) is the most intensively investigated system for photocatalytic CO₂ reduction. For example, very recently, Tesbihi and Fresno [102] reported a mesoporous SiO₂ supported Pt/TiO₂ catalyst, which was synthesized by classic deposition-precipitation method. CO is the main product with only traceable CH₄ and CH₃OH using TiO₂ alone as the photocatalyst, while using Pt/TiO₂, CH₄ becomes the major product with a selectivity of ~100% with optimum Pt loading. *In-situ* near ambient pressure X-ray photoelectron spectroscopy (NAP-XPS) characterization indicates that the Pt NPs on TiO₂ can strongly chemisorb the CO intermediate, thus preventing CO to be the main product and further promoting the total reduction of CO₂ to CH₄. Zhang et al. [103] loaded Pt and Cu₂O on TiO₂ surface for CO₂ reduction. In the hybrids, Pt usually tends to promote the production of CH₄ with undesired H₂. On the other hand, Cu₂O is an effective material to suppress the production of H₂; however, it shows lower CH₄ selectivity than that of Pt. Thus, the combination of both with an appropriate ratio can largely improve CH₄ production. It is found that Pt shows dual functions to accelerate separation and transport of photo-generated electrons, and increase the electrons density of Cu₂O NPs, which is beneficial for selective CH₄ formation. In another report of Pt/In₂O₃ system, researchers [104] found that due to electronic and steric effect, Pt NPs can modulate the surface feature of In₂O₃, reducing the formation of bicarbonates (HCO₃[−]), bidentated carbonate (b-CO₃^{2−}) and monodentated carbonate (m-CO₃^{2−}) species toward the production of HCOOH, CH₂O and CH₃OH. More importantly, Pt play a key role in the selective formation of CH₄, as it weakens H-Pt bond and facilitate the bonding of C in CO₂ with protons to form CH₄, which simultaneously restrains CO production. As the most studied catalyst, Pt has been widely employed to couple with various semiconductors, such as g-C₃N₄, CeO₂, Zn₂GeO₄, LaPO₄ [61,99,120,121], and composites of In₂O₃/g-C₃N₄, NaNbO₃/g-C₃N₄, HNb₃O₈/SiO₂, CdSe/TiO₂, CdS/SiO₂ etc [74,100,101,122,123], to improve reaction activity and selectivity.

Pd has also been decorated to semiconductors to improve reaction efficiency of photocatalytic CO₂ reduction. Through a density functional theory (DFT) study, Liu et al. [124] had proposed that Pd/In₂O₃ is a promising catalyst with high activity for CO₂ reduction to methanol, because Pd is expected to improve the catalysis by offering metal sites for H₂ dissociation-adsorption and interfacial sites for CO₂ adsorption-hydrogenation, though there is still challenge experimentally. Very recently, they have synthesized the Pd/In₂O₃ hybrid *via* a thermal decomposition method, which successfully prevented the formation of PdIn alloy at composite interface [125]. Highly-dispersed

small Pd-NPs are exposing predominately the {111} facets on In₂O₃ surface. The Pd NPs demonstrate better ability to adsorb–dissociate hydrogen, thereby providing active H for the hydrogenation and accelerating the generation of oxygen vacancies on semiconductor surface. The Pd-In₂O₃ interfacial sites are also vital to promote CO₂ adsorption and hydrogenation. As a result, a superior performance of the Pd/In₂O₃ catalyst for CO₂ reduction to methanol is reached with a CO₂ conversion > 20% and methanol selectivity > 70%. Bai et al. [105] investigated the relationship between Pd NP facet and catalytic selectivity, by loading single-crystal Pd nanoclusters (NCs) or Pd nanotubes (NTs) enclosed by {100} and {111} facets on g-C₃N₄ nanosheets. The Pd/g-C₃N₄ samples all showed enhanced charge separation efficiency; however, they found that the Pd NT/g-C₃N₄ showed a much higher selectivity (80%) than that of Pd NC/g-C₃N₄ (20%) in CO₂ reduction to CO, C₂H₅OH, and CH₄. This facet selectivity relationship is attributed to the higher adsorption energy (EA = 0.23 eV) and lower activation energy barrier (EB = 3.98 eV) on Pd {100} than those on Pd {111}, respectively.

Au, Ag and Cu NPs are well-known materials as cocatalyst for visible light driven photocatalytic water splitting, due to their unique optical property of surface plasmon resonance (SPR). These plasmonic nano-hybrids have also been used for CO₂ reduction. Au NP is deemed to be the most famous SPR material with strong and tunable visible to near infrared absorption. Various Au/TiO₂ photocatalysts are used for CO₂ reduction under visible light irradiation [126,127]. For example, mesoporous Au@TiO₂ yolk-shell hollow spheres with highly crystalline and thin TiO₂ has been reported by Zou's group [127]. The SPR-induced local electric field at Au/TiO₂ not only enhances the separation of photo charge carriers in TiO₂ shells to improve the CO₂ reduction rate but also favors the formation of high-grade carbon species (C₂H₆), which is rarely reported in CO₂ reduction systems. They also reported the Ag/TiO₂ catalyst for efficient CO₂ reduction owing to the SPR and electron sinker effect of Ag component, which is closely related with the amount and size of loaded Ag. In this system, diverse hydrocarbons were produced, mainly including CH₄ and methanol [127]. Cu NPs have also been hybridized on TiO₂ surface (Cu/TiO₂) to increase the production yield of CH₃OH, as they exhibit a dual role as electron sink to improve the photo-charge separation and light harvesters to enhance the visible light absorption due to their localized SPR [128,129]. Besides the SPR property, these noble metals also show catalytically active sites in reactions. Small Ag NPs have been loaded on ZnGa₂O₄, ZnTa₂O₆, SrNb₂O₆ and Sr₂Nb₂O₇ for photoreduction of CO₂ [130–132]. Tanaka et al. [131] proposed the reaction mechanism on Ag/SrNb₂O₆ nanorod, where the reduction of CO₂ led to the formation of CO mainly on the top of the Ag/SrNb₂O₆ nanorods, while O₂ was generated mainly on the sides of the nanorods. The separation of the reduction and oxidation sites greatly suppressed the recombination of the photogenerated charge carriers; Ag-loaded SrNb₂O₆ nanorods thus exhibit good activity and selectivity. In another report, Vajda et al. [133] found small Cu clusters on Fe₂O₃ surface favor the activation of hydrogen, which can spill over to the neighboring Fe sites, and thus enhance the conversion CO₂. Other Ag based compound catalyst, such as AgBr NPs have also been used for efficient CO₂ reduction [134].

Recently, Ru has attracted increasing attentions as a promising replacement to expensive noble metals (i.e. Pt), as they show good activity and stability if rationally designed and more importantly price advantage compared with Pt [112,135–137]. For example, Zhang et al. [135] studied the effect of different oxide support (Al₂O₃, CeO₂, MnO₂ and ZnO) of Ru based catalysts on CO₂ reduction. For the pristine oxides alone, CO was the major product due to a lack of H₂ dissociation sites on these oxides. The addition of Ru created H₂ dissociation sites and led to a significant increase of CO₂ conversion and CH₄ selectivity. The ZnO support resulted in the formation of lowest Ru-CO coverage with a weak CO adsorption and the reverse water-gas shift was the dominant reaction. CeO₂ showed a moderate Ru-CO coverage in between Al₂O₃ and ZnO, which favors the creation of H₂ dissociating sites

and remains the high Ru-CO adsorption strength. Zeng et al. [136] reported a mesoporous silica nanowire encapsulated Ru NP catalyst (Ru@mSiO₂) for CO₂ reduction. CO was the main product for 1–3 nm Ru NPs within mesoporous silica nanowires, while CH₄ was the major one for bigger Ru NPs (5–20 nm). This difference is mainly ascribed to the different reaction intermediates formed on Ru@mSiO₂ catalyst surface: CO-Ruⁿ⁺ on 1–3 nm and formate species on 5–20 nm.

Bimetallic NPs, including alloys, core-shell and intermetallic structures, usually contains at least one noble metal, which have demonstrated the so-called synergistic effect on promoting the photocatalytic CO₂ reduction. In most cases, these bimetallic NPs are distributed on semiconductor surface as cocatalysts for photoreactions. For example, Song et al. [138] reported a SiO₂ supported Pd-Cu alloy NP catalysts for selective CO₂ hydrogenation to methanol. In the alloy structure, the component ratio of Pd could be varied in the range of 25–34 mol %. It was found that the alloy with 25 mol % Pd (Pd(0.25)-Cu/SiO₂) demonstrated the highest activity with a methanol formation rate twice higher than the simple sum of monometallic Cu and Pd catalysts, indicating a synergistic effect for catalysis. It is proposed that the alloys could provide a source of chemisorbed hydrogen atoms, which favors the formation of CH₃OH. Zhao and co-workers [116] reported a three-dimensionally ordered microporous (3DOM) TiO₂ supported Au-Pd core-shell-like NPs. Since bimetallic AuPd nanoparticles with the relatively low Fermi level have good capacity of trapping electron, they can efficiently promote the separation of photogenerated electron-hole pairs in TiO₂. The AuPd/3DOM-TiO₂ catalysts demonstrate excellent activity for photocatalytic CO₂ reduction. In particular, Au₃Pd₁/3DOM-TiO₂ catalyst exhibits the highest activity and selectivity for CO₂ reduction to CH₄ with a formation rate of 18.5 μmol g⁻¹ h⁻¹ and selectivity around 93.9%. In photocatalysis, upon light absorption, the excited electrons in CB of TiO₂ are transferred to Au NPs. And then the electrons further transfer from Au to Pd, which further decreases the recombination rates of electron-hole pairs. Electrons assemble on metal NPs react with the adsorbed CO₂ to form CH₄, while holes on the VB of TiO₂ oxidize H₂O. Therefore, Au-Pd core-shell NPs not only offers the reduction sites but also serves as the electron sinks, leading to an effective charge separation and photocatalytic activity enhancement. AuFe, AuAg and Pd-In based catalysts have also been reported and show large activity enhancement for CO₂ reduction into hydrocarbon products [118,119,139].

b) Noble metal free catalyst

Compared with the noble metal-based catalyst, non-noble metal one exhibits superior cost advantage, implying higher feasibility for mass-production or commercialization. Ni is a famous material as non-noble metal cocatalyst for various catalytic reactions, including CO₂ reduction [140–142]. For instance, Dai et al. [143] reported a Y₂O₃ supported Ni NP catalyst as photocatalyst for CO₂ reduction. By changing different synthetic methods, the authors found the approach using YO(NO₃) acting as a unique matrix to afford anchoring sites to interact with Ni²⁺ ions, can result in a moderate interaction between Ni metal and Y₂O₃ support, thus inducing excellent catalytic activity and stability towards

CO poisoning in photocatalytic CO₂ reduction. Garcia and Albero [130] synthesized GR supported NiO/Ni NPs (NiO/Ni-GR) as efficient photocatalyst for gas phase CO₂ reduction with H₂. The hybrid with an optimal Ni loading of 23 wt % showed the highest activity with the maximum specific CH₄ formation rate (642 μmol g_{Ni}⁻¹ h⁻¹ at 200 °C). Under the same conditions, Ni NPs supported on SiO₂-Al₂O₃ or NiO NPs alone only showed much lower CH₄ production rates than NiO/Ni-GR. In another report, the presence of Ni@NiO core@shell co-catalyst increased the photoactivity of N doped InTaO₄ (N-InTaO₄) for CO₂ reduction to CH₃OH under visible light irradiation [30]. Zou's group [144] reported a KOH-modified Ni/LaTiO₂N photocatalyst for visible light CO₂ reduction, showing high performance in CO₂ reduction with CH₄ generation rate of 9.69 μmol g⁻¹, about 5 times higher than that upon LaTiO₂N. The significant activity enhancement is mainly attributed to a formation of Schottky barrier at Ni/LaTiO₂N interface boosting the separation of electron-hole pairs. The OH⁻ of KOH promotes the activation of CO₂ into CO₃²⁻ species, greatly enhancing the reaction kinetics of CO₂ reduction, and the OH⁻ can also act as hole acceptor, accelerating the proton transfer from H₂O oxidation. Metallic Cd has also been used as cocatalyst to couple with semiconductors for photocatalytic CO₂ reduction. Inoue et al. [145] reported that the Cd decorated ZnS (Cd/ZnS) increased the reaction efficiency of photocatalytic reduction of CO₂ to HCOOH.

c) Non-metallic (or metal free) hybrid catalyst.

Although most efforts have been concentrated on the metal-based hybrid catalyst with superior activity, the cost is still very high, as those metals are limited in supply, and refining process is less environmental-friendly. By stark contrast, the non-metallic nanohybrids, mainly composed of semiconductor-based (mainly oxides, compound semiconductors and g-C₃N₄), carbon based (e.g., GR, reduced graphene oxide (rGO), carbon nanotube (NT)) or metal-organic framework (MOF)-based materials show many excellent features, such as easy synthesis, highly designable morphologies, high surface area, good electric conductivity, nontoxic, inexpensive, and feasible for mass fabrication, leading to a promising material for photocatalytic CO₂ reduction. For example, recently, Guo et al. [146] reported a g-C₃N₄@CeO₂ hollow heterostructure with rich OVs. This hybrid demonstrates a significant synergetic effect in catalysis. The OVs of g-C₃N₄@CeO₂ is found to play the vital role for CO₂ reduction, resulting in the generation of CH₄ much earlier with higher concentration than that upon pristine g-C₃N₄ and CeO₂ alone. Yu et al. [96] reported a g-C₃N₄/ZnO structure, which exhibited stronger and wider light absorption than pure g-C₃N₄ in the visible range. The photocatalytic activity of this g-C₃N₄/ZnO for CO₂ reduction to CH₃OH is 2.3 times higher than that of pure g-C₃N₄. Rather than the conventional heterojunction-type mechanism, a direct Z-scheme mechanism was proposed to interpret the enhanced properties of the g-C₃N₄/ZnO system, where the intimate contact of the two components results in more efficient electron transfer from ZnO to g-C₃N₄ without an electron mediator can take place at the g-C₃N₄/ZnO interface (Fig. 6). The mechanism is further confirmed by PL analyses, photocurrent measurements and DFT calculations.

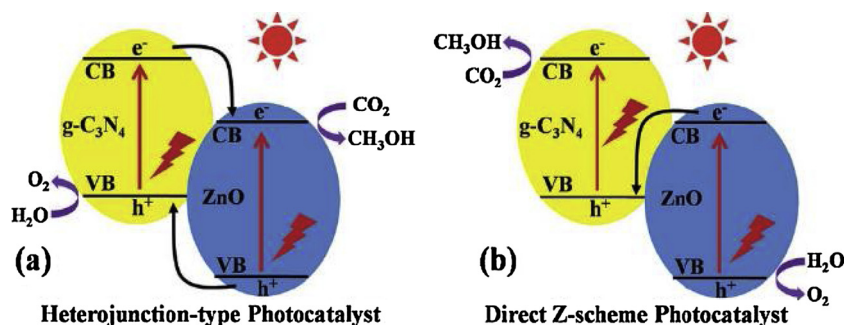


Fig. 6. Scheme of the two different mechanisms for charge carrier separation: (a) conventional heterojunction-type and (b) direct Z-scheme mechanisms [96]. Reprinted with permission.

Koci et al. [147] find kaolinite/TiO₂ composite shows higher photoactivity than P25 for CO₂ conversion to CH₄. The enhanced performance is attributed to two key factors: (1) the decrease of anatase crystallite size when TiO₂ NPs was introduced into the kaolinite structure; (2) the modification of acidobasic properties of catalyst surface inhibiting the charge recombination and preventing the aggregation of TiO₂ during reaction. Backov and Fécant [148] also reported novel SiO₂-TiO₂ self-standing porous foam with a size of millimeter length scale for 3D-photodriven CO₂ catalytic reduction. The foams bear a strongly multidiffusive performance, in which photons can be greatly trapped within the cores by increasing the light pathway. This 3D process largely promotes selectivity for the hydrocarbon production of methane (~80%) and ethane (~18%). Olivo et al. [149] reported that N-doped CuO-TiO₂ photocatalyses CO₂ photoreduction in gas phase under a very mild reaction condition. The study of N and Cu amount effect on catalytic performances showed that the CH₄ formation is sensitive to the amount of Cu, and the reagent ratio also strongly affects the catalytic performance. Fang et al. [150] reported CuO-doped TiO₂ hollow microspheres in light-driven CO₂ conversion with H₂O to CH₄, and the crystal structure effect on CO₂ conversion has also been investigated. Hollow spherical mesoporous TiO₂ NPs possess large surface areas and layered nanostructures, with a large number of surface-active sites. The CuO clusters on TiO₂ surface act effectively as co-catalyst to improve photocatalytic activity. Compared with the most prevailing photocatalyst, e.g. P25 TiO₂, the TiO₂ hollow microsphere catalyst hybridized with CuO exhibited higher photocatalytic activity for photo-driven reduction of CO₂ with H₂O into CH₄. Cuprous oxide (Cu_xO_y) nanoclusters coupled with binuclear units of ZrOCo^{II} were covalently anchored on a silica mesopore surface to form a hierarchical assembly for CO₂ reduction. The oxidation state of the Cu on surface can be tuned by the reduction of Cu_xO_y cluster via a metal-to-metal charge transfer state of the ZrOCo^{II} light absorber. The production yield of the HCOOH showed strong dependence on the oxidation state of the surface Cu, indicating that the heterobinuclear unit functions as light absorber to donate electrons to the Cu_xO_y catalyst to drive the CO₂ reduction [151].

GR materials possess excellent conductivity and optical property, thus have been broadly applied in photocatalysis to enhance the efficiency of photo-charge separation and transportation. rGO modified TiO₂ reveals improved activity for photoreduction of CO₂ to CH₄ under visible light, which is six-fold higher than the pure TiO₂ [152]. Tu et al. [153] successfully fabricated robust hollow spheres which consist of molecular alternating Ti_{0.91}O₂ NPs and rGO nanosheets toward the photocatalytic conversion of CO₂ in the presence of water vapor. The conversion of CO₂ using rGO-Ti_{0.91}O₂ hollow spheres is 5-times higher than pure Ti_{0.91}O₂ hollow spheres and 9-times higher than P25 [154,155], since i) the ultrathin nature of the material favors the rapid migration of charge carrier to surface, ii) the strong interaction of Ti_{0.91}O₂ with rGO enhances the lifetime of charge carriers, and iii) the hollow structure increases the incident light trapping by multi-scattering effect. A core-shell structured rGO@CuZnO@Fe₃O₄ microspheres was fabricated by Jain et al [156], which is a highly efficient, recyclable and magnetically separable catalyst for CO₂ reduction under visible light to produce methanol. The excellent activity of this hybrid is ascribed to the restoration of the *sp*² hybridized aromatic system of rGO, which promotes the movement of electrons and leads to efficient charge separation. The synthesized heterogenous photocatalyst could readily be collected by magnet and reused for several cycles without significant activity loss.

MoS₂-based nanomaterial has attracted wide attention as they possess a suitable band gap for visible-light harvesting and large surface area for reactant adsorption, rendering them a promising catalyst for photocatalysis [157–159]. For example, very recently, Li and co-workers [158] synthesized a marigold-like nanoflower constructed by SiC@MoS₂ nanosheets, which demonstrated excellent activity for CO₂ reduction under visible light irradiation to form CH₄ (Fig. 7). The CH₄ evolution efficiency was reported to reach the value of 323 μL·g⁻¹ h⁻¹

along with nearly stoichiometric evolution of O₂ under visible light without using any sacrificial reagents during reaction, which is a record for simultaneously visible-light driven photocatalytic CO₂ reduction to CH₄ and water oxidation to O₂. This superior photocatalytic performance can be ascribed to (1) the Z-scheme heterostructure of the SiC@MoS₂ nanosheets, which favors electron transfer upon more negative CB of SiC and more positive VB of MoS₂; (2) the higher hole mobility of MoS₂ and higher electron mobility of SiC. (3) the large surface area of marigold flower-like morphology of SiC@MoS₂; (4) the gas-solid reaction mode, which is beneficial for adsorption/desorption of reactants/products.

Bismuth based semiconductors, such as Bi₂WO₆, BiOX (X = Cl, Br, I) and Bi₂S₃ are cheap materials, and show excellent photocatalytic activity due to their unique optical and structural features [160–168]. For example, Fu's group [168] reported a Bi₂WO₆-TiO₂ binanosheet Z-scheme heterostructure toward high selectivity CH₄ formation (Fig. 8). They revealed that an interaction and a competition between light-driven carbonaceous residues decomposition and photocatalytic CO₂ reduction are coexisted during reaction, suggesting the importance of removing organic residues from photocatalysts for an efficient CO₂ reduction. Moreover, this work could provide some enlightenment on designing and/or synthesizing more efficient photocatalysts for CO₂ reduction. BiOX photocatalysts possess unique layered crystalline structure and visible absorption property. Under visible/near-infrared-light, BiOI has been used as catalyst to convert CO₂ into CO and CH₄ [169]. Yu et al [170] developed a novel 2D/2D heterojunction of untrathin Ti₃C₂/Bi₂WO₆ nanosheets, where Bi₂WO₆ was grown along the surface of Ti₃C₂ nanosheet. This hybrid possesses a short charge transfer pathway and a large interfacial surface, leading to superior charge transfer performance. Moreover, the high surface area as well as high porosity enables Ti₃C₂/Bi₂WO₆ hybrids enhanced CO₂ adsorption capability. This 2D/2D hybrid demonstrated largely enhanced catalytic activity for photoreduction of CO₂. The production yield of CH₄ and CH₃OH upon the hybrids is 4.6 times higher than that using pristine Bi₂WO₆ nanosheets. Bismuth sulfide (Bi₂S₃) is a p-type semiconductor with a narrow band gap (1.49 eV), and the CB potential is more negative than that of most photocatalysts indicating a good visible light absorption. Recently, Bi₂S₃ nanoribbons with very high aspect ratio were synthesized and used for the photocatalytic reduction of CO₂ to methanol [161]. Bi₂S₃ NPs were also used as co-catalyst to conjugate with other semiconductors, such as CeO₂ [171] and CdS [172], to form nanocomposite catalyst for visible light CO₂ reduction to CH₃OH, and demonstrated dramatically enhanced activity, compared with the reactions catalyzed by each single component, which is attributed that the Bi₂S₃ co-catalyst effectively inhibits the electron-hole recombination and favors charge transfer. Since surface OVs are believed to play a decisive role in determining the efficiency of photocatalytic reactions, very recently Zhang and co-workers [173] published an excellent review discussing about the OV-mediated photocatalysis at the surface molecular level using 2D BiOCl as the platform, indicating the importance of Bi based semiconductor in photocatalysis.

Besides the inorganic materials, coordination polymers and MOF have been largely applied in photocatalytic CO₂ reduction [174–181]. These organic metal complex materials provide a newly emerging platform to integrate light-harvesting and catalytic centres for photocatalysis due to their high diversity of structure and controllable synthetic procedures [150–155]. An artificial Z-scheme system of p-type InP/Ru complex polymer-TiO₂ hybrid photocatalyst was introduced for the photoelectrochemical reduction of CO₂ to formate. Upon this hybrid material, selective photoreduction of CO₂ to HCOO⁻ was achieved in aqueous media, in which H₂O was used as both an electron donor and a proton source. The selective yield of HCOO⁻ is more than 70% and the conversion efficiency from solar energy to chemical energy is 0.03 ~ 0.04% [182]. Amino-functionalized NH₂-UiO-66(Zr), MOF-253 supported active Ru carbonyl complex (MOF253-Ru(CO)₂Cl₂), amine-functionalized Ti-based porous MOF (NH₂-MIL-125(Ti),

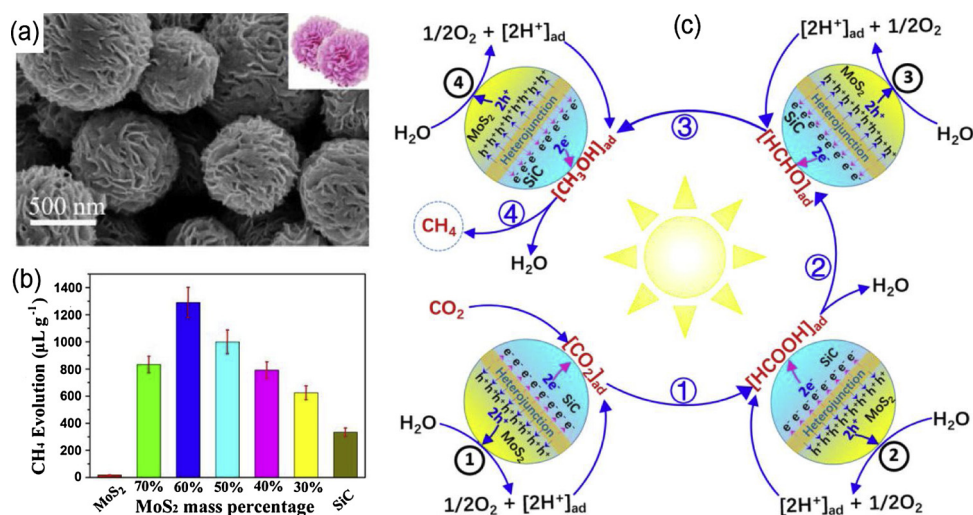


Fig. 7. (a) Scanned electron microscopy (SEM) image of the SiC@MoS₂ nanoflowers. (b) CH₄ evolution on the photocatalyst SiC@MoS₂ with different MoS₂ content for 4 h reaction. (c) Proposed reaction pathway of photocatalytic CO₂ reduction with H₂O and SiC@MoS₂ [158]. Reprinted with permission.

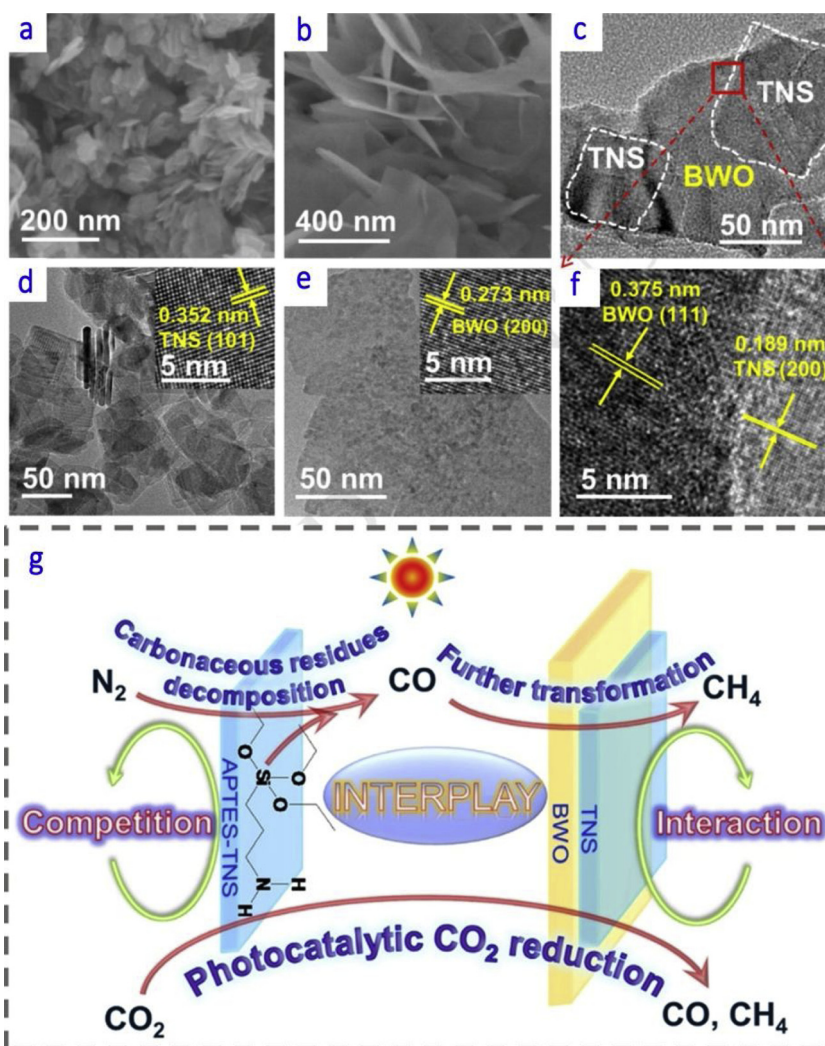


Fig. 8. (a–f) TEM images of the Bi₂WO₆-TiO₂ binanosheets. (g) Proposed Z-scheme process of the photocatalytic CO₂ reduction upon the binanosheets [145]. Reprinted with permission.

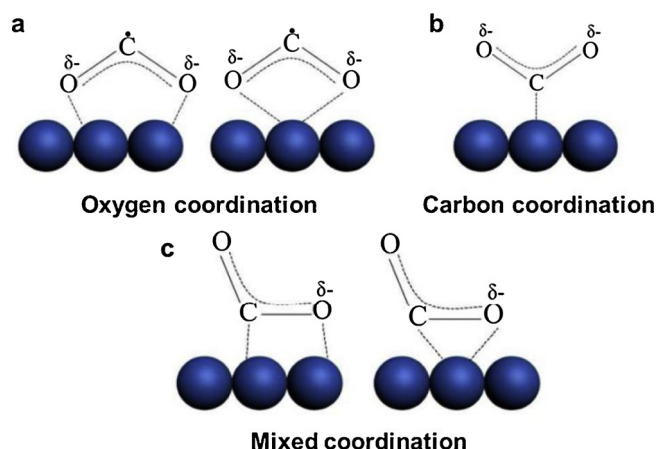


Fig. 9. Proposed structure modes of CO_2 bonding on catalyst [25,191–193]. Reprinted with permission.

($\text{Ti}_8\text{O}_8(\text{OH})_4(\text{NH}_2\text{-BDC})_6$, BDC = benzene-1,4-dicarboxylate) and other types of MOFs were synthesized and used for visible light photocatalytic CO_2 reduction [40,175,183–186]. For example, Xu and co-workers [186] reported the application of a porphyrin-based MOF PCN-222 in the photo organic synthesis. Their study showed that this MOF structure can selectively capture and further photo-reduce CO_2 efficiently under visible light. The deep electron trap states present in the unique structure of PCN-222 effectively suppress the electron-hole recombination compared to the corresponding porphyrin ligands, leading to significantly enhanced photocatalytic conversion of CO_2 to form formate anion. There are still many other types of photocatalysts in this research domain, such as Perovskite oxide and biological catalysts, this information can be found in other excellent reports and reviews [25,27–30,187–190].

2.1.3. Factors affecting products

In general, the heterogenous photocatalytic CO_2 reduction is started from the adsorption and activation of CO_2 on catalyst surface; subsequently, PET from catalysts to the adsorbed CO_2 triggers chemical reactions which eventually determine the final products and the efficiency of the photocatalysis [191–193]. The process of adsorption and activation of CO_2 on catalyst surface is the key step which significantly affects the following hydrogenation of CO_2 and the suppression of competing H_2 evolution reaction. Basically, CO_2 adsorption induces the formation of partially charged species $\text{CO}_2^{\cdot-}$, which present on catalyst surface in three modes [191–193]. If $\text{CO}_2^{\cdot-}$ is interacted with surface atoms of catalyst via O atom(s) (Fig. 9a), it prefers to take a H atom to form a formate anion (HCOO^-) and then form formic acid (HCOOH) through protonation as a final product, where the C–O bond is stable and no cleavage occurs [194,195]. If the bonding is taken place between C atom of $\text{CO}_2^{\cdot-}$ (Fig. 9 and c), $\text{CO}_2^{\cdot-}$ tends to combine with a H to form carboxyl radical ($\cdot\text{COOH}$) and then split into the adsorbed CO, where the C–O bond breaks easily [195,196]. The adsorbed CO can be subsequently hydrogenated to form various hydrocarbons. Therefore, in principle, by the rational design of catalyst surface, the adsorption and activation of CO_2 on catalyst surface may be regulated, leading to the formation of desired products [191–193]; however, a good control to the adsorption process is a considerable challenge in practice and the understanding of the exact mechanism of catalysis is still limited. There are also many factors influencing the activity and selectivity of the catalysis, such as OV, exposed facet, surface area (or porosity), heterojunctions and so on, which may show combined effects to reactions. In many cases, the results are unpredicted from the initial design. Although a clear law affecting the selectivity of the reaction is too complicate to be concluded, several important parameters (co-catalyst, surface chemical and solution pH) are extracted from some published

results.

1) Cocatalyst effect:

As mentioned above, today, nearly all efforts have been concentrated on development of heterostructures, among which the hybridization of semiconductor with cocatalysts dominates the research domain. The cocatalyst system can greatly improve the efficiency of photocatalytic CO_2 reduction, as it can essentially improve the surface reaction kinetics by decreasing the activation energy. A report of the CuO loaded P25 from Gunlazuardi et al. [197] showed a lower activation energy than P25 (23 vs. 26 KJ mol^{-1}), indicating that the presence of CuO enhanced the catalytic efficiency [197]. The Schottky barrier at the interface of metal NP-semiconductor can improve the charge separation leading to an electron accumulation at the metal side for catalysis [198]. The adsorption of CO intermediate on catalysis, the hydrogen evolution and CO_2 activation overpotentials are the key factors determining the selectivity [199,200]. The metals, such as Pb, possessing high hydrogen evolution and CO_2 activation overpotentials usually lead to the formation of formate as the major product; while for the metals, e.g. Au, with medium hydrogen evolution overpotential and weak CO interaction, CO turns to be the major product. For Pt and Fe, as they have very low hydrogen evolution overpotential and strong CO bonding ability, the major product is preferable to be H_2 . An exception is Cu, which can still improve the reaction of adsorbed CO with hydrogen to form CH_4 and CH_3OH [42,49].

Noble metals, e.g., Pd, Pt, Au etc., are excellent cocatalyst to improve the reaction rate and vary the selectivity. For pristine TiO_2 , CO was the main product with only traceable amount of CH_4 . By stark contrast, after loading with Pd and Pt, CH_4 became the main product instead of CO [201]. Fine structure of metal NPs also shows important effect on activity and selectivity. For example, the edge sites of Au nanowires are highly beneficial for CO generation. The increase of edge to corner ratio of the Au atoms on NP surface led to higher production of CO. In general, metals loaded on semiconductor surface mainly act as electron traps to promote electron-hole separation, and form a high local electron density area at the metal, which is favorable for the generation of CH_4 [139].

2) Surface chemical effect:

The catalysts are obtained through various synthetic methods, e.g., hydrothermal, wet-synthesis, physical treatment etc., leading to different surface features of the materials. Catalysis is fundamentally a surface reaction, which highly relies on the surface chemistry of the catalyst. Therefore, surface features of the catalyst, such as functional groups, play a crucial role affecting the CO_2 reduction from the aspects of activity and selectivity. As water is involved in nearly all heterogenous CO_2 reduction photocatalytic process, surface wetting or hydrophilic-hydrophobic property becomes a primary factor impacting on the subsequent steps. By varying hydrophilic-hydrophobic feature of photocatalyst, some reports have shown that selective production of either CH_4 or CH_3OH could be feasible. For example, the hydroxyl groups ($-\text{OH}$) on Ti-beta zeolites surface can be tuned by using OH^- and F^- anions during hydrothermal synthesis to form Ti-beta (OH) and Ti-beta (F), which showed different adsorption ability to CO_2 and water [202]. CO_2 photoreduction under UV light over the two catalysts demonstrated quite distinct results. Hydrophilic Ti-beta (OH) demonstrated much higher reactivity than hydrophobic Ti-beta (F), whereas the selectivity of CH_3OH formation from Ti-beta (F) is much higher than that from Ti-beta (OH) (41% vs. 11% in all products), indicating that increase hydrophobicity of this material favors the selective formation of CH_3OH with a reduction of CH_4 proportion [202]. This observation was confirmed again by introducing F into Ti/FSM-16 to increase its hydrophobicity, where the production yield of CH_3OH was increased greatly [203]. Amine groups [204] also show impact on the reaction selectivity of product formation, since they can

interact with CO₂ via the formation of C–N bonding, leading to the formation of carbamate (NH₂COO[−]) and subsequent carbonate. This process resulted in the generation of carboxyl radicals and then decomposed into CO on catalyst surface as the main product.

3) Solution pH effect:

CO₂ solubility in water can be changed by varying pH value in solution, which also affects the concentration of CO₃^{2−} and HCO₃[−] in solution. The different chemical species generated by dissolved CO₂ lead to different adsorption modes and reactions on catalyst surface. It is also found that the pH can affect the completing hydrogen evolution during CO₂ reduction. Reaction is preferable to produce H₂ at low pH [42]. An early study [205] of electrochemical CO₂ reduction test using Cu electrode and various electrolyte solutions showed that the adsorption strength of CO on Cu is much weaker than that on Pt. Adsorbed CO is reduced to CH₄, C₂H₄, EtOH and isopropanol at more negative potentials. The product types depend strongly on the electrolytes employed. Formation of C₂H₄ and alcohols is favored in solution of KCl, K₂SO₄, KClO₄ and dilute HCO₃[−] with pH ~6–7, whereas CH₄ is the major product in relatively concentrated HCO₃[−] (pH = 9.6) and phosphate solutions (pH = ~6). The product selectivity depends on protons on electrode surface, which is controlled by pH or the electrolyte, since OH[−] is released in the electrode reactions. However, whether this observation in electrochemical catalysis can be applied in heterogenous photocatalysis is still unknown. The pH of the reaction solution may play an important role in the preferred surface reaction, leading to different final products.

2.2. Photocatalytic conversion of organics

In chemical industry, the synthesis of many important organic chemicals usually requires harsh operating conditions, such as high temperature and pressure, with extreme amount of energy consumption. Heterogenous photocatalytic organic synthesis is a concept to use light as an energy source and small hydrocarbons as the raw material (reactant) to produce value-added organics, which indicates a more promising route to drive chemical reactions. Moreover, many chemicals synthesized upon photocatalytic process can be achieved in simple “one-pot” reactions. The following content briefly reviews the state-of-the-art progresses of the heterogenous photocatalytic organic conversions. Depending on the reactions, this section is mainly divided into four parts, including the oxidation of alcohol and aromatics, carbon-carbon coupling, esterification and epoxidation, nitrogen containing chemical formation.

2.2.1. Oxidation of alcohols and aromatics

In heterogenous photocatalytic water splitting, alcohols (e.g. CH₃OH) have been mainly employed as hole scavengers to promote the reaction, because the redox potentials of alcohols are less positive than the VB edge of the semiconductor catalysts [206]. In principle, alcohols

can be photocatalytically oxidized to the corresponding carbonyl compounds [207–214]. However, due to the difficulty of the reaction control, this reaction usually produces carboxylic acids or even CO₂, which are products of over-oxidizing or fully oxidizing (decomposed) processes. Therefore, the control of oxidizing extent and the selectivity toward desired products is the primary concern for heterogenous photocatalytic oxidation of organics. Studies have shown that the selectivity can be influenced by many parameters, such as the medium (solvent), the photocatalyst itself, the presence of O₂, and the type (structure) of the alcohol used.

Another similar photocatalytic oxidation process is the oxidation of aromatics, which leads to the formation of many important chemicals, such as resins and pharmaceutical products, where phenol, catechol and hydroquinone have been widely used as precursors in this reaction. The heterogenous photocatalytic oxidation of aromatic compounds was firstly reported by Fujihira et al. [215], where the role of various reaction parameters, such as oxygen, solution pH, and additional of ions, have been investigated in the selectivity of the hydroxylated products.

Friend et al [216] studied the formation of methyl formate by oxidizing methanol on TiO₂ (110) surface. They found that exposure of the TiO₂ surface to O₂ is important to promote the photo-oxidation reaction in order to heal surface and near-surface defects that can serve as hole traps. Based on measurement using mass spectrometry and scanning tunneling microscopy, two consecutive photo-oxidation steps for this reaction were proposed. The first step is to form CH₃O and water via thermal dissociation of the O–H bond, followed by the formation of formaldehyde through hole-mediated oxidation of CH₃O. In the second step, transient HCO is produced from formaldehyde, which can react with residual CH₃O to produce methyl formate as the final product. CeO₂, as a reducible metal oxide, can replace TiO₂ as the supporting material of Au NPs, which may endow different catalytic properties. Kominami et al. [217] prepared Au/CeO₂ plasmonic photocatalyst by reducing H₄AuCl₄ on CeO₂ surface with citric acid as reducing agent. Upon 530 nm-wavelength excitation, Au/CeO₂ can catalyze the selective oxidation of aromatic alcohol to aromatic aldehydes with O₂ in aqueous phase, and the reaction is almost quantitative. In addition, the catalytic activity of the catalyst mainly depends on the specific surface area of Au NPs loaded on CeO₂, rather than the total amount of Au NPs. The sample with Au NPs of 30 nm demonstrated the most efficient catalytic performance. Compared with the single-step synthesis, the multi-step method allows the formation of the Au NPs with larger particle size and higher catalytic activity, and their reaction rate is twice higher than those NPs obtained using the single-step synthesis method. The oxidation of alcohols over the Au/CeO₂ composites proceeds with high selectivity, e.g. the photocatalytic system endows the oxidation of p-aminobenzyl alcohol to p-aminobenzaldehyde at high product yield (99%) without exerting any side effect to amino groups (Fig. 10) [218,219]. Due to the SPR effect of Au under visible light irradiation, hot electrons are injected to the CB of adjacent CeO₂, resulting in the electron-deficient Au. The efficient oxidation of benzyl

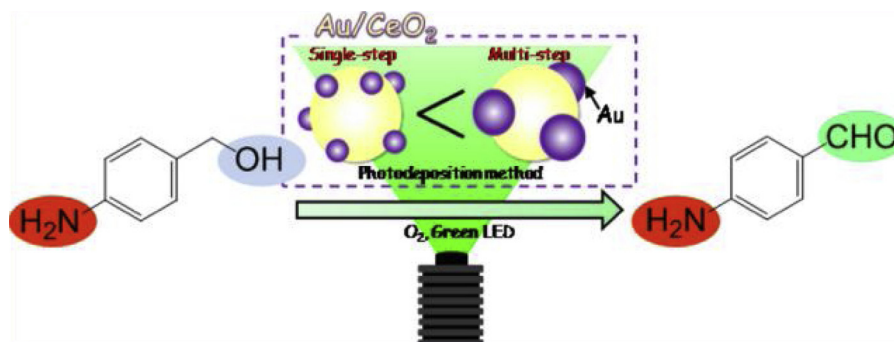


Fig. 10. Selective oxidation of p-aminobenzyl alcohol into p-aminobenzaldehyde over Au/CeO₂ catalyst under green light irradiation [218]. Reprinted with permission (For interpretation of the references to colour in this figure legend, the reader is referred to the web version of this article).

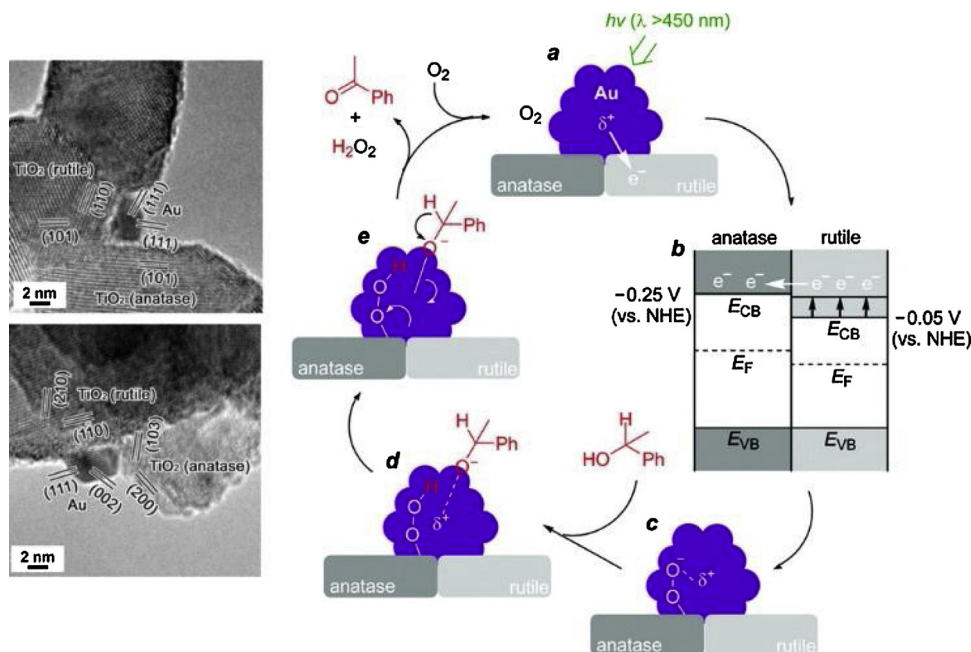


Fig. 11. HR-TEM images of the Au NPs loaded on the interface of anatase/rutile TiO₂. And the proposed process of oxidation of aromatic alcohols on the interface of mixed crystal structure [222]. Reprinted with permission.

alcohol may be attributed to smooth electron transfer from electron-rich benzyl alcohol to the electron-deficient Au. Because in this reaction O₂ is involved, electrons trapped by O₂ may form highly active oxygen species, such as O₂^{•-} radical and/or H₂O₂. In the presence of metal co-catalyst, one-electron reduction of O₂ takes place more efficiently in photocatalytic oxidations than the multielectron reduction of O₂. The high selectivity of benzaldehyde implies that those active oxygen species may be exhausted in the reaction system. The Au based plasmonic catalyst can also catalyze hydrogen peroxide to oxidize aromatic alcohols to corresponding carbonyl compounds [220] with a conversion rate close to 95%, under visible light irradiation. Li et al. [221] also presented a plasmonic Au/CeO₂ hybrid nanofiber catalyst for selective oxidation of benzyl alcohol to benzaldehyde with O₂ under visible light irradiation. The Au loading effect on catalysis was studied and showed that an optimal level over 0.5 wt. % Au-loaded CeO₂ nanofibers led to the highest selectivity of 100% benzaldehyde formation. Shiraishi et al. [222] prepared Au/TiO₂ plasmonic photocatalyst by loading Au NPs smaller than 5 nm on the interface of anatase/rutile TiO₂ mixed crystal structure (Fig. 11). At room temperature, aromatic alcohol can be efficiently converted to oxo-compound with high catalytic selectivity using Au/TiO₂ as the catalyst with visible light irradiation.

Hollmann et al. [223] have developed a photocatalytic technique, combining photochemical water-oxidation catalysis with peroxygenase catalysis to achieve visible-light-driven, aerobic oxidation of hydrocarbons with high selectivity. The generation of H₂O₂ during photocatalytic water oxidation process promoted peroxygenase-catalysed, selective oxyfunctionalization reactions. This concept was testified for the reaction of the selective photoenzymatic hydroxylation of ethyl benzene using Au-TiO₂ photocatalyst in the presence of Agrocybe aegerita (AaeUPO) under visible light irradiation (Fig. 12a). More importantly, a broad range of aliphatic and aromatic compounds have also been converted into their corresponding alcohols, verifying the versatility and robust of this technique. Immobilized Au NPs containing layered titanate in interlaminar space as catalyst promoted the oxidation of benzene in the presence of water to the corresponding phenol with high product yield and selectivity (96%) under visible light irradiation [224]. Huang and co-workers [225] prepared a series of plasmonic catalyst M@TiO₂ (M = Au, Pt, Ag) using a simple in-situ growth approach to load noble metals onto TiO₂ (Fig. 12b). Among the three

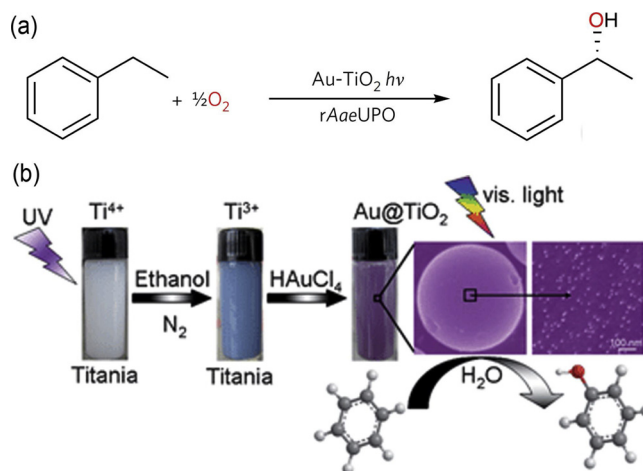


Fig. 12. (a) Reaction scheme of the photoenzymatic hydroxylation of ethyl benzene [223]. (b) Schematic presentation for the synthesis of noble-metal@TiO₂-microspheres [225]. Reprinted with permission.

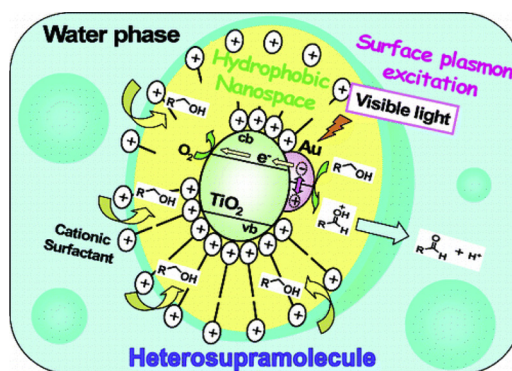
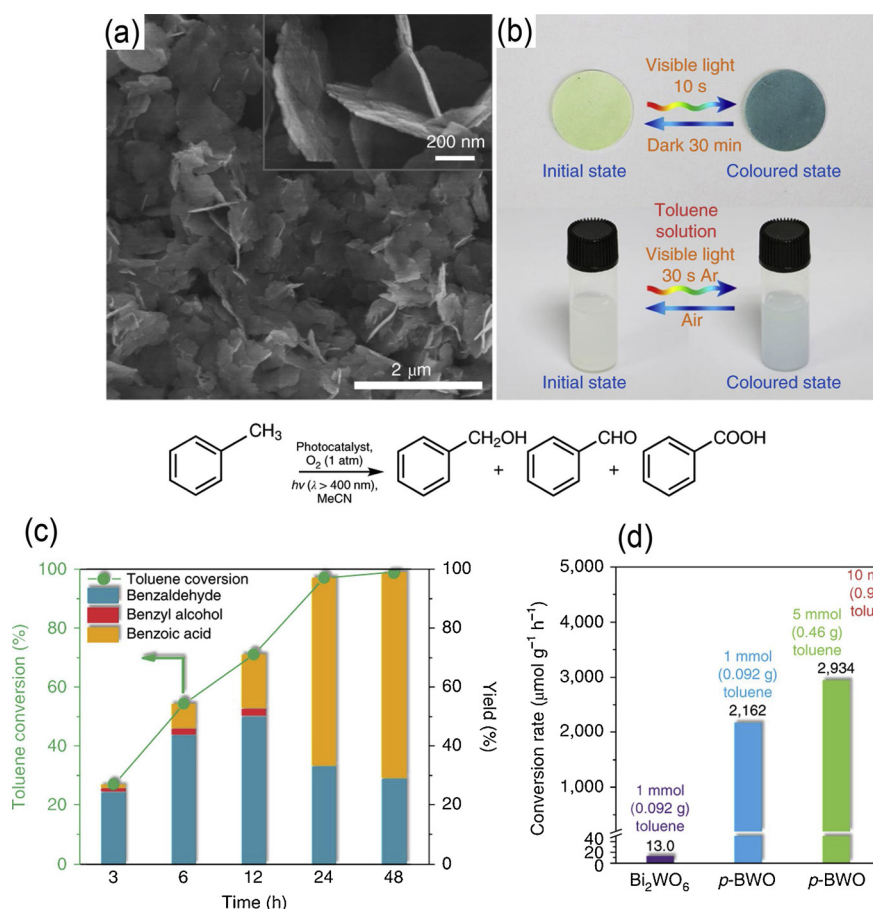


Fig. 13. Schematic illustration of the self-assembled heterosupramolecular visible light photocatalyst [226]. Reprinted with permission.



catalysts synthesized, Au/TiO₂ demonstrated the highest catalytic activity for visible-light hydroxylation of benzene in the aqueous phase. The selectivity of the reaction can reach 91% with the phenol yield of 63%.

Tada et al. [226] found that the oxidation of alcohols into carbonyl compounds in aqueous phase could be effectively catalyzed by the addition of trimethyl octadecyl ammonium chloride (C₁₈TAC) in the system of Au/TiO₂ under visible light irradiation (Fig. 13) with high selectivity (> 99%). Compared with the reaction without surfactant, the addition of cationic surfactant C₁₈TAC to the photocatalytic system with an appropriate concentration leads to the increase of the production yield with a factor of 3.3–5.7 due to the formation of stable micelles as nanoreactors which favor the surface reactions at the strictly confined region. As a result, for some individual alcohol reactants, the yield can be increased by 29.6 times.

Very recently, Li and co-workers [227] reported an application of Bi₂WO_{6-x}/amorphous BiOCl (*p*-BWO) nanosheets for photocatalytic activation of benzylic C–H bonds in toluene via a selective photocatalytic oxidation process. The *p*-BWO nanosheets show distinct appearance of blue color from pristine Bi₂WO₆, with the irradiation of visible light and the presence of atmospheric O₂, as shown in Fig. 14a and b. Structural characterization confirmed that abundant W(VI)O_{6-x} units are presented in the hybrid, which serve as the active sites to rapidly capture and consume the photogenerated electrons, thus effectively favoring the separation of electron–hole pairs. Due to this unique advantage, *p*-BWO nanosheets could effectively activate C(sp³)–H bonds in photocatalytic oxidation of toluene, which is a challengeable and significant reaction in chemical synthesis. This catalyst demonstrated a remarkable enhancement in performance for the photocatalytic oxidation of toluene to produce benzaldehyde and benzoic acid with high selectivity. The highest conversion rate reached 2162 μmol g⁻¹ h⁻¹, which is 166 times higher than that using pristine

Bi₂WO₆ nanosheet (Fig. 14c and d).

Alloy NPs of noble metals with strong visible light absorption are capable of effectively increasing the conversion of several reactions, including Suzuki–Miyaura cross-coupling, oxidation addition of benzyl amine, selective oxidation of aromatic alcohols, and phenol oxidation. The reaction of oxygen oxidation of benzyl alcohol catalyzed by Au–Pd/ZrO₂ [228,229] or Au–Cu/TiO₂ [230] can be further improved by visible or solar irradiation. For Au–Pd/ZrO₂ system, the distribution of Pd active sites and the heterogeneity of electrons around the NP surface are determined by the molar ratio of Au–Pd, playing a critical role in catalysis. Further study reveals that Au–Pd alloy can also drive the

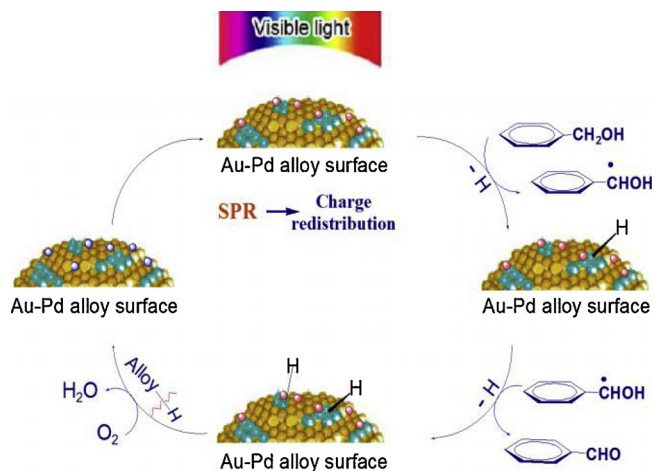


Fig. 15. Aromatic alcohol oxidation over Au–Pd alloy NPs under visible light irradiation [229]. Reprinted with permission.

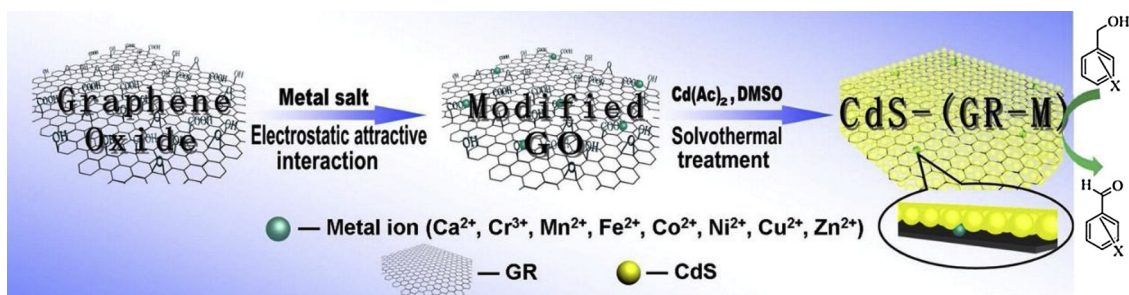


Fig. 16. Schematic illustration of the fabrication of CdS-(GR-M) ($M = \text{Ca}^{2+}, \text{Cr}^{3+}, \text{Mn}^{2+}, \text{Fe}^{2+}, \text{Co}^{2+}, \text{Ni}^{2+}, \text{Cu}^{2+}, \text{and Zn}^{2+}$) nanocomposites in which metal ions are introduced to the interfacial layer matrix between GR and semiconductor CdS [233]. Reprinted with permission.

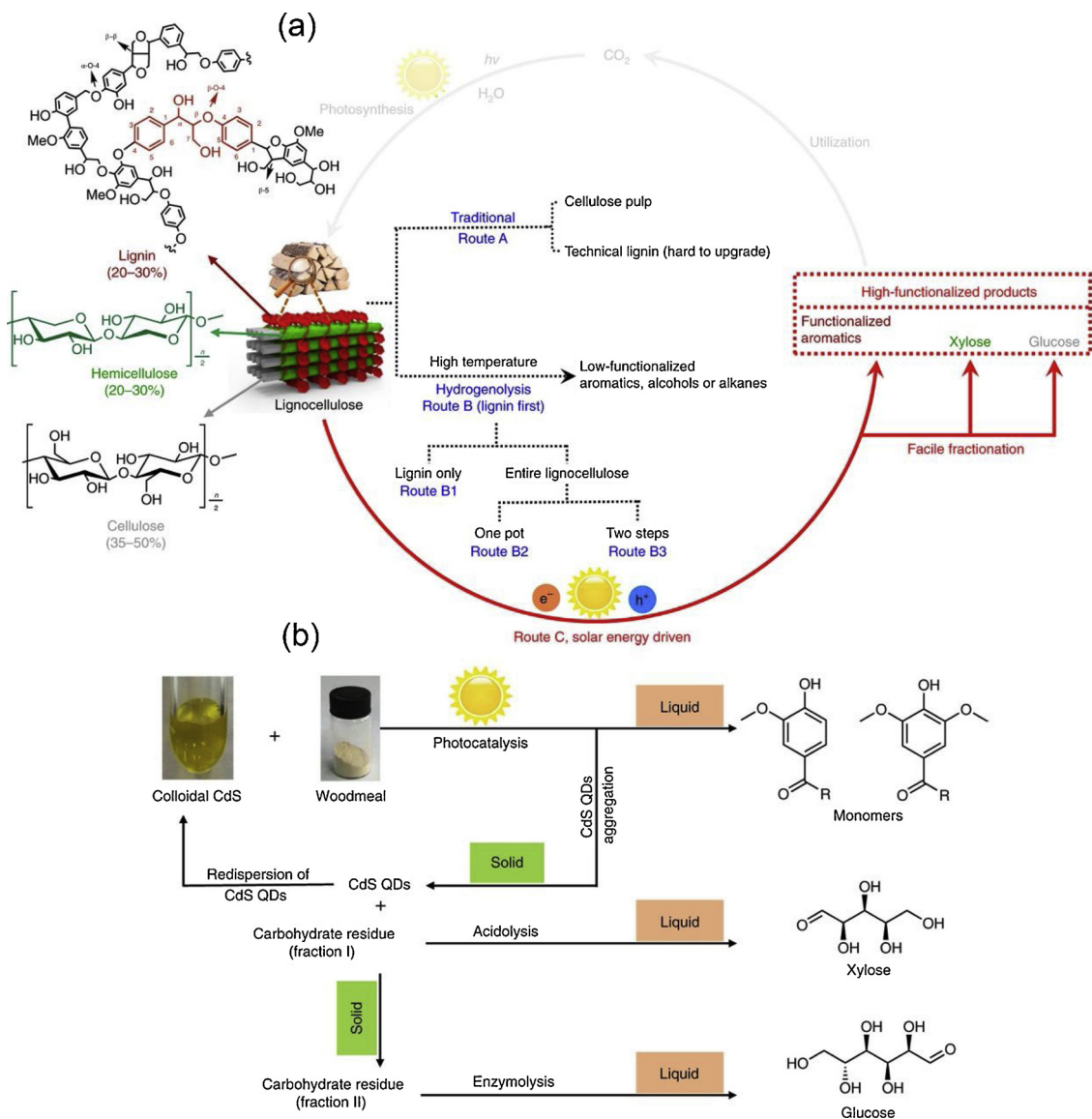


Fig. 17. (a) Schematic illustration of the routes to fragment β -O-4 linkage for conversion of lignin. Route A, traditional biorefinery process forming cellulose pulp and technical lignin. Route B, lignin-first approach with high-temperature hydrogenolysis upon a conventional thermal catalysis process using supported metal catalyst. Route C, lignin-first approach with solar energy-driven photocatalytic process under mild conditions. (b) Scheme of the light-driven lignin-first valorization of birch woodmeal using CdS QDs as photocatalyst [237]. Reprinted with permission.

dissociation of α -H from aromatic alcohols under visible light irradiation, favoring the oxidation reaction in a mild condition instead of high temperature and highly concentrated oxygen (Fig. 15) [229].

By introducing a small amount of metal ions ($\text{Ca}^{2+}, \text{Cr}^{3+}, \text{Mn}^{2+}, \text{Fe}^{2+}, \text{Co}^{2+}, \text{Ni}^{2+}, \text{Cu}^{2+}, \text{and Zn}^{2+}$) in to CdS (see Fig. 16), the mobility

of photogenerated carriers at the interface between GR and CdS semiconductor can be largely enhanced [231]. This simple design can significantly improve the efficiency of selective photo-oxidation-reduction reactions under visible light, including aerobic oxidation of alcohols and anaerobic reduction of nitro compounds. It also favors the

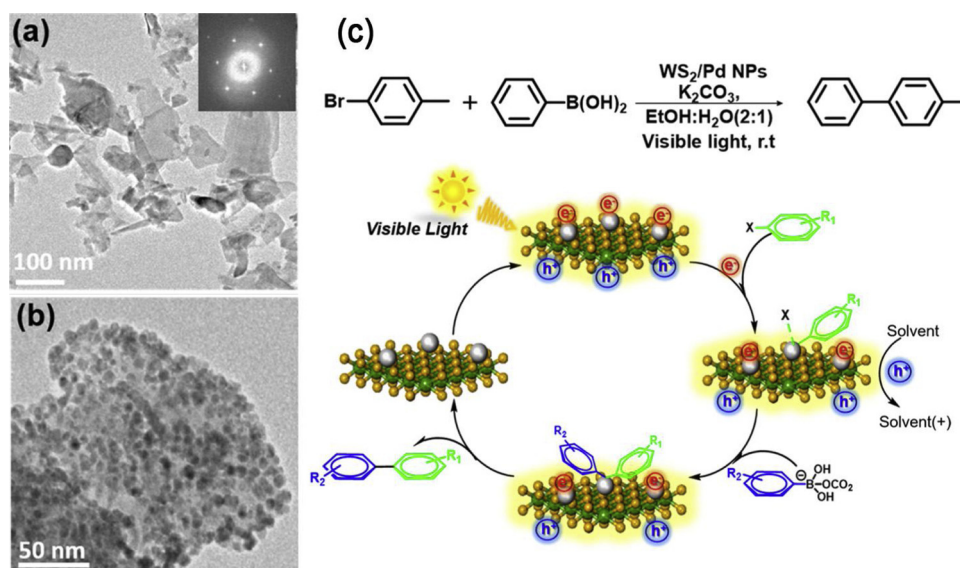


Fig. 18. (a, b) TEM images of the WS₂/Pd nanohybrids. (c) Photocatalytic Suzuki C–C coupling reaction over WS₂/Pd and proposed reaction mechanism [238]. Reprinted with permission.

suppression the recombination of electron-hole pairs, while retards the negative "shielding effect" caused by the high concentration of GR. Under the same reaction conditions in the presence of CdS-GR (10 wt %) catalyst, the conversion of benzyl alcohol to benzaldehyde after 2 h irradiation was approximately twice higher than that obtained using CdS with 5 wt % GR as catalyst [231,232]. A series of CdS-GR nanocomposites with different weight addition ratios of GR was also synthesized by a simple one-step solvothermal method. CdS-GR nanocomposites have been shown to be of high efficiency for selective aerobic oxidation of alcohols and reduction of heavy ion Cr(VI) rather than water. In addition, the photocatalytic activity of CdS-GR nanocomposites can be effectively improved by using solvent stripped GR (SEG) instead of GO as a precursor of GR, which can effectively convert benzyl alcohol to benzaldehyde in water [231–233]. The ternary nanocomposite has been reported to be a more efficient photocatalyst compared to CdS-GR for the selective oxidation of benzyl alcohol to benzaldehyde [234].

Oxidation of CH₄ to methanol with high selectivity has recently been reported by Tang et al. [235] using a Fe species decorated TiO₂ photocatalyst at ambient conditions. The catalyst with an optimal composition demonstrated a 15% conversion rate for CH₄ with an alcohol selectivity of more than 97%, where the methanol selectivity is over 90%. The production of 18 mol of alcohol per mole of iron active site has been achieved in 3 h. Various characterization technique confirm the function of the major iron-containing species—namely, FeOOH and Fe₂O₃, which enhance charge transfer and separation, decrease the overpotential of the reduction reaction and improve selectivity towards methanol over carbon dioxide production. The mechanism of this catalysis was proposed that upon photon absorption, electron / hole pairs are generated on TiO₂ surface. As the CB potential of Fe₂O₃ is lower than that of TiO₂, photogenerated electrons can be then transferred to the CB of Fe₂O₃, leading to the reduction of H₂O₂ to form $\cdot\text{OH}$ radicals. Simultaneously, CH₄ can react with photogenerated holes at the VB of TiO₂ to form methyl radicals (CH₃ \cdot), which then react with the $\cdot\text{OH}$ radicals to form methanol on Fe species.

To increase the sustainability and production of biorefinery, intensive effort has been focused on the efficient utilization of the three components of lignocellulose from biomass, in which lignin is believed to be the most abundant source of renewable aromatics. However, challenge still exists in the direct transformation of native lignin from biomass. For example, conventional approaches, such as Kraft and Organosolv processes, usually involve the fractionation of

lignocellulose, which can cause transformation of lignin structure. In particular, the condensation to form more C–C linkages by consuming β -O-4 bonds, inducing the inactivation of the extracted lignin [236]. Very recently, a more advanced achievement of the heterogenous photocatalytic selective organic oxidation has been reported. The concept is based on the selective fractionation / oxidation of cheap biomass (macromolecules or polymer composite) to form valuable organic products. A report from Wang et al. demonstrates a lignin-first strategy based on solar energy-driven β -O-4 ether bond cleavage under mild conditions using CdS quantum dots (QDs) as the photocatalyst (see Fig. 17) [237]. The distinct advantage of CdS QDs is their high selectivity in this reaction without segmenting other bonds, thus the functional groups of lignin compounds can be secured. More importantly, upon the photocatalytic process using CdS QDs, native lignin compounds in birch woodmeal can be directly converted into functionalized monomeric aromatics with a yield of 27 wt%, which reaches 84% of the theoretical maximum calculated from the cleavage of the β -O-4 linkages. A new electron-hole coupled (EHCO) mechanism has been proposed for the precisely cleaving the C–O (β -O-4). In principle, the C $_{\alpha}$ –H bond is first fragmented upon oxidation by holes, forming C $_{\alpha}$ radical intermediate, which greatly decreases the bond dissociation energy (BDE) of the β -O-4 bond. Therefore, upon the photo-excitation of CdS QDs, β -O-4 bond breaking is promoted by the C $_{\alpha}$ radicals. The remarkably reduced BDE of β -O-4 bond in the C $_{\alpha}$ radical intermediate is the dominating factor, leading to the high activity and selectivity of the lignin transformation. After reaction, CdS QDs can be facily separated by forming aggregates upon an addition of acetone into the liquid.

2.2.2. Carbon-carbon bond formation (C–C coupling)

Kim et al. [238] reported a hybrid structure composed of Pd NPs on exfoliated 2H-WS₂ nanosheets (WS₂/Pd). This catalyst demonstrated extraordinarily high photocatalytic activity in Suzuki reactions for C–C coupling under visible light (Fig. 18). The photocatalytic activity of the WS₂/Pd showed size-dependence on Pd NPs. The increase of Pd NP size on WS₂/Pd hybrid led to the enhancement of photocatalytic activity in Suzuki reactions at room temperature. Moreover, the protic organic solvents also affected the catalysis, which can activate WS₂/PdN catalysts in photocatalyzed Suzuki reactions; whereas they had been considered less active compared with the polar aprotic ones in conventional Suzuki reactions. A plausible mechanism suggested that photogenerated holes can be transferred to the protic organic solvents, while the photogenerated electrons are transferred to Pd NPs, which

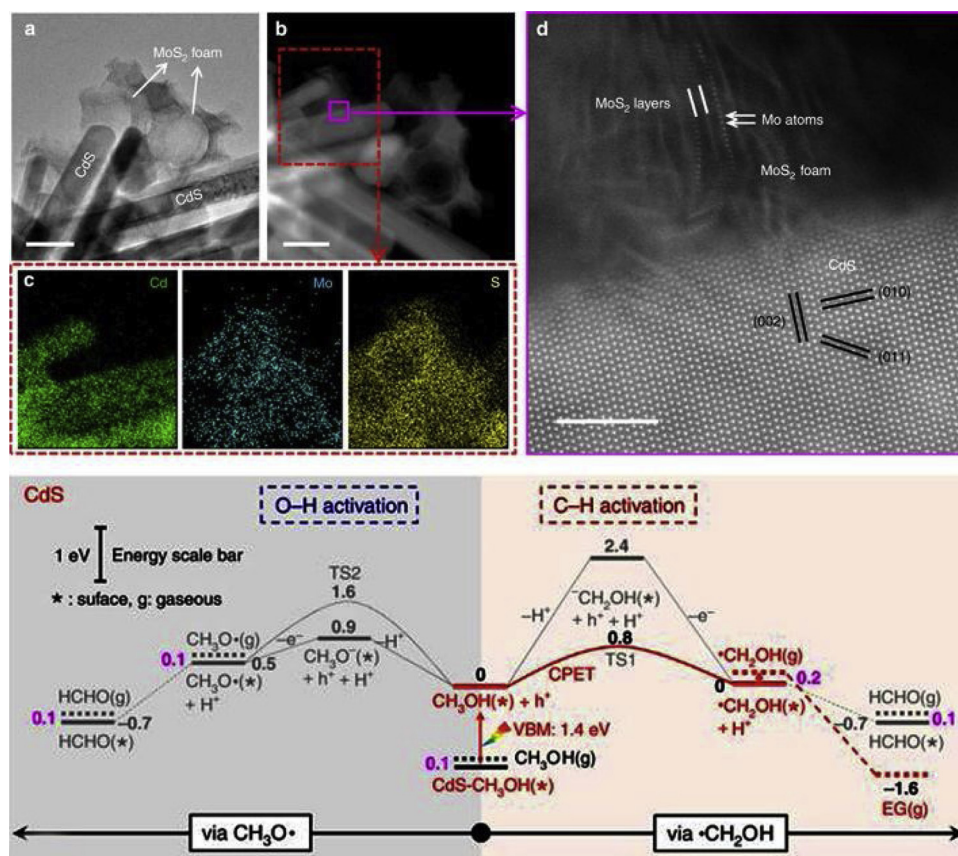


Fig. 19. (Upper) TEM and HR-TEM images of the CdS-MoS₂ catalyst and corresponding elemental distribution. (Lower) Schematic illustration of reaction energy profiles via $\cdot\text{CH}_2\text{OH}$ and $\text{CH}_3\text{O}\cdot$ on CdS(100) [239]. Reprinted with permission.

favor the efficient electron / hole separation. This charge transfer process endows the electron-enrichment on Pt NPs and accelerates the oxidative addition of aryl halides reactions. Xie et al. [239] report the visible-light-driven dehydrogenative coupling of methanol into ethylene glycol, using CdS NPs (TEM images in Fig. 19) as the heterogeneous catalyst and methanol as the raw material under a mild condition. Conversion ratio of ethylene glycol over CdS nanorod catalyst modified by MoS₂ nano-foam reached 90% with high selectivity. Mechanism study indicates that the activation of C–H bond rather than O–H bond in CH₃OH by photogenerated holes on CdS through a concerted PET (CPET) process results in the generation of the hydroxymethyl ($\cdot\text{CH}_2\text{OH}$) intermediate on CdS surface, and the weak adsorption of CH₃OH and $\cdot\text{CH}_2\text{OH}$ radical enables them to be readily desorbed from CdS surfaces for subsequent C–C coupling to form EG. Additionally, the MoS₂ nano-foam with rich edge position is highly beneficial to the reaction efficiency. The reaction selectivity of EG has also been increased by the enrichment of mesoporous MoS₂ nano-foam.

Wang et al. [162] reported a unique truncated tetragonal bipyramidal bismuth vanadate (BiVO₄, BVO) single crystal structure, with tuneable {010} and {110} facets, for photocatalytic C–C coupling of formaldehyde into EG under visible light. Chloride anions were used to control the growth of the single crystals as well as the ratio of exposed {010} and {110} facets. The BVO with the facet ratio of 1 : 1 allows the highest conversion yield of C2 compound. Pt@MoO and MoO NPs were loaded to the two facets of the BVO, respectively, which further enhanced the conversion ratio (Fig. 20). This greatly increased property is attributed to the unique architecture, where photo-charge separation can be largely accelerated by the Pt and MnO_x NPs, while the HCHO coupling may be catalyzed at the MoO_x shell via a redox process.

2.2.3. Esterification and epoxidation

Using alkyl alcohol as the reactant, ester has been synthesized via a heterogeneous photocatalytic approach [240]. With H₁₄[NaP₅W₃₀O₁₁₀] loaded silica as catalyst, Fatemeh and co-workers successfully demonstrated the esterification of salicylic acid with fatty alcohol and benzyl alcohol. When the reaction time is 3 h and the starting molar ratio of acid to alcohol is 1:5, the yield of ester reaches 85%.

Zhu and Sarina [241] reported the photocatalyzed selective epoxidation of alkenes using TiN supported Cu NPs (Cu@TiN) as the photocatalyst (Fig. 21). During photocatalysis, a chemisorb of reactant alkenes on Cu NPs takes place and form Cu-alkene complexes at catalyst surface, which can be activated by photon absorption. The cyclic ether solvent also plays a crucial role, which can facilitate the reaction by reacting with the adsorbed O₂ on Cu NPs under irradiation to produce oxygen adatoms. The activated surface Cu-alkene complexes can then react with the adatoms to form corresponding epoxides. This photocatalyst exhibits excellent activity and selectivity with various types of alkenes for photocatalytic epoxidation. Irradiation wavelength and intensity showed important effect on the epoxidation, indicating that photogenerated electrons of Cu NPs drive the reaction.

Plasmonic photocatalyst has also been applied for visible-light-driven selective epoxidation of organics [242]. Ethylene can be selectively oxidized to ethylene oxide catalyzed by Ag cubes supported on Al₂O₃ with the side length of 60 nm under visible light. At 450 K, the oxidation rate under visible light irradiation is 4 times higher than that in the conventional heat-driven system. The increase of reaction rate is dependent on the temperature, which varies from 8 times at low temperature to 3 times at high temperature, without affecting the selectivity in reaction [243]. Under ambient conditions with visible light, the ZnS-GR nanocomposite exhibited photocatalytic activity for aerobic selective oxidation of alcohol and epoxidation of alkenes. The GR in

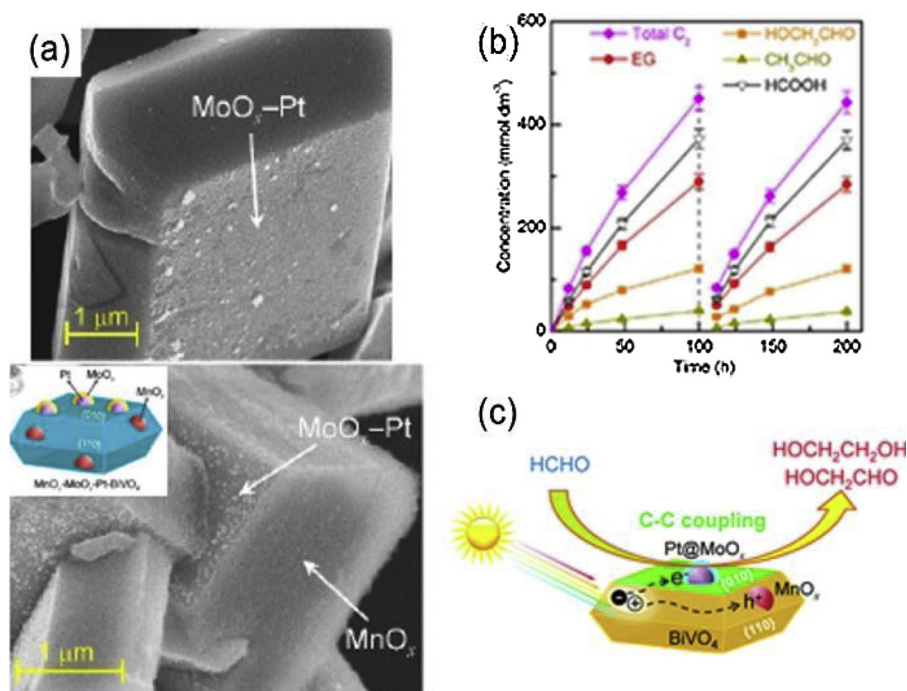


Fig. 20. (a) SEM images of the nanostructure of Pt@MoO₃ on BVO. (b) EG conversion efficiency of the catalysts under visible light irradiation. (c) Proposed mechanism for the photocatalytic synthesis of EG over Pt@MoO₃/BVO [162]. Reprinted with permission.

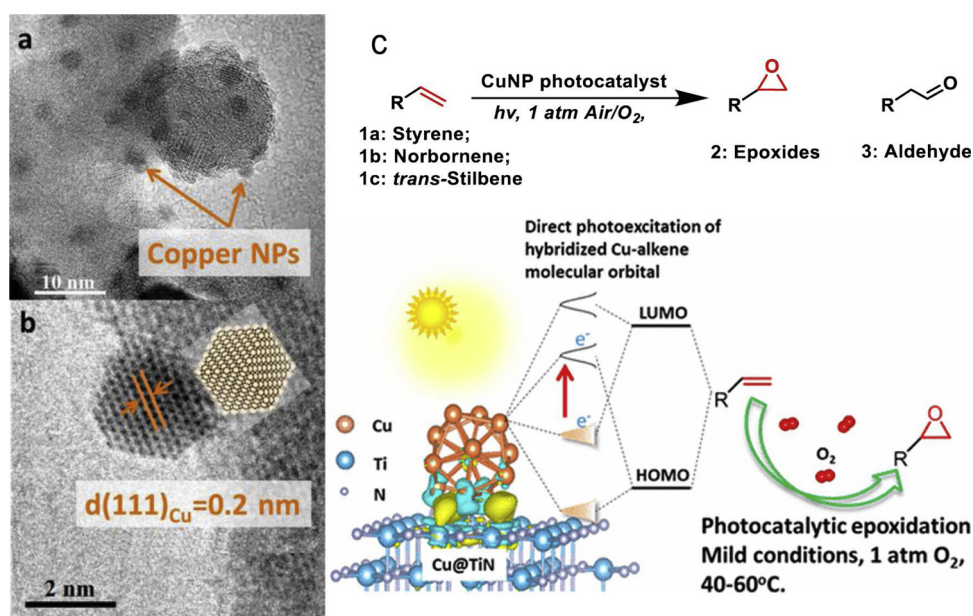


Fig. 21. (a, b) TEM and HR-TEM images of the Cu@TiN catalyst. (c) Schematic illustration of the reaction process of the photocatalytic epoxidation of alkenes using Cu NPs as catalyst [241]. Reprinted with permission.

ZnS-GR works as an organic dye-like macromolecule "photosensitizer" for ZnS rather than an electron reservoir. Cu can also be used as a catalyst for some reactions, but it is rarely used to catalyze epoxidation of alkene as it can be easily oxidized. Linic et al. [244] used Cu NPs with an average size of 41 ± 9 nm attached on SiO₂ (Cu/SiO₂) for catalyzing the epoxidation of propylene. Under visible light irradiation, the selectivity of the reaction is greatly enhanced. The reason is that the localized surface SPR effect of CuNPs weakens the Cu-O bond, thus promoting the reduction of Cu₂O to Cu⁰ and the consequent electron transport.

2.2.4. Carbon-nitrogen bond transform

Photocatalytic N-alkylation of ammonia in alcohol to amines has been studied by Ohtani et al. in an early report, using Pt-TiO₂ as photocatalyst, where Pt plays an important role of the selectivity of the reaction [245]. Secondary amines have also been synthesized using primary amines in alcohols aqueous solution (Fig. 22) [245]. Pt decorated TiO₂ and CdS catalysts showed good activity to synthesize amino acids (e.g. glycine, alanine, serine, aspartic acid, and glutamic acid) in an aqueous solution of ammonia and methane [246–248].

Recently, Střáhal et al. [249] reported the photocatalytic N-alkylation of aniline with Au-TiO₂ as catalyst and primary alcohols as reactant (Fig. 23). The overall selectivity of the mono alkylation and two

$$\begin{array}{l}
 \text{R-NH}_2 \xrightarrow[\text{H}_2\text{O, Ar}]{h\nu, \text{Pt/TiO}_2} \text{R-CHO} + \text{NH}_3 + \text{H}_2 \\
 \text{R-OH} \xrightarrow[\text{Ar}]{h\nu, \text{Pt/TiO}_2} \text{R-CHO} + \text{H}_2 \\
 \text{R-CHO} + \text{R-NH}_2 \xrightarrow[\text{-H}_2\text{O, Ar}]{h\nu, \text{Pt/TiO}_2} \text{R-N=CH-R} \xrightarrow{\text{H}_2, \text{Pt/TiO}_2} \text{R-NH-CH}_2\text{-R} \\
 \text{R-CHO} + \text{NH}_3 \xrightarrow[\text{-H}_2\text{O, Ar}]{h\nu, \text{Pt/TiO}_2} \text{HN=CH-R} \xrightarrow{\text{H}_2, \text{Pt/TiO}_2} \text{H}_2\text{N-CH}_2\text{-R}
 \end{array}$$

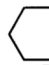
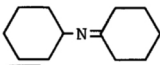
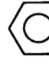
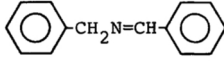
Run	Substrate (RNH ₂) R =	Conversion %	Product/ μmol		
			H ₂	NH ₃	Schiff base
1	CH ₃ CH ₂ CH ₂ -	65	42	13	CH ₃ (CH ₂) ₂ N=CHCH ₂ CH ₃ 40
2	(CH ₃) ₂ CH-	49	40	13	(CH ₃) ₂ CHN=C(CH ₃) ₂ 30
3 ^{b)}	CH ₃ CH ₂ CH ₂ -	46	57	16	CH ₃ (CH ₂) ₂ N=CHCH ₂ CH ₃ 20
	(CH ₃) ₂ CH-	44			(CH ₃) ₂ CHN=C(CH ₃) ₂ 3
					CH ₃ (CH ₂) ₂ N=C(CH ₃) ₂ 16
					(CH ₃) ₂ CHN=CHCH ₂ CH ₃ 18
4	CH ₃ (CH ₂) ₅ -	46	25	16	CH ₃ (CH ₂) ₅ N=CH(CH ₂) ₄ CH ₃ 32
5		31	18	14	 7
6		≈ 100	44	25	 41

Fig. 22. Scheme of reactions of synthesis secondary amines using primary amines as starting materials upon Pt/TiO₂ photocatalyst, and a summary of the products (chart) [245]. Reprinted with permission.

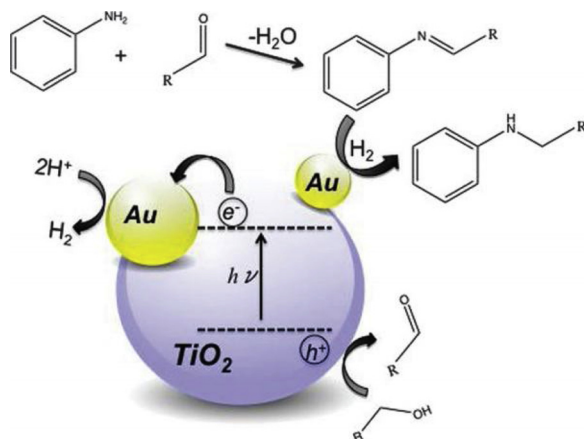


Fig. 23. Proposed reaction mechanism for the photo-alkylation of aniline over Au-TiO₂ [249]. Reprinted with permission.

alkylation products is always higher than 70%, and depends on the alkyl alcohol used. It is proposed that the reaction is triggered by the oxidation of the primary alcohol to the corresponding aldehyde through the R-O[•] or OH[•] radical intermediates by the photo-generated holes of TiO₂. The photo-generated electrons transferred to the Au surface reduce the resultant protons to molecular hydrogen, which subsequently react with the aldehyde to accomplish the alkylation. TiO₂/magnetite-silica nanocomposite as a photocatalyst has also been reported for the selective oxidation of benzyl alcohol to benzaldehyde. When the conversion of benzyl alcohol is about 50%, the unprecedented selectivity of benzaldehyde in organic medium reaches 90% [250].

Nitroaromatic compound (e.g. 4-nitrophenol (4-NP)) can be reduced onto corresponding aminoaromatic (e.g. 4-aminophenol (4-AP)) in the presence of Au or Pt catalyst with NaBH₄ as the reducing agent [251–253]. A recent study from Ma's group [254] showed that the reaction rate of this reduction process can be further increased under photo-irradiation using a Au-TiO₂ catalyst. As illustrated in Fig. 24, it is proposed that under UV light, Au works as electron sink to accept the photo excited electrons from the CB of TiO₂. The electrons are then injected into the LUMO of the 4-NP for reduction. Meanwhile, the high electron density on Au favors the formation of hydrogen or Au-H species on Au surface for more efficient hydrogenation to 4-NP. On the other hand, under visible light, a hot-electron mechanism plays dominant role for reaction rate enhancement. Due to the SPR effect of Au, hot electrons were injected to CB of TiO₂, which can be further transferred to the LUMO of 4-NP for reduction to 4-AP.

Nitrobenzene can be transferred to imines upon the photocatalytic process using TiO₂ as the photocatalyst and alcohol as dispersant (Fig. 25). This reaction showed high selectivity for the cases using C1–C3 alcohols [255]. It has shown that surface properties of the TiO₂ exerts important effect on selectivity [256]. Anatase structure with a much higher Lewis acidity than rutile one can favor imine formation, while Rutile exhibited a higher selectivity for the formation of aromatic amino compound. Pt/TiO₂ [257] and Au/CeO₂ [258,259] are able to promote photocatalytic azobenzene reduction using alcohol as a sacrificial electron and proton donor. Very recently, Shiraishi et al. [260] reported that the photocatalytic hydrogenation of azobenzene to hydrazobenzene on CdS NPs under visible light irradiation reached the selectivity more than 95%.

Homoallyl amines can be obtained using olefins and trisubstituted imines as reactants and CdS based materials as photocatalyst. Shiraishi

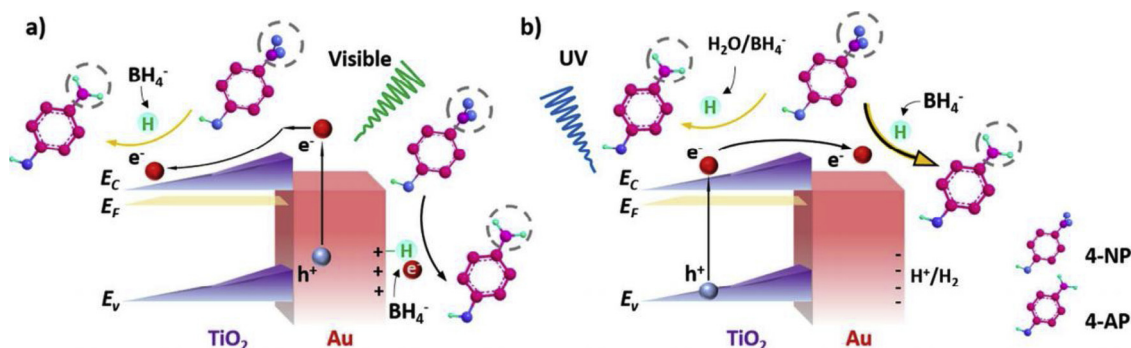


Fig. 24. Schematic illustration of the photocatalysis promoted 4-NP reduction into 4-AP under visible (a) and UV light (b) irradiation [254].

et al. [261] showed the study of photocatalytic cyclisation reactions, where benzimidazoles were synthesized using 1,2-diaminobenzene in the presence of Pt–TiO₂ photocatalysts in alcohol solution. Using nitroaromatic compounds in alcohols as the starting materials, Hakki et al. [262] reported the photocatalytic formation of polyalkylated quinolines over TiO₂ decorated with acid modified mesoporous SiO₂ catalyst (Fig. 26). In this reaction, nitro compound reduction and the alcohol oxidation are proceeded simultaneously upon the photo-generated electrons and holes, respectively. An imine is then produced upon condensation of the generated aldehyde and amino compounds. The surface attached arene–SO₃H acid group strongly affected the selectivity of the products and production yield of the quinolines.

Morpholine derivatives are important substance for pharmacological study. Plasmonic photocatalysts can be used to catalyze the oxidative condensation of aldehydes and morpholine under visible light irradiation. Luque group [263] found that in the presence of H₂O₂ and strong alkali KOH, under 532 nm laser irradiation with Au/SiO₂ as photocatalyst, amides can be synthesized by the reaction of morpholine with benzaldehyde. MOFs have also been used for imine formation from amines. Li et al. [185] reported a visible light assisted aerobic photocatalytic oxidation of amine to imines over NH₂-NIL-125(Ti), where the photo-generated Ti³⁺ and O₂^{•−} formed through the reaction between Ti³⁺ and O₂ promoted this organic transformation.

Unsupported Ru NPs have also been used as photocatalyst to direct aminate octanol and other alcohols into primary amines in the presence of ammonia (Fig. 27) [264]. Octylamine was obtained at a lower reaction rate using small Ru NPs (~ 2 nm) with the selectivity of ~ 90% and conversion ratio of 92%; whereas for larger Ru NPs and supported NPs, a lower selectivity was observed for the octylamine formation with a conversion decreased to 70–80%. The primary reaction of alcohol amination into octylamine showed nearly structure-insensitive reaction, as all Ru NPs presented comparable turnover frequency values. The self-coupling of octylamine was sensitive to the NP size. Amine self-coupling is inhibited upon small NPs, which can be attributed to the structural and electronic effects during hydrogenation of the secondary imine.

2.2.5. Factors affecting products

Although value-added organics can be “one-pot” synthesized using heterogenous photocatalytic process from simpler starting materials, which bears the distinct advantages of mild reaction conditions, less energy consumption and environmental-friendly, the challenges exist in

promoting reaction selectivity and reaction rate. The key issue in photocatalytic oxidation reactions is to minimize the mineralisation of products and reactants to achieve good selectivity, thus a suitable catalyst as well as optimal reaction conditions need to be systematically investigated. As aforementioned, there are many impressing factors, such as solvent, catalyst structure and its surface functionality etc., which may present together as combined effect during reaction. We here briefly summarize several possible factors affecting the reaction efficiency and selectivity.

1) Effect of solvent

In reaction, solvent plays the role to disperse and transport reactants to the reaction sites of the catalyst, and also may join the reaction, therefore, solvent features, such as structure and polarity, strongly influences the interaction between the surface of the photocatalyst and the chemicals. By simply varying the solvent, photocatalytic reaction rate can be tuned. A report from Brezova et al. [265] showed that the photocatalytic reduction rates of nitroaromatic compounds in different solvents follow the order as: methanol > ethanol > iso-propanol, because the formation of α -hydroxyalkyl radicals in methanol is more efficient than that in other solvents [266]. Solvents with different properties, such as diffusibility and polarity possess different ability to transport all species during reaction, including reactants, highly active intermediates and products, which exert important impact on electron transfer kinetics, subsequent reaction rates and selectivity [267]. Almquist et al. [268] reported the solvent effect using the reaction of TiO₂ catalyzed oxidation of cyclohexane in various solvents including acetone, isopropanol, dichloromethane, chloroform, carbon tetrachloride, benzene and n-hexane. It was found that selectivity to cyclohexanol, cyclohexanone and reaction rates were influenced by the type of solvent. Non-polar solvents (e.g. hexane and benzene) led to low selectivity with cyclohexanol being completely oxidized to water and CO₂, due to their strong adsorption on catalyst surface. In polar solvents, adsorption of cyclohexanol to the TiO₂ NPs is weaker as the competition for adsorption sites with the solvent, and thus the selectivity is higher. Solvent induced competitive adsorption, to an extent, determines the overall reaction rate and selectivity to cyclohexanone and cyclohexanol. Dichloromethane allowed the highest reaction rate; by contrast, chloroform and isopropanol dramatically inhibited the desired reactions. The optimal solvent for this reaction with high selectivity is the one that can minimize product adsorption on catalyst

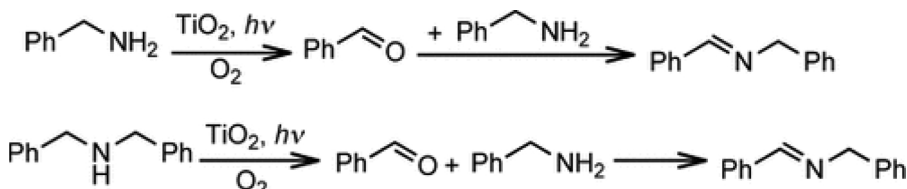


Fig. 25. Photocatalytic formation of imines using TiO₂ as catalyst and nitrobenzene as reactant [255]. Reprinted with permission.

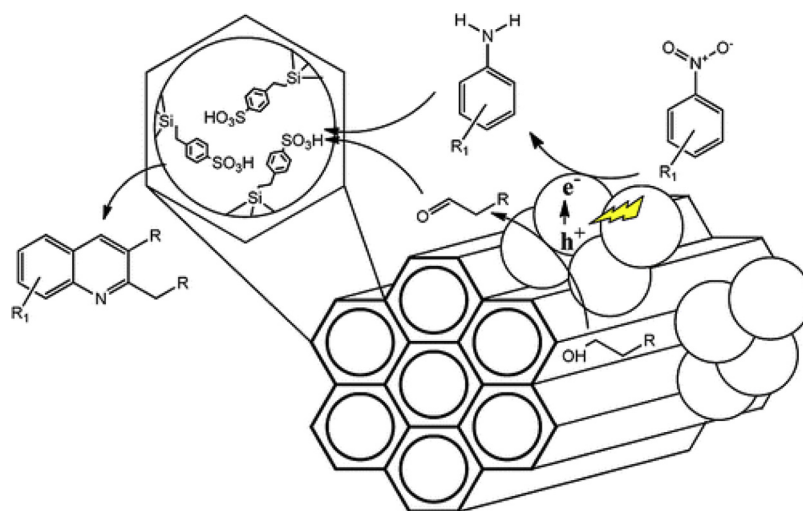


Fig. 26. Schematic illustration of quinolines synthesis from nitroaromatic compounds and alcohols using arenesulfonic acid functionalized $\text{SiO}_2\text{-TiO}_2$ photocatalyst [262]. Reprinted with permission.

and improve reactant adsorption on catalyst surface. Colmenares et al. [250] also reported the similar phenomenon, where photocatalytic oxidation of benzyl alcohol to benzaldehyde in acetonitrile demonstrated better selectivity than that in aqueous medium. Soana et al. [269] reported the effect of an organic solvent to slow down the reaction and improve selectivity.

Water is a good “green” solvent for heterogenous photocatalytic reactions, it is of high polarity and can easily interact with the surface of the photocatalysts to react with photo-generated holes to form strong oxidizing radical of -OH^\bullet , thus resulting in a difficult control to the oxidation extent and hence inducing a poor selectivity. Therefore, polar organic solvents (e.g. the alcohols introduced above, dimethyl carbonate [270] and acetonitrile) or their mixtures are most often employed as dispersant for photocatalytic organic synthesis. For instance, acetonitrile has been used as solvent in many photocatalytic organic syntheses, including oxidation of liquid cyclohexane [271], benzyl alcohol [250], naphthalene [272], primary aliphatic amines [273], and epoxidation of propylene with high selectivity [244], as it is a stable solvent which usually cannot be oxidized by the photogenerated holes. The pH value of the solution also affects the dissociation of the reactant as well as their adsorption on catalyst surface. For example, Zhu et al. [274] reported an efficient photocatalysis to selectively oxidize 5-hydroxymethylfurfural (HMF) to 2,5-furandicarboxylic acid (FDCA) under mild conditions using O_2 in air as the oxidant and g- C_3N_4 supported cobalt thiophorpyrazine (CoPz) as photocatalyst. This reaction showed pH dependence of the solution, where the FDCA can be achieved with a

yield of 96.1% in an aqueous solution at pH = 9.18, while at lower pH (4.01), the main product is 2,5-diformylfuran.

1) Effect of catalyst surface feature:

In heterogenous photocatalytic organic synthesis, reaction is proceeded following two major steps [12,13,24]. The 1st step is the adsorption/dissociate process, where reactants adsorbed on catalyst surface; the 2nd step is the desorption process, where products leave the catalyst surface. Therefore, strong adsorption between organics and catalysts (mainly semiconductors) usually induce high reaction rate, however it may lead to the mineralisation with CO_2 and water as the final products. A rational design to the catalyst surface, such as specific functional groups, can result in a suitable and preferential adsorption, and thus increases the selectivity of the reaction.

Hakki et al. [262] reported that the formation of polyalkylated quinolines via a cyclization using nitroaromatic compounds as reactants reaches a selectivity up to 53% catalyzed by arene- SO_3H acid group functionalized mesoporous $\text{SiO}_2\text{-TiO}_2$ hybrid, whereas this value is only 6% for pure TiO_2 , and 18% for $\text{SiO}_2\text{-TiO}_2$. Notestein et al. [275] designed a novel catalyst with nanocavities constructed by depositing a shape-selective sieving layer of Al_2O_3 on an oxide (TiO_2) catalyst surface, which bears high selectivity for both reduction and oxidation reactions as shown in Fig. 28. Nitrobenzene and benzyl alcohol can be photocatalytically reduced and oxidized into their corresponding products with selectivity up to 90%, respectively, while no reaction was

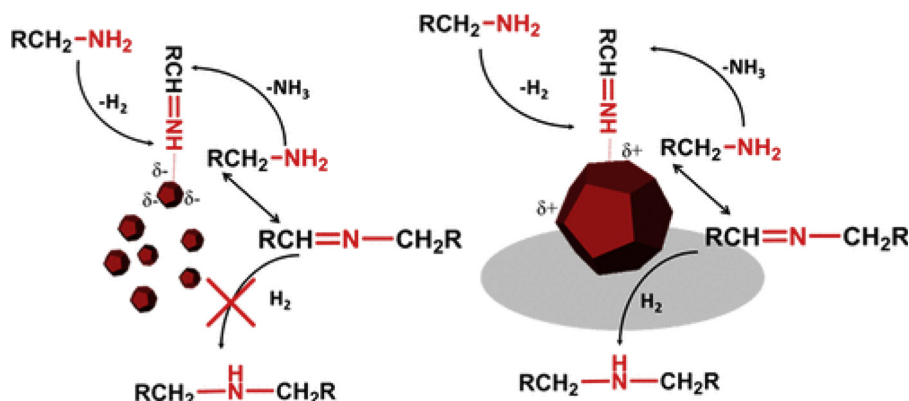


Fig. 27. Ru NP size (left: small and unsupported NPs) and support effect (right: large and supported NPs) on self-coupling of primary amines [264]. Reprinted with permission.

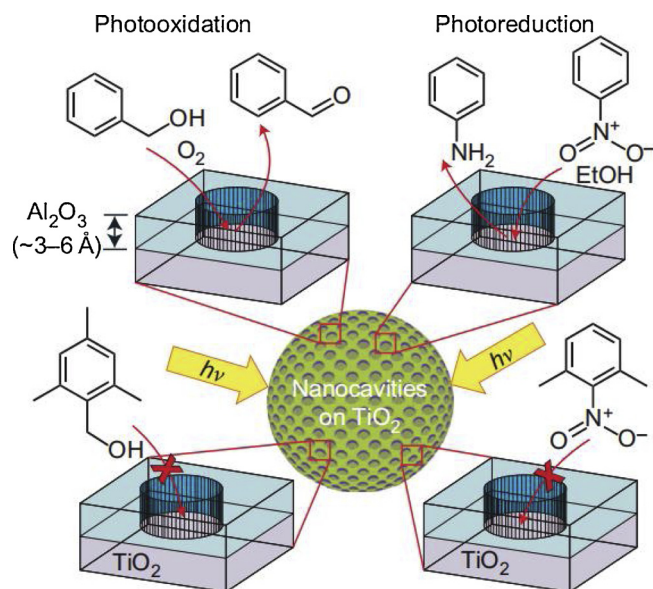


Fig. 28. Schematic illustration of selective photocatalytic oxidations and reductions of mixtures over templated nanocavities [275]. Reprinted with permission.

taken place for the ortho methylated derivatives. The excellent selectivity is resulted from the size-sieving effect induced adsorption alignment of reactants to the catalyst surface. Ohtani et al. [276] found the selectivity of photocatalytic synthesis of pyridine 3-carboxylic acid (PCA) from diamines using CdS is higher than that using TiO_2 as photocatalyst. High purity racemic PCA product was obtained in the presence of CdS, whereas for the case using TiO_2 , PCA was produced with an excess of the L-isomer as by-product. The selectivity difference was ascribed to the adsorption difference of the amino group in L-Lys on catalyst surface, which underwent distinct oxidation reactions [277].

1) Effect of incident light wavelength:

The efficiency of charge carrier's generation on photocatalyst is of high importance for photocatalysis, which depends on the energy levels of the semiconductor and the energy of the incident light. By varying the wavelength of the incident light, the process for photogeneration of electron-hole pairs may be tuned to favor the selectivity and reaction rate for the organic transformations.

For example, as shown in Fig. 29, under visible light irradiation

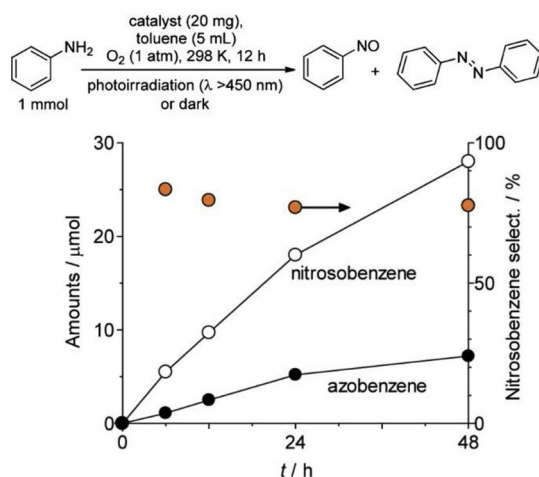


Fig. 29. Amount of products and nitrobenzene selectivity during photocatalytic reaction of aniline using Pt/P25 and proposed mechanism of selective oxidation of aniline on Pt/P25 under visible light irradiation [278]. Reprinted with permission.

($\lambda > 450$ nm), Pt NP decorated P25 (Pt/P25 catalyst) favored selective aerobic oxidation of aniline to form nitrosobenzene as the main product (selectivity: 90%) [278]. By contrast, under UV irradiation azobenzene turned be the major product. It is proposed that upon visible light absorption, an inter-band electronic excitation of Pt atoms takes place, which promotes the electrons to be transferred to the CB of TiO_2 , followed by the formation of $\text{O}_2^{\cdot-}$ radicals on Pt surface. The $\text{O}_2^{\cdot-}$ radicals are highly active to attract the H atoms from aniline upon its dissociation on Pt NPs, producing hydroperoxide species. The following reaction between anilino anion and hydroperoxide species results in the formation of nitrosobenzene.

Pt/ TiO_2 photocatalyst has also been used to catalyze aromatic ring hydroxylation of benzene derivatives when illuminated with light of appropriate wavelength, in the presence of water as oxidant [279]. It was observed that under irradiation with 365 ± 20 nm light, the selectivity of phenols, produced via photocatalytic hydroxylation of toluene or p-xylene was low; however, the yield and selectivity was significantly increased under 405 ± 20 nm light irradiation (Fig. 30). This wavelength dependant selectivity is attributed to that upon incident light at ~ 405 nm photogenerated charge carriers mainly form at the surface of the catalyst, which are more efficient to participate the hydroxylation reaction than those generated from the deeper area of the catalyst excited under ~ 365 nm light. The lower selectivity at 365 nm was resulted from the retardant of charge separation due to the electron transfer from toluene to TiO_2 upon the absorption of toluene at ~ 360 nm, leading to the generation of benzyl radicals to form dibenzyl.

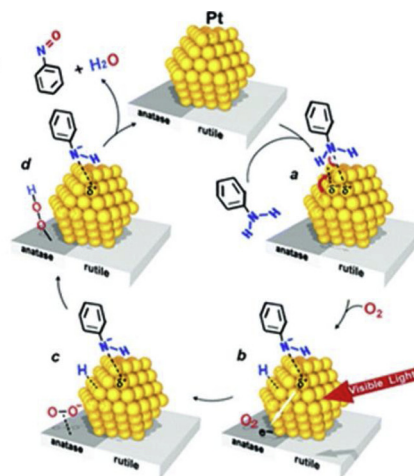
3. Photoresponsive NP initiated radical polymerization

Apart from the photocatalytic synthesis of small organic molecules, we here introduce the advances of heterogenous photocatalytic synthesis of polymers or macromolecules from their monomers, to demonstrate the fundamental achievements including the reaction mechanisms and technical advantages. Compared with CO_2 reduction and organic transform introduced above, this domain is relatively less developed, because it needs more background from polymer chemistry and specific characterization technique of macromolecules, including structure and mechanics analysis, differing from those for small molecules. We choose the free radical polymerization system, as it is the most classic and major topic in polymer research.

3.1. Free radical polymerization

3.1.1. Simple semiconductor system

The use of semiconductors to photo-initiate polymerizations were



Substrate	Catalyst ^b	Irradiation light/nm	Organic products/ μmol				Gas products/ μmol		Total yield ^f / μmol	Conversion ^g (10 ² %)	Phenols selectivity ^h (%) S_{OH}
			Phenols Y_{OH}	Coupling products ^c Y_{C}	Carbonyl products ^d Y_{CHO}	Hydrogenated compounds ^e Y_{HCP}	H ₂	CO ₂ Y_{CO_2}			
Benzene	TiO ₂	All ⁱ	n.d.	n.d.	—	n.d.	2.4	3.1	0.5	0.5	0
	Pt(0.1)/TiO ₂	All ⁱ	8.9	0.4	—	0.4	62	11	12	11	75
	Pt(0.1)/TiO ₂	405 \pm 20 ^j	3.7	0.4	—	0.5	9.4	n.d.	4.7	4.3	76
Toluene	Pt(0.1)/TiO ₂	All ⁱ	11	7.8	0.3	0.5	240	11	29	32	38
	Pt(0.1)/TiO ₂	254 \pm 20 ^j	1.5	0.1	n.d.	n.d.	3.0	n.d.	1.7	1.9	88
	Pt(0.1)/TiO ₂	365 \pm 20 ^j	3.5	1.7	0.1	n.d.	31	n.d.	7.0	7.8	50
	Pt(0.1)/TiO ₂	405 \pm 20 ^j	5.7	1.4	0.1	n.d.	31	n.d.	6.6	7.3	86
	Pt(1)/TiO ₂	405 \pm 20 ^j	6.1	0.1	n.d.	n.d.	7.4	n.d.	6.3	7.0	97
Ethylbenzene	Pt(1)/TiO ₂	405 \pm 20 ^j	3.4	0.3	n.d.	n.d.	6.0	n.d.	3.7	4.1	85
<i>tert</i> -Butylbenzene	Pt(1)/TiO ₂	405 \pm 20 ^j	2.0	n.d.	n.d.	n.d.	6.3	n.d.	1.2	1.3	>99

Fig. 30. Photocatalytic oxidation of benzene and alkylbenzenes by Pt/TiO₂ photocatalysts using incident light with different wavelengths [279]. Reprinted with permission.

first attempted by Markham and Oster et al. [280,281]. Both reported that ZnO NPs can initiate the free radical polymerization of methyl methacrylate (MMA) under UV ($\lambda = 365 \text{ nm}$) irradiation. They also demonstrated that the presence of O₂ adsorbed on ZnO surface is crucial for the reaction, as no catalytic activity could be observed when using ZnO NPs undergone a thermal treatment, where the surface adsorbed O₂ was removed upon heating. However, excess O₂ in solution can inhibit the polymerization, as expected for any radical polymerization. Solvent effect study showed that solvents of higher dielectric constants with good proton-donating or hydrogen-bonding characteristics favor the initiation reaction via the intervention of photo-excited surface O₂. The anionic nature of the excited surface oxygen was evidenced by the fact that the polymerization can proceed readily for electrophilic monomers such as MMA and acrylonitrile, but not for styrene [280]. It was thus proposed that photo-activated oxygen was formed on the surface of ZnO during irradiation and converted into radical anion (such as O₂^{•−}) which could then initiate the polymerization [280,281].

The photo-generation of active species on the semiconductor surface and the following initiating step of photo-radical polymerization were further investigated using quantum sized TiO₂, ZnO and CdS by Hoffman and co-workers [256,282]. The effect of solvent, monomer concentration, NP concentration, light intensity and NP size on polymerization rate were examined. The quantum sized semiconductors exhibited significantly higher quantum yields than their bulk counterparts. Fig. 31a presents the proposed reaction mechanism consisting of the surface reduction of the monomer by the photoexcited electrons present at CB, leading to a radical anion which can initiate the free radical propagation. An alkyl alcohol solvent (such as isopropanol) must also be present in the system. It acts as hole scavenger in order to suppress charge recombination, and the resulting oxidation product can also initiate the polymerization, either directly or via monomer oxidation. The implication of a radical anion as pivotal initiating species was confirmed by the inhibition of the reaction by O₂ or acetonitrile, both of which are not only electron scavengers, but also radical anion scavengers. For the case of the MMA polymerization triggered by ZnO NPs, Hoffman noticed that the reduction potential ($E_{\text{A}}^{\text{red}}$) of MMA (−1.1 V vs NHE) is more negative than the energy of CB (E_{CB}) of ZnO (−0.2 V vs NHE). Thus, MMA should not be reduced by photo-excited electrons. It was proposed that stored electrons with more negative redox potential ($< -2.0 \text{ V}$), and thus potentially able to reduce MMA, may be localized at surface-trap sites or trapped under the form of Zn⁺ ion at the NP surface [283]. Later investigations using annealed ZnO NPs in an unstirred solution pointed toward reaction details which differ from the polymerization in stirred reaction medium with non-annealed ZnO NPs [284]. In the former case, the polymerization reaction takes place preferentially at the NP surface, leading to a polymer-NP composite. Remarkably, unlike PMMA prepared by a conventional

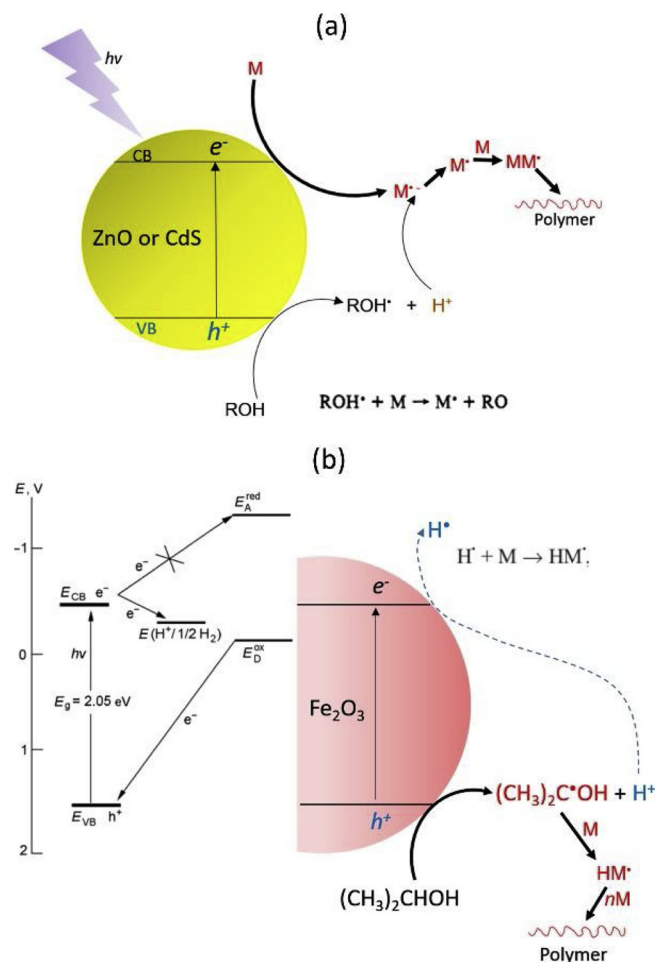


Fig. 31. Schematic illustration of photoinduced MMA and BMA polymerization using ZnO (or CdS) [280,281] (a) and Fe₂O₃ (b) NPs [285], respectively. Reprinted with permission.

thermal radical process, the resulting PMMA product is predominantly syndiotactic with significant crystallinity [284].

A disadvantage of the aforementioned ZnO and CdS NPs is their limited sensitivity to visible light [255,256,282,284,286–289]. The spectral sensitivity range was considerably expanded by using Fe₂O₃ NPs as photoinitiator to polymerize butyl methacrylate (BMA) in isopropanol solution under visible light [285,290]. As illustrated in Fig. 31b, since the $E_{\text{CB}} \approx -0.45 \text{ V}$ (vs NHE) of Fe₂O₃ is less negative than the $E_{\text{A}}^{\text{red}}$ (−1.1 V vs NHE) of BMA monomer, the direct transfer of

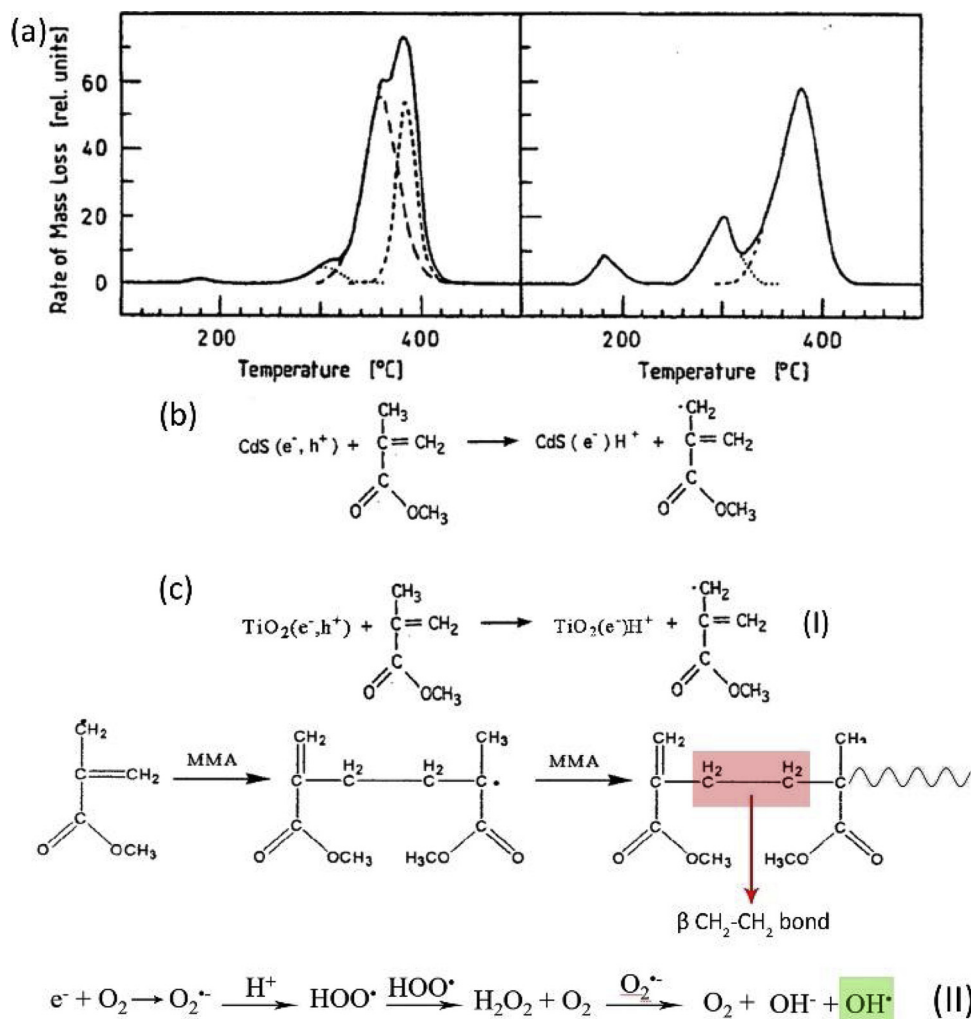


Fig. 32. (a) Deconvolution of the DTG curves of PMMA prepared using CdS (left) and AIBN (right). (b) Scheme of the generation of monomer radical using CdS [285]. (c) Two possible radical generation mechanisms using TiO_2 [291]. Reprinted with permission.

the photoexcited electron from the CB to the monomer is not feasible. However, isopropanol can be oxidized by the holes in the VB, leading to the formation of isopropoxy radicals, as the redox potentials of 2-propanol ($E_D^{\text{ox}} = -0.244$ V vs NHE) is less positive than the energy of VB (E_{VB}) of Fe_2O_3 [285]. Moreover, the protons formed during the oxidation of isopropanol may accept the excited electrons from the Fe_2O_3 CB to form active hydrogen species (noted, for the sake of simplicity as H^{\cdot}) which can further react with BMA or alcohol molecules to generate radical initiating species. Thus, although the direct electron transfer from the CB of the photoinitiator to the monomer molecule is thermodynamically prohibited, the electron and hole generated upon the absorption of light may nevertheless lead to formation of monomer radicals capable of initiating a chain reaction [285].

The photopolymerization of MMA using CdS was reported by Popovic et al. who proposed a different mechanism based on the analysis of the thermal stability of the resulting PMMA [255,286]. Differential thermogravimetry (DTG) results show that the thermal stability of PMMA synthesized with CdS photoinitiator was greater than PMMA thermally prepared with AIBN, but was comparable to PMMA prepared by anionic polymerization. The DTG curves of the CdS initiated PMMA (Fig. 32a left) was composed of four peaks, three of which correspond to radical PMMA prepared with AIBN (Fig. 32a right). The additional peak of the photopolymerized PMMA suggested a CH_2CH_2 segment in β position relative to a vinyl end-group, which is the signature of the initiation process [285]. Therefore, a plausible mechanism (Fig. 32b)

was that the positive hole oxidizes a MMA molecule, leading to the formation of a proton and a very stable acrylic radical stabilized by $-\text{CO}_2\text{Me}$. Addition of a MMA unit on this stable radical leads to the formation of a propagating chain containing the CH_2CH_2 moiety in β position of an unsaturated chain-end. It was suggested that these unsaturated chain-ends are thermally more stable than the conventional unsaturated chain ends arising from radical disproportionation, thus resulting in a photopolymerized PMMA with improved thermal stability [285].

The MMA photo polymerization reaction was performed using TiO_2 NPs as photoinitiator in a non-degassed solution [291]. Using ^1H Nuclear Magnetic Resonance (^1H -NMR) spectroscopy, the polymer was found to contain 6.9% of isotactic, 38.1% of heterotactic and 54.9% syndiotactic triads. Such a microstructure is consistent with a radical PMMA. Interestingly, DTG analysis and theoretical calculations indicate that a fraction of the PMMA chains possess the characteristic CH_2CH_2 moiety β to an unsaturated chain-end (red area in Fig. 32c), implying an initiation mechanism similar to the CdS-MMA system (Fig. 32c, (I)). In this study, due to the presence of dissolved O_2 in the non-degassed liquid medium, $\text{O}_2^{\cdot-}$ species can be formed by electron transfer from the CB of photoexcited TiO_2 to O_2 , which then react with holes to generate the highly reactive OH^{\cdot} radical. These hydroxyl radical are known to initiate MMA radical polymerization (Fig. 32c, (II)), as observed in the case of a conventional MMA polymerization initiated by a redox $\text{Fe}^{2+}/\text{H}_2\text{O}_2$ system. The generation of OH^{\cdot} radicals was detected

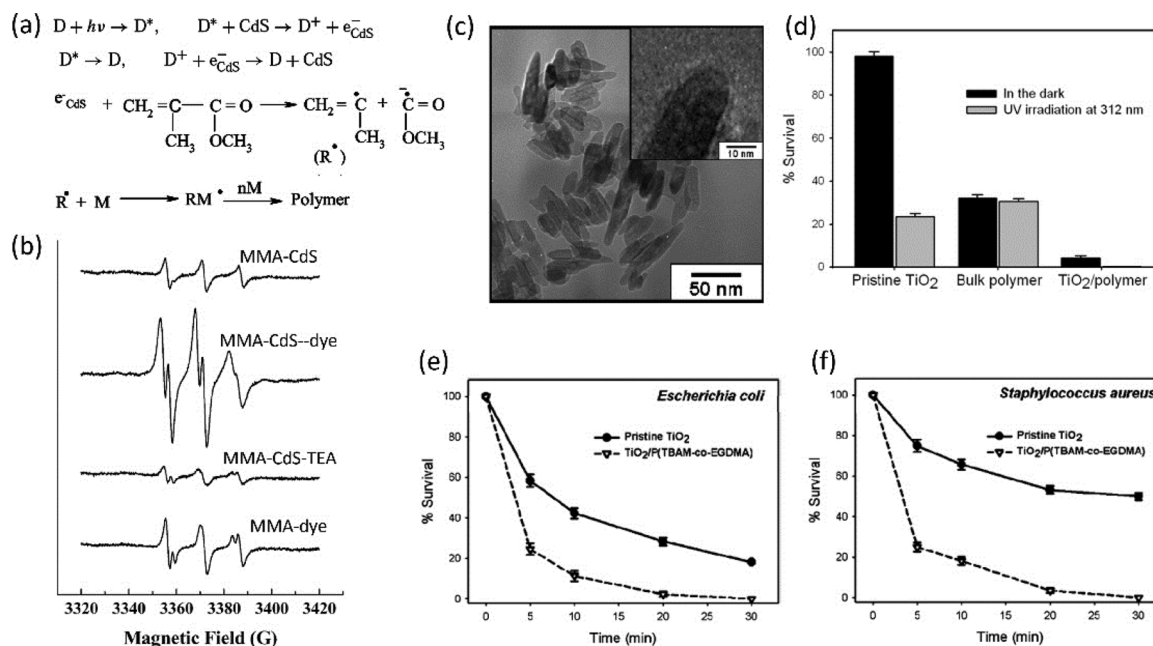


Fig. 33. (a) Scheme of radical generation and chain growth using dye-sensitized CdS. (b) EPR spectra of different semiconductor system [292]. (c) Transmission electron microscopy (TEM) images of the TiO_2 / poly(TBAM-co-EGDMA) core/shell NPs. (d) Bacteria survival (%) after treatment with pristine TiO_2 , bulk poly (TBAM-co-EGDMA), and TiO_2 /poly(TBAM-co-EGDMA) nanoparticles in the presence and the absence of UV light irradiation. Bacteria survival ratio (%) vs. UV-irradiation time on the surface of pristine TiO_2 and TiO_2 /poly(TBAM-co-EGDMA) nanoparticles against (e) *Escherichia coli* and (f) *Staphylococcus aureus* [293]. Reprinted with permission.

experimentally by Electron Spin Resonance (ESR) spectroscopy using dimethyl pyridine N-oxide (DMPO) as spin trap, thus confirming the proposed mechanism where both holes and OH^\cdot radicals work to generate initiating species [291].

The improvement of the semiconductor quantum efficiency is essential to enhance the reaction efficiency [294,295]. After dye sensitization, the oxidation power is measured by the HOMO of the dye, which is usually less powerful as an oxidant than the electron hole [295]. Dye sensitized semiconductors, i.e., CdS and ZnO NPs, demonstrate significantly enhanced activity as initiators in photopolymerization [288,292]. Xanthene dyes in combination with ZnO NPs are able to trigger the photopolymerization of BMA under visible light [288]. Eosin was used to sensitize CdS NPs for the photopolymerization of MMA [292], leading to a higher polymer yield in comparison to the system initiated with CdS NPs alone, or with CdS in combination with triethylamine, NEt_3 . Analysis by ESR spectroscopy confirmed that the CdS + eosin system generated more free radicals than the two other systems (Fig. 33b). The dye sensitized CdS photoinitiator also showed good photostability for a long time because the dye molecules were not photodegraded. It is believed that (Fig. 33a) upon light absorption, an electron transfer occurs between the photoexcited dye (D^*) and the CB of the semiconductor. The electrons in the CB band can then be transferred to the monomer molecules, leading to the formation of an organic radical anion which can initiate polymerization [292]. Carbon doped TiO_2 also demonstrated visible / solar light activity to initiate the polymerization of MMA on NP surface to form PMMA-grafted TiO_2 nanostructure [296]. Compared with non-surface confined PMMA, the photopolymerized PMMA confined at the surface the TiO_2 particle possesses a high thermal stability as shown by TGA analysis. As shown by XRD, it is also crystalline, and its unit cell is unlike the one of syndiotactic PMMA which is obtained by low temperature radical polymerization. Hybrid polymer TiO_2 nanocomposites obtained by photochemical grafting also exhibit interesting properties. For example, the *in-situ* polymerization of amine-containing 2-(*tert*-butylamino)ethyl methacrylate and ethylene glycol dimethacrylate initiated by TiO_2 NPs led to the formation of a core@shell TiO_2 @polymer nanocomposite

which exhibits high antibacterial activity. This antibacterial activity is ascribed to the combined action of the photocatalytic degradation by TiO_2 NPs, the biocidal polymeric amine containing polymer and the antifouling characteristic of the ethylene glycol units (Fig. 33c–f) [293].

Ravoo and coworkers developed a TiO_2 NP photoinitiating system to carry out step-growth polymerization, which can be potentially be used for microcontact printing in a simple, rapid and economic way [297]. This technique took advantage of photoinduced electron / hole charge carriers from semiconductors to induce reduction / oxidation of ethanol amine to initiate its step-growth polymerization. As illustrated in Fig. 34, the photogenerated hole species of TiO_2 oxidized the ethanol amine monomer (or the alcohol groups on the substrate surface) to the corresponding aldehyde, which reacts with another ethanol amine molecule to generate an imine. This imine was finally reduced by the photoexcited electrons of CB to form a secondary amine, leading to the step growth polymerization of ethanol amine. A similar step-growth polymerization was also reported in the synthesis of polypyrrole using TiO_2 -based nanostructures [298].

To increase the initiation efficiency, co-initiators, such as amines can be introduced to the photopolymerization system to promote the generation of free radicals as reported by Yagci *et al.* when using ZnO NPs [5,299]. In degassed water, in the absence of co-initiators, the photopolymerization of acrylamide can be initiated by ZnO alone due to the formation of OH^\cdot radicals from the reaction of H_2O / O_2 with charge carriers (Fig. 35a). However, this reaction is completely inhibited in organic medium. Co-initiators such as tertiary amines (TEA) and iodonium salt ($\text{Ph}_2\text{I}^+\text{PF}_6^-$) can be added to the system to trigger the photopolymerization of MMA in the absence of water. It is proposed that the lone pair on the N atom of TEA reacts with the photogenerated hole to form a radical cation, which can initiate the polymerization (Fig. 35b). In the case of the iodonium salt, a different route is proposed, consisting in the direct reduction of the iodonium salt by the photogenerated electrons, as shown in Fig. 35c. Carboxylic acids can also work as co-initiator in photopolymerization [300,301]. Fe_3O_4 NPs stabilized by lauric acid (LA) ligands (Fig. 36a) are capable of initiating the polymerization of MMA in the absence of any co-initiators, as the

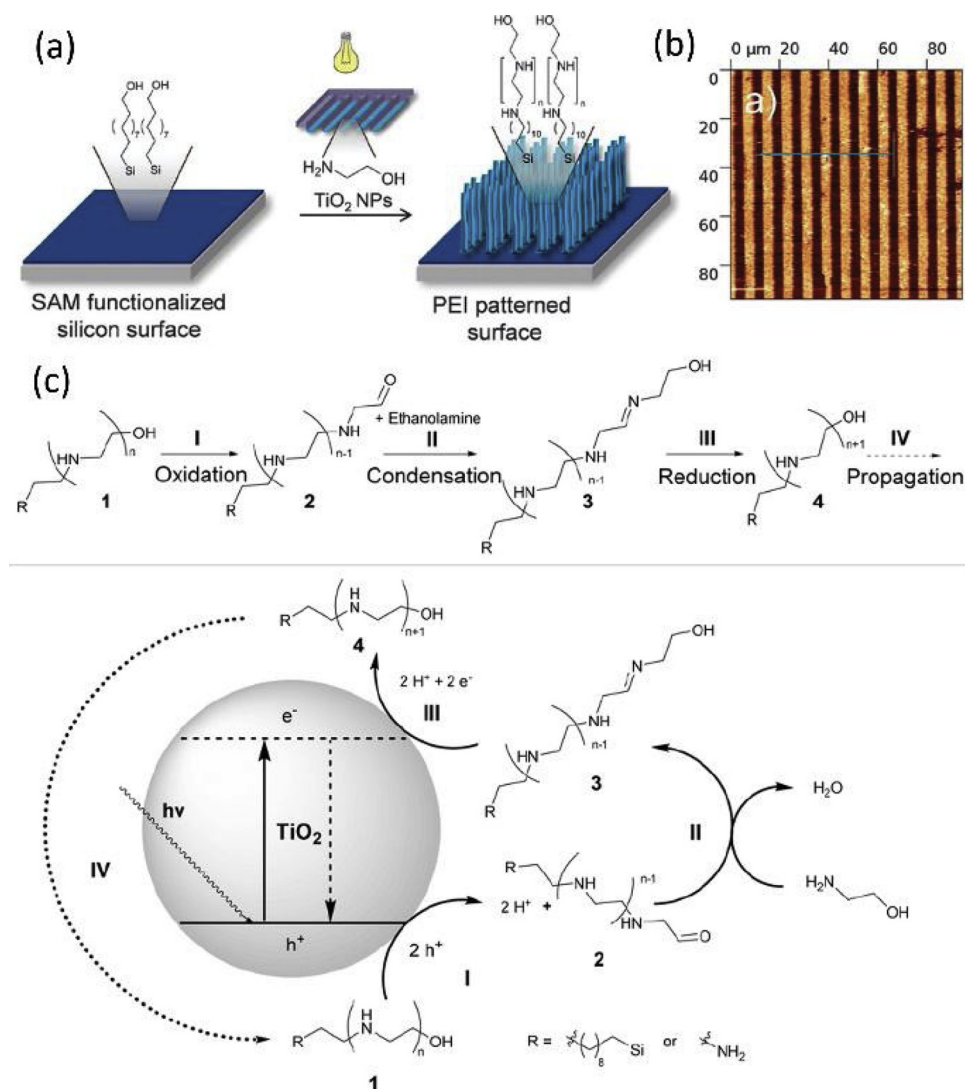


Fig. 34. (a) Scheme of the photocatalytic polymerization by printing of ethanol amine with TiO_2 on a 11-(trichlorosilyl)undecan-1-ol self-assembled monolayer. (b) Atomic force microscope (AFM) image of the patterned PEI brushes. (c) Proposed reaction mechanism of the photocatalytic step-growth of ethanol amine [297]. Reprinted with permission.

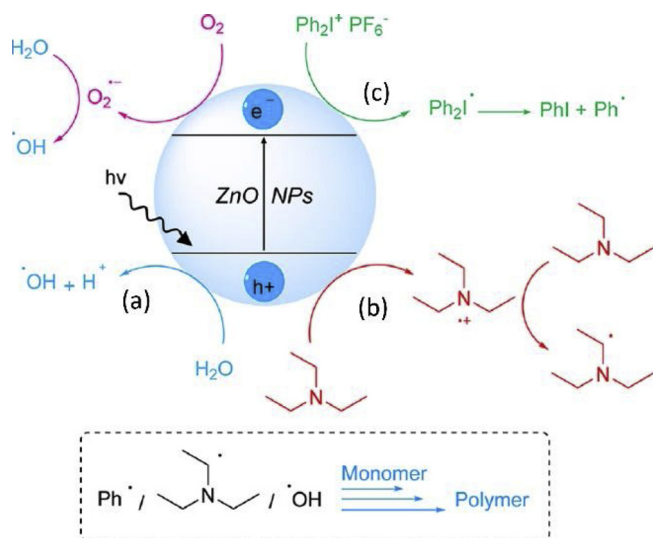


Fig. 35. Interaction of the photoexcited electron and hole species with different co-initiators in a ZnO initiating system [299]. Reprinted with permission.

interaction of the photogenerated holes with the carboxylic acid groups leads to the decarboxylation of LA and the formation of free radicals, which can then initiate the polymerization (Fig. 36b). However, in the presence of TEA, α -amino radicals can form and initiate the polymerization (Fig. 36c). A similar decarboxylation process has also been reported during the photoinduced polymerization initiated by TiO_2 NPs in the presence of butyric acid [302].

It is well-known that halide perovskites in optoelectronic applications can be in part attributed to their high absorption and long carrier lifetime, leading to a promising material for the application of photocatalysis and photovoltaics. Very recently, Tüysüz et al. [303] reported a visible light driven *in-situ* photosynthesis of poly(3,4-ethylenedioxythiophene), PEDOT, over cesium lead iodide (CsPbI_3) Perovskite QDs (Fig. 37). Higher concentration of the CsPbI_3 QDs increased polymerization rate, and after synthesis CsPbI_3 QDs were encapsulated and stabilized by PEDOT to form a composite. During catalysis, 1,4-benzoquinone was used as the electron acceptor to promote polymerization, and to secure the desired cubic crystal structure of CsPbI_3 perovskite from oxidation. This novel approach enables a single-step synthesis of CsPbI_3 /PEDOT composite, which could be promising for optoelectronic applications.

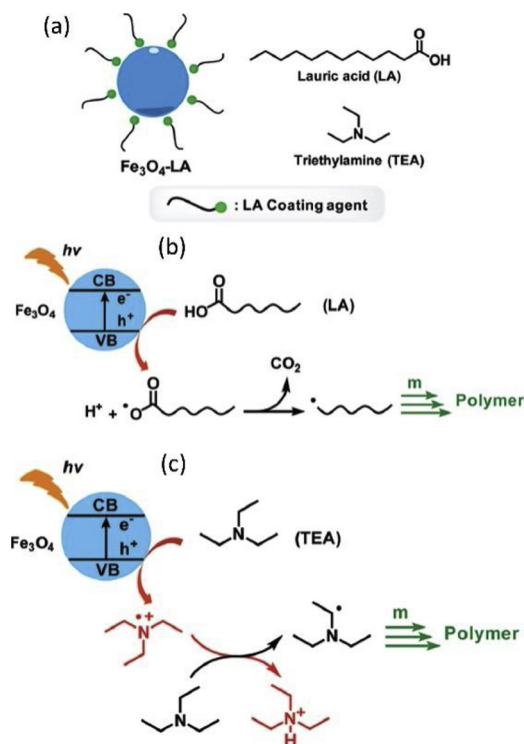


Fig. 36. (a) Illustration of the LA coated Fe_3O_4 and the amine co-initiator. Proposed mechanism for the photopolymerization of vinyl monomers using LA- Fe_3O_4 NPs without (b) and with co-initiator (c) [301]. Reprinted with permission.

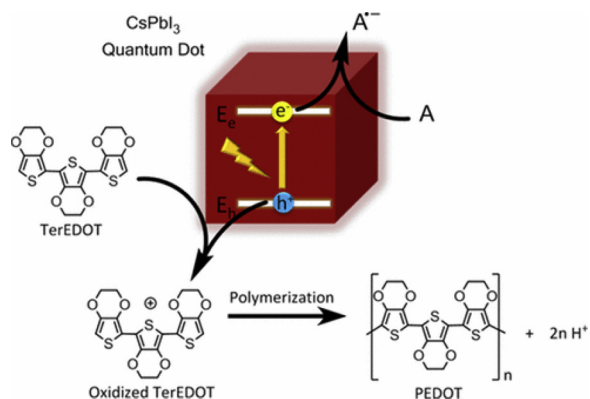


Fig. 37. Schematic illustration of PEDOT synthesis using CsPbI_3 as the photo-initiator [303]. Reprinted with permission.

3.1.2. Heteronanostructure or hybrid system

Semiconductor-metal composite heteronanostructures have been widely used as photocatalyst for photosynthesis. Recently, $\text{ZnO}@\text{Ag}$ composite nanostructures have been applied as photo-initiator to trigger the free radical photopolymerization [302]. As shown in Figure 38 a–c, $\text{ZnO}@\text{Ag}$ heteronanostructure was prepared by depositing Ag NPs on ZnO nanoflowers using a redox active poly(ionic liquid), poly(1-vinyl-3-butyliimidazolium ascorbate) (P[VBUIm][As]). Under UV light irradiation, this material demonstrated good activity and stability (Fig. 38d and e) to initiate the polymerization of MMA and N-isopropylacrylamide (NIPAM) in various solvents, such as water and dichloromethane (DCM), indicating a high versatility of this initiator. In comparison with ZnO nanoflower alone, the $\text{ZnO}@\text{Ag}$ NPs showed much higher activity in photopolymerization, which can be ascribed to that the Ag NP on ZnO surface works as electron trap promoting the separation of photocharges as well as suppressing the recombination of

electron-hole pairs at surface. Moreover, the authors proposed that the adsorbed H_2O molecules on NP surface, due to the presence of highly hygroscopic P[VBUIm][As], are critical for the generation of OH^\bullet radical species to initiate the polymerization, since no polymerization occurred if the reaction system was completely free from traces of moisture [303,304].

Besides inorganic semiconductor NPs, $g\text{-C}_3\text{N}_4$ can also be used as photoinitiators, due to their unique properties combining the characteristics of a middle-band semiconductor and conductive graphite carbon with high surface area [305]. Indeed, $g\text{-C}_3\text{N}_4$ was found to be an active visible light catalyst, useful in water splitting, photodegradation of pollutants, Friedel–Crafts reactions, reduction of CO_2 and selective oxidation [305]. Yagci and co-workers reported that mesoporous $g\text{-C}_3\text{N}_4$ in the presence of alkyl amines as co-initiators can photoinitiate the free radical polymerization of MMA under visible light [305]. The initiation mechanism was presumed to be similar to the $\text{ZnO}\text{-TEA}\text{-MMA}$ reaction system, with the amine being photooxidized in an initiating radical cation [299].

3.2. Controlled/living radical polymerization

Despite the popularity and economic feasibility of free radical polymerization, the major limitation of this synthetic technique is the poor control over the synthetic process that usually generates wide polydispersity of molecular weight (M_w) and difficulty to achieve well-defined polymers with controlled composition, chain architecture, and site-specific functionality [48,306]. Controlled / living radical polymerization (CRP) has revolutionized and revitalized the field of synthetic polymer chemistry over the last twenty years and it is now possible to prepare a wide variety of previously inaccessible macromolecules under relatively mild conditions [48,306]. CRP realized the well-defined microstructure design of the polymers in a controlled fashion to synthesize bioconjugates, organic/inorganic composites, and surface-tethered copolymers with a narrow M_w polydispersity [48,306–308]. Several methods including transition-metal-catalyzed atom transfer radical polymerization (ATRP), reversible addition-fragmentation chain transfer (RAFT) polymerization, single-electron-transfer living free radical polymerization (SET-LRP) as well as nitroxide mediated polymerization (NMP) are increasingly well-developed CRP processes for the construction of macromolecular architectures [309]. Very recently photochemistry with CRP techniques has revolutionized for the synthesis of well-defined macromolecules [306]. In the following content, the ATRP and RAFT photopolymerizations upon photosensitive NP initiating system are highlighted.

In conventional ATRP synthesis, generally a transition metal complex catalyst, such as Cu(I) -ligand complex, is necessary to establish the control over the polymerization [136,306,311]. Alkyl halide compounds were used as initiators to react with transition metal catalyst to generate active initiating species in a reversible manner. In the example using cooper catalyst, the polymer growth highly depends on the redox cycle of $\text{Cu(I)} / \text{Cu(II)}$, acting as a reversible activation / deactivation process for initiation. An optimal control to the $\text{Cu(I)} / \text{Cu(II)}$ ratio is crucial to maximize the reaction rate while extending the lifetime of propagation chains [299,310,312]. Liu et al. report the ATRP synthesis of several polymer brushes using TiO_2 as the photo-reductant and Cu(II) complex as the catalyst to trigger the polymerization under UV irradiation via a one-electron transfer process [309]. Fig. 39a displays the mechanism of the UV-induced ATRP, where the air-stable Cu(II) -ligand was *in situ* reduced to active Cu(I) -ligand via accepting the photo-generated electrons from the CB of TiO_2 , which then reacted with the alkyl halide to produce alkyl radicals for initiating the polymerization; the Cu(I) can be facily recovered to Cu(II) by oxidation reaction with O_2 in air [309]. In this study, it is found that decreasing the Cu catalyst amount to ppm level did not retard the reaction significantly. The living nature of this UV-ATRP synthetic process was verified by its ability to form copolymer brushes (Fig. 39b, c). Under irradiation, a new chain

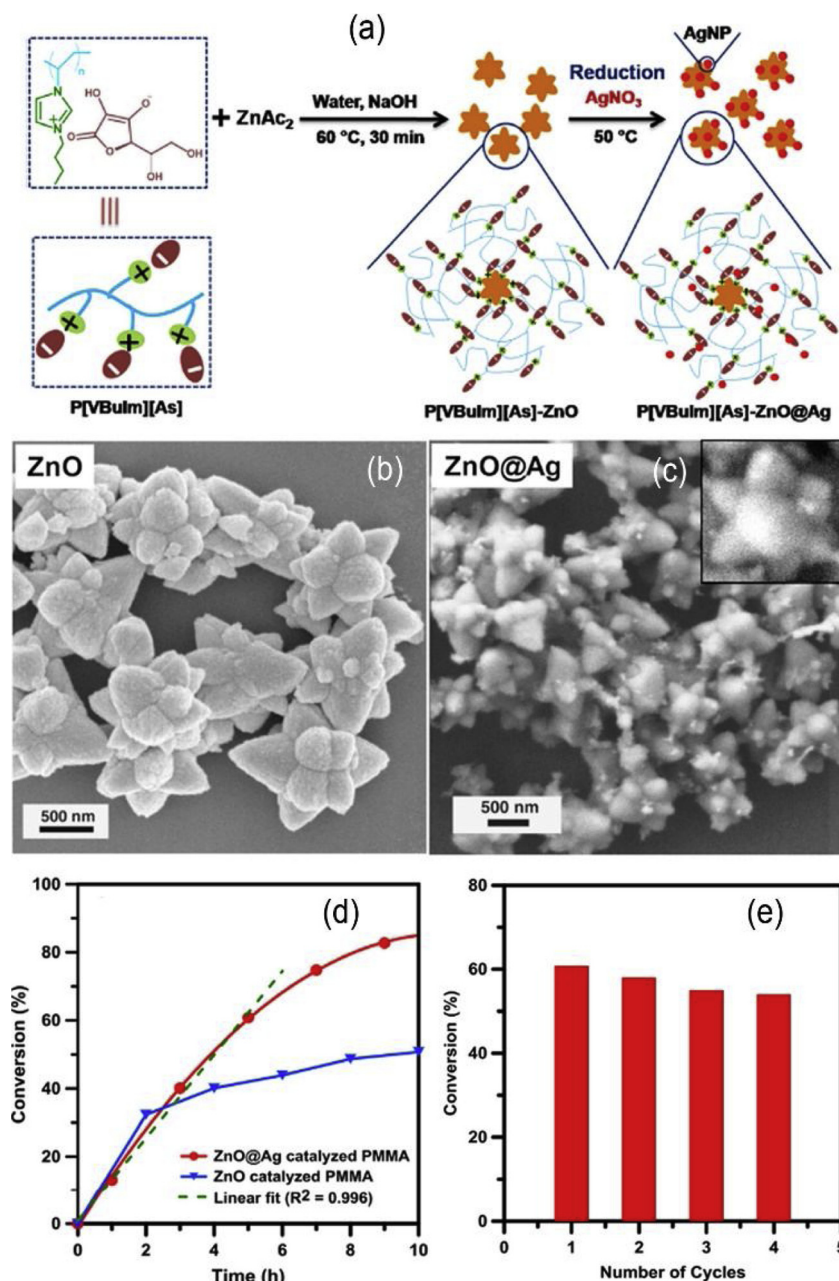


Fig. 38. (a) Synthesis of ZnO@Ag composite heteronanostructure using P[VBulm][As]. (b, c) SEM images of ZnO nanoflowers and ZnO@Ag NPs. (d) Conversion ratio of MMA polymerization using ZnO@Ag NPs as photoinitiator. (e) Continuous cycles of polymerization using ZnO@Ag NPs [302]. Reprinted with permission.

segment of poly(sulfopropyl methacrylate) (PSPMA) can be grafted onto the chain-end of the pre-synthesized poly(dimethylamino)ethyl methacrylate (PDEAEMA) to form a block polymer brushes (Fig. 39c) [309]. The break-off and re-start of the ATRP polymerization can be simply programmed by interval light on-off (Fig. 36d) [310]. Moreover, under irradiation, if successive monomer was introduced to the reaction, the polymer chain can grow continuously (Fig. 39e). Both observations confirmed the living nature of the RAFT process with NP photoinitiator. The M_w of the synthesized PMMA has a small polydispersity and the experimental polymer conversion ratio showed good correlation with theoretical calculation. Polymer brushes were also synthesized through the visible-light-driven ATRP synthesis in the presence of dye-sensitized TiO₂ NPs and TiO₂-rGO nanocomposite [313,314]. The light induced ATRP allows the application potential of micro-contact printing, where multi-functional groups with complex architectures can be built / arranged orderly along the brush chain. On

account of the same one-electron transfer principle, ZnO, Fe-doped ZnO NPs, g-C₃N₄ NPs were also used as photo-initiators in ATRP synthesis [299,310,311].

Recent research efforts have also been concentrated on developing new catalytic system which can work efficiently under milder and environmentally benign conditions. For example, instead of using toxic Cu, more biologically tolerable metal complexes including Ru and Fe at ppm level have been reported in ATRP synthesis [299,310,311], offering a “greener” reaction environment [5]. In addition, metal-free photoinitiated ATRP using semiconductors has recently reported by Liu and co-workers, where Nb(OH)₅ NPs with benzyl alcoholate ligand (NbBA) were used as the visible light active initiator (Fig. 40a) [315]. In the presence of NbBA and Ethyl 2-bromoisobutyrate (EBiB) as catalyst, the ATRP synthesis of poly(isopropylacrylamide) (PNIPAAm) was initiated under visible light. The proposed mechanism was illustrated in Fig. 40b, upon the photoexcitation, electron transfer occurs via ligand-

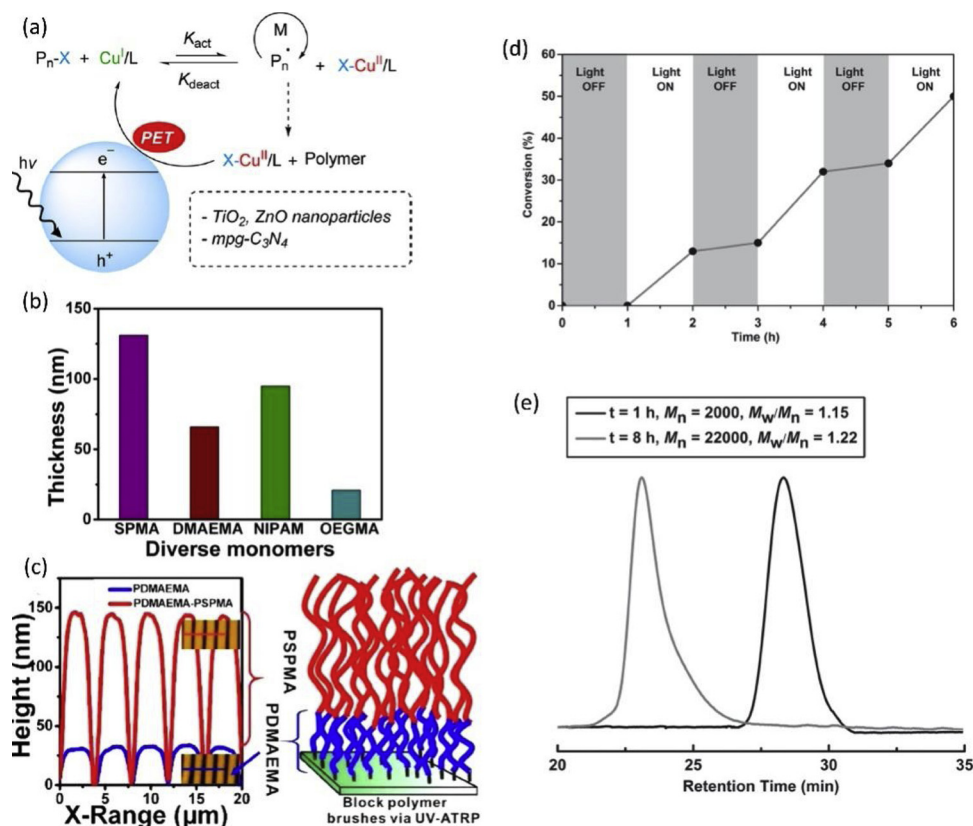


Fig. 39. (a) Photoinduced ATRP using semiconductor NPs as photoinitiators [6]. (b) Thickness of the polymer brushes obtained from various monomers after 1 h ATRP reaction. (c) Left figure shows the line traces of the PDMAEMA and PMAEMA-PDMAEMA brushes AFM images. The right image is the schematic illustration of the PMAEMA = PDEAEMA multi-layer brushes produced by UV-ATRP [309]. (d) UV-light on-off test during the ATRP of MMA. (e) Gel permeation chromatography (GPC) of the PMMA during chain extension process before (black) and after (gray) sequential monomer addition [310]. Reprinted with permission.

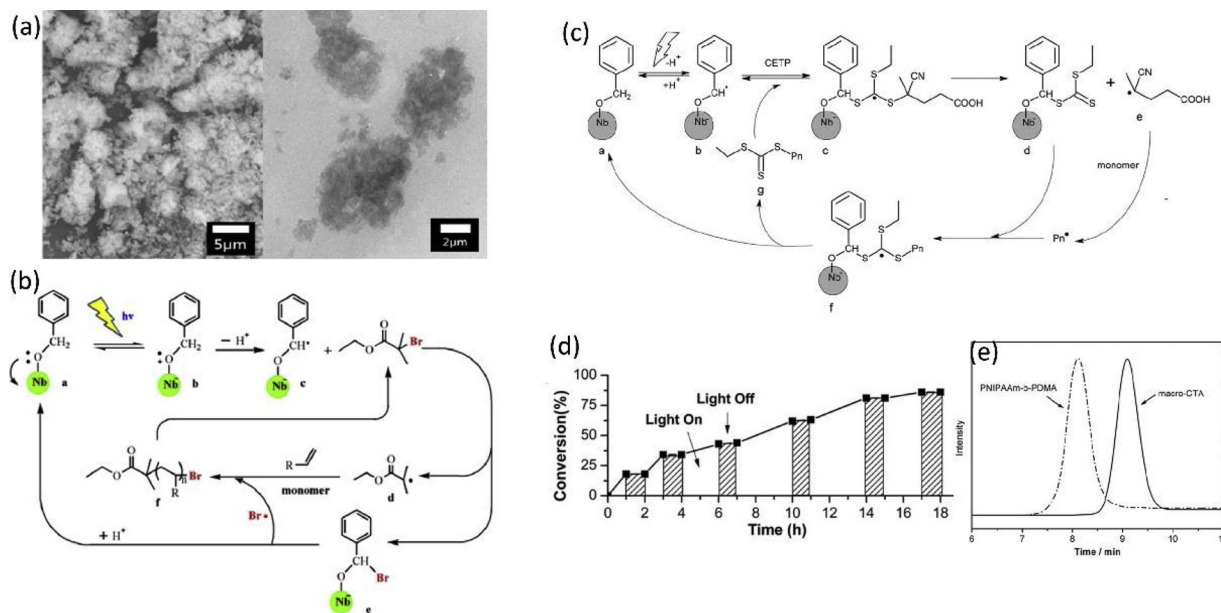


Fig. 40. (a) Scanned electron microscopy (left) and TEM (right) image of NbBA NPs. (b) Proposed mechanism of a visible light driven ATRP (b) and RAFT (c) polymerization using NbBA as the photoinitiator. (d) Light on-off test of RAFT polymerization of NIPAAm using NbBA as photoinitiator. (e) GPC traces of PNIPAAm-b-PDMA (dashed line) and PNIPAAm (macro-CTA, solid line) to confirm the living character test of RAFT polymerization using NbBA photoinitiator [315,316]. Reprinted with permission.

to-metal charge transfer process from the surface complex ligand to the metal atom of the NP, leading to the formation of radical cations of the ligand followed by the generation of a $-\text{O}-\text{CH}^\bullet-\text{Ph}$ radical after losing the α -hydrogen. The resulted alkoxy substituted radical is highly active to react with the EBiB catalyst to yield the alkyl radical to initiate polymerization. As presented in Fig. 40a, the regeneration of NbBA, homolysis of the C–Br bond, chain propagation can take place

repeatedly in the cyclical process. Without using EBiB catalyst, this reaction undergoes a solely free radical polymerization process with poor control over M_n and polydispersity. The NPs can be easily separated by centrifuge and reused for successive reactions. Another advantage is that this metal free reaction system enables the producing of clean products without additional efforts to remove the ionic metal residues [315].

Compared with the ATRP synthesis, RAFT polymerization renders a metal ion-free environment, which is promising for biological relevant applications. The NbBA NPs were also successfully applied in visible light-driven RAFT polymerization, in which PNIPAAm with controlled M_n and narrow polydispersity index was obtained if the feeding ratio of NP to RAFT agent was controlled properly [316]. Like the mechanism proposed in the above ATRP case, in RAFT synthesis, the photoinduced $-O-CH^{\bullet}-Ph$ radical can attack the $C=S$ bond of the RAFT agent to generate the highly reactive intermediate, initiating the RAFT polymerization (Fig. 40c). Afterward, $C=S$ bond of the RAFT agent can be reformed with a radical fragment by the decomposition of the radical intermediate. The radical fragment can initiate the chain propagation and subsequently react with the NbBA-RAFT to produce a highly active polymeric intermediate again (f), which could decompose into the polymer with RAFT active center (g) and NbBA NP for the following repeating reactions. Like the ATRP process, the well-controlled manner of this photo-induced ATRP was evidenced by light on-off test (Fig. 40d). The living nature was confirmed by a continuous growth of the polymer chain upon the introduction of additional monomers under irradiation (Fig. 40e) [316].

3.3. Free radical photopolymerization induced by other NPs

Apart from the semiconductors, other photo-responsive nanostructures have been developed to assist the radical polymerization. Lanthanide-doped upconverting NPs (UCNPs) have revealed profound potential as fluorescent probes in bio-applications, such as bio-imaging and bioassays [317]. In particular, UCNPs are able to transfer low-energy near-infrared (NIR) incident photons to high-energy UV or visible emission based on the sequential absorption of two or more photons. NIR light serving as the excitation source offers a distinct advantage for bio-system, as it enables higher penetration depth in tissues without photo-damage to living cells. Haupt et al. [318] reported generic

strategy to construct a cross-linked polymer coating with plenty of optional functional groups on UCNPs. As illustrated in Fig. 41, upon the NIR ($\lambda = 980$ nm) irradiation, the UV emission was generated by the UCNPs, which was then captured by the dye molecules to generate active species [318]. Co-initiators were activated by the excited dye to generate free radicals initiating the polymerization. Since the emission from the UCNPs is weak as compared to the direct light, the polymerization is proceeded only at the confined, close proximity of the UCNP surface, and thus resulting in the formation of a UCNP@polymer core@shell structure. By simply varying the monomers, polymer coating with various properties can be programmed facilely, which can be hydrophilic or hydrophobic, bio-compatible or sensitive, chemically reactive or inert. Multilayer polymeric coating was also achievable by sequentially introducing different monomers with variety of functionalities [318].

SiO_2 NPs are considered to be non-toxic, biocompatible materials with unique surface features, such as the rich of $-OH$ groups, high porosity as well as large surface area, which render them to be a versatile platform for surface functionalization to meet various applications. Ruthenium complex (RuL^{2+}) was immobilized in a Nafion (Nf) coating wrapped on SiO_2 NP to form a visible-light-active hybrid catalyst ($SiO_2/Nf/RuL$) for radical polymerization (Fig. 42a) [319]. Due to the presence of a great number of negatively charged sulfonate groups in Nafion, RuL^{2+} can be bound to surface of the $SiO_2@Nf$ structure, attributed to a strong electrostatic attraction between RuL^{2+} and Nafion (Fig. 42b). In the presence of the $SiO_2/Nf/RuL$, free radical polymerization of MMA can be performed at ambient temperature under visible light irradiation using EBIB as initiator. As shown in Fig. 42c, the $Ru^{II}L$ confined in the Nafion coating was excited to Ru^*L upon photon absorption, which is reduced by an electron donor, isodipropylethylamine (Pr_2NET), via electron transfer process, to form a highly active single electron reductant Ru^IL . The interaction of Ru^IL and EBIB initiator produced a carbon-centered radical for polymerization and reduced $Ru^{II}L$ back to Ru^IL again in the photoredox cycle [319]. Schlögl and co-workers developed photoactive SiO_2 core-photo-cleavable shell NPs by immobilizing bis(acyl)phosphane oxide and aromatic α -hydroxyketone derivatives on SiO_2 NP surface using silanization method, which can efficiently undergo Norrish type I photo-fragmentation reactions [320]. They studied the photo-activity of these photoactive core-shell structures as photo-initiators for free radical polymerization of thiol-ene. Results revealed that the photoactivity of the NPs is not only influenced by the type of initiating species of the organic shell but also by the grafting method used for NP synthesis, since the latter can control the size, dispersion and surface functionalization of the NPs [320].

Metal NP-polymer composites have attracted increasing research interest for the development of functional materials with unique electrical, optical or mechanical properties in the application of optics, bio-imaging and sensors [321,322]. In particular, Au NPs have been an intense research topic due to their fascinating properties and catalytic activity in various reactions [323–325]. Neckers and co-workers studied the polymerization of acrylates using 5-Mercapto-2,2-bithiophene (BTS) capped Au NPs under UV and visible light irradiation, where the function of the Au was highly dependent on the excitation light [326,327]. Upon exposure to the UV irradiation ($\lambda = 350$ nm, corresponding to BTS absorption), the BTS ligands on Au surface were excited to generate highly active radical cations at the thiophene rings of Au NP-BTS $^{++}$ via electron transfer to the conductive Au NP, which consequently became the unstable acryl radical through deprotonation to initiate the polymerization (Fig. 43a). As the polymerization was only taken place in a close vicinity to the NP surface, which strictly localized reaction largely reduced the rate of product diffusion. On the other side, visible light irradiation ($\lambda > 450$ nm, Fig. 43b) led to different photo-radical generation mechanism due to the SPR effect of Au [326]. Au NPs can act as electron donors upon excitation at the SPR band to generate active surface species, although BTS is not light-

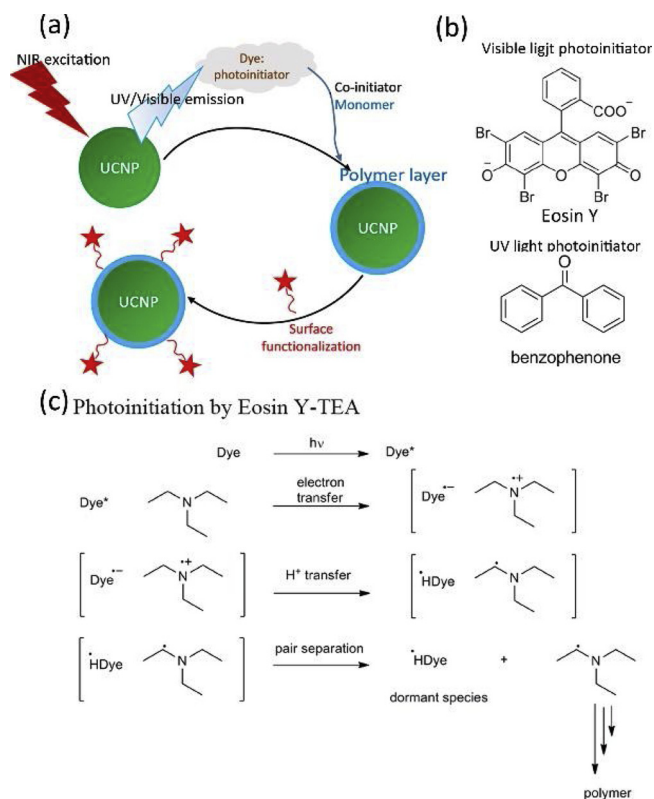


Fig. 41. Scheme of the UCNP assisted photopolymerization (a) in the presence of UV and visible light photoinitiators (b), and the detailed radical formation process (c) [318]. Reprinted with permission.

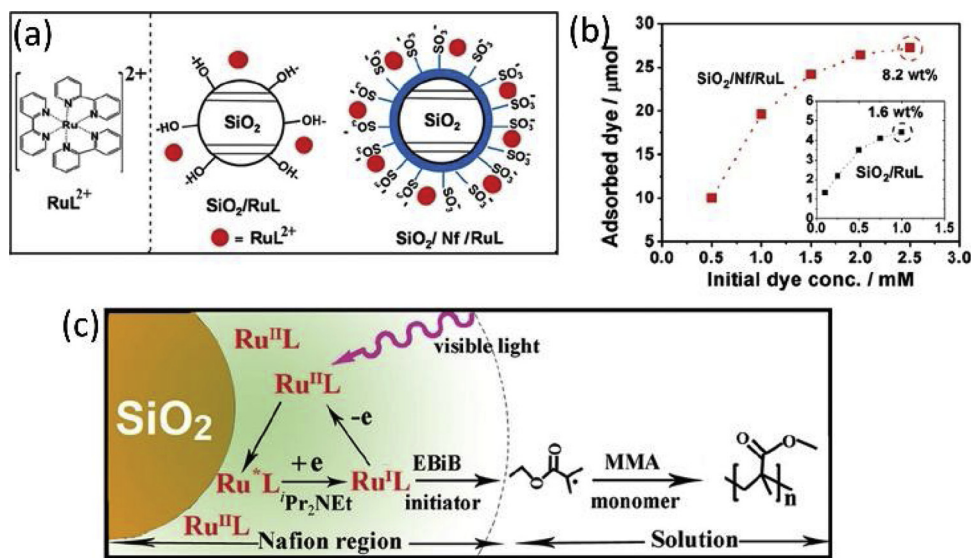


Fig. 42. (a) Structure scheme of the SiO_2/RuL and $\text{SiO}_2/\text{Nf}/\text{RuL}$. (b) Dye adsorption ability of SiO_2/RuL and $\text{SiO}_2/\text{Nf}/\text{RuL}$. (c) Scheme of the photopolymerization using $\text{SiO}_2/\text{Nf}/\text{RuL}$ as photoinitiator [319]. Reprinted with permission.

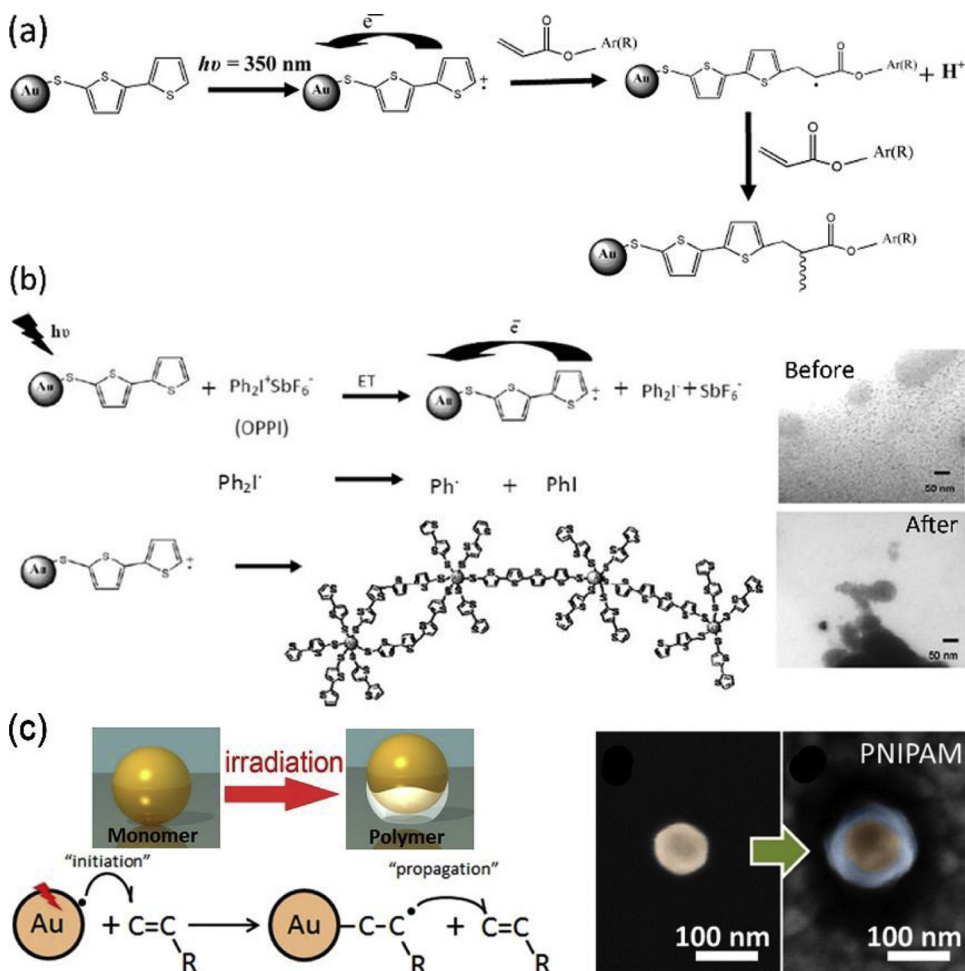


Fig. 43. Schematic mechanism of the photopolymerization under UV (a) and visible light (b) using light responsive Au NP-BST [326,327]. TEM images show the Au NP-BST before and after light irradiation without monomers [326]. (c) Scheme of the plasmon initiated polymerization and the scanned electron microscopy (SEM) images of Au NPs before and after irradiation, showing the formation of polymer [328]. Reprinted with permission.

responsive at visible region. It is suggested that on account to the excitation of Au NP SPR in the presence of an oxidizing chemical of [4-[(octyloxy)phenyl] phenyl] iodonium hexafluoroantimonate (OPPI) as co-initiator, electron was transferred from the Au NP to OPPI inducing the decomposition of OPPI to form phenyl radicals for polymerization. This proposal was evidenced by the fact that without the presence of monomers, intraparticle coupling took place though BTS ligand connection to form NP aggregates via intramolecular electron transfer and subsequent charge recombination.

Baymberg et al. reported SPR-induced radical polymerization via plasmonic “hot” electrons using Au NPs [328]. As illustrated in Fig. 43c, Au NPs were deposited on a Au “mirror” surface with tunable gap, where strong electric fields were formed due to the coupling of Au substrate and SPR. Under visible light (laser) illumination, N-isopropylacrylamide (NIPAM) polymer growth was triggered around the junction of the Au NP and substrate, without using any additional initiator. It is proposed that upon the absorption of visible photons, due to the strong localized SPR electric fields, hot-electron transfer takes place from Au NP surface to monomers to form initiating free radicals for polymer growth, demonstrating the radical polymerization initiated by light-directed programmable plasmons [328,329].

3.4. Reaction kinetics in polymerization

According to classic kinetic theory of a conventional free radical polymerization reaction with a given monomer concentration, the overall rate of polymerization, R_p , is given by the following equation [47]:

$$-\frac{d[M]}{dt} = R_p = k_p k_t^{1/2} [M] R_{in}^{1/2}$$

where R_{in} is the initiation rate, $[M]$ is the monomer concentration; k_p and k_t are the rate constants of propagation and termination, respectively, which can be referred from literature values. Clearly, in a given monomer system, R_p is proportional to the square root of the initiation rate, indicating that the reaction ratio is mainly dominated by the initiation step. In the presence of a photoinitiator, the initiation process is the only photochemical step. The chain initiation rate can thus be determined from the following expression [256,282]:

$$R_{in} = Q_i I_a = Q_i I_0 (1 - 10^{-A})$$

where Q_i is the photoinitiation quantum yield, A presents the absorbance of the NPs in solution, I_0 and I_a are the incident and the absorbed light intensity. Once the monomer radical is formed, subsequent chain propagation will comply with the classic free radical chain growth mechanism. Hence, the overall rate of a free radical polymerization under the steady state using NP photoinitiator can be expressed as follows [256,282]:

$$R_p = k_p k_t^{1/2} [M] (Q_i I_0 (1 - 10^{-A}))^{1/2}$$

Therefore, with regard to the materials, quantum efficiency is a crucial factor significantly determining the rate of photo-polymerization. NP photoinitiators with high quantum efficiency and good charge separation feature are of large benefit to the photopolymerization. The kinetic nature of photopolymerization has been investigated experimentally via varying the reaction parameters, such as irradiation time, intensity of incident light, monomer concentration and NP concentration. In most cases, the monomer consumption ($[M]/[M_0]$) basically follows a first-order dependence of the polymerization rate as shown in Fig. 44a [136]. The polymer yield increases linearly with the extension of irradiation time, indicating that the rate of polymerization was independent of time (Fig. 44b) [284]. The plot of the polymerization rate versus the square root of light intensity is linear, which is in perfect agreement with the kinetic theory shown above (Fig. 44c) [256]. Besides the quality of the NPs, monomer, solvent or co-initiator also may influence the reaction (Fig. 44d). For example, in an early report of

Hoffman, the polymerization efficiency of vinyl acetate, methyl acrylate, acrylonitrile, MMA and styrene was assessed using a CdS quantum dot photo-polymerization system. It is found that besides the reduction potential of the monomers, their intrinsic reactivity and polarity played more essential roles in the reaction [282]. The relationship between quantum yield of NPs and dielectric constant of the solvent was also discussed, but such solvent effect may not applicable to other reaction system [282]. Nonetheless, usually the solvent with reduction potential compatible with the energy level of semiconductor NPs, which may work as a good hole scavenger to promote the charge separation, is preferred. Moreover, the choosing of co-initiators needs to be carefully considered. The co-initiators can dramatically enhance the efficiency of the polymerization, as they may interact with the surface of the NPs, where photo-excited charge carriers are inherently located [300,329]. The effect of various amine co-initiators on the one- and two-photon induced polymerization of MMA using CdS QDs implied that some amines, i.e. TEA, can interact more strongly with trapped carriers than other amines (such as n-butylamine and diethylethlenediamine), although the nature of the interaction is still unknown [329].

4. Conclusion and perspective

In line with the concept of “green” and sustainable chemistry, photocatalytic organic synthesis, e.g. photocatalytic conversion of CO_2 , aromatic alcohols, fatty alcohols and other compounds to fuel, organic molecules and polymers, as one important branch and a frontier in photosynthesis has opened a promising and environmental-friendly venue for the production of organics. In this paper, we mainly highlighted the most recent advances about the CO_2 conversion, organic molecule transformation, and photopolymerization initiated by photo-active NPs and. The introduction of photocatalytic CO_2 reduction is categorized depending on the catalyst types; and at the end of the introduction we briefly discussed several important factors affecting catalysis. The section of photocatalytic organic transform is classified based on the reaction types, and ended with a summary of factors influencing reaction selectivity. In the third part, for the first time, we summarized the application of photoresponsive NPs, which have long been used as photocatalysts in heterogenous catalysis, in the radical polymerization system working as photo-initiators. The semiconductor NPs or nanocomposites are good light-sensitive materials undergoing photon adsorption followed by the generation of charge carriers, which can induce the formation of initial radicals. The possible reaction mechanism is highly dependent on the type of the NPs, reactants and solvents. Compare with the conventional heterogenous catalysis system, the organic synthesis and photopolymerization initiated by NPs is more complex since monomers, solvents and co-initiators all participate the reaction. In addition to the good activity, several outstanding merits of using NP photoinitiator, including, but not limited to the mild reaction conditions, products with high purity related to the easy separation of NPs, and facilely recyclable / reusable NP initiators, make them highly attractive for many applications.

Despite the achievements over the past decades, there are many challenges still existing in the domain of photocatalytic organic synthesis. The photoconversion efficiency and selectivity for desired products are lower than photocatalytic H_2 evolution or natural photosynthesis. In addition to continue developing of highly active catalyst, the exact mechanism needs to be systematically investigated, in particular the adsorption and activation of reactants on catalyst surface which are playing key role affecting reaction rate and selectivity. Other processing factors determining the reaction selectivity need to be systematically studied. The investigation using nanomaterials for photopolymerization is still largely limited in comparison to those in heterogenous catalysis. To further expand the application of photoresponsive nanomaterials in radical polymerization, more efforts need to be devoted to the following aspects: Firstly, it is critical to develop more active NP photoinitiators. Regarding the materials,

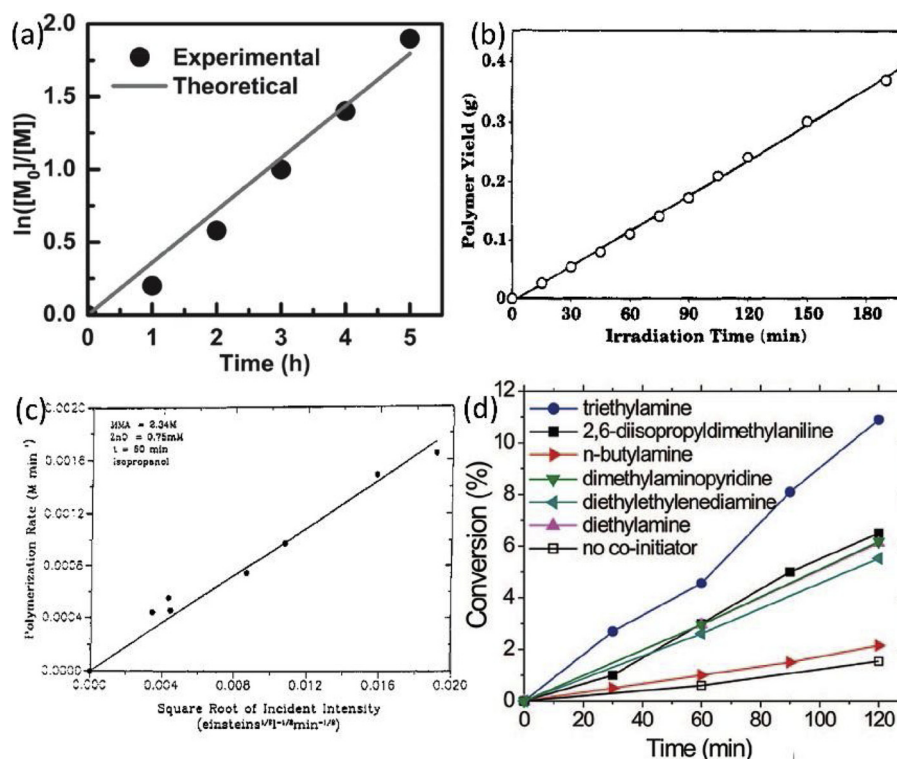


Fig. 44. (a) Monomer consumption ($\ln([M]/[M_0])$) vs. reaction time [136]. (b) polymer yield as a function of irradiation time [284]. (c) Polymerization rate vs. Square root of light intensity [256]. (d) Co-initiator effect on the polymerization [329]. Reprinted with permission.

although classic semiconductors show good performance in photopolymerizations, there is a large ascendant space to develop high performance photoresponsive nanostructures, such as larger surface area, broader spectral absorption, higher quantum efficiency as well as better charge separation. Nanocomposites containing semiconductors, metal NPs or carbon materials with rationally designed architectures may be promising solutions. Also, it is timesaving but interesting to transfer the recently developed novel nanocatalysts from heterogeneous catalysis into the photopolymerization system to assess the reaction efficiency and explore the possible mechanism. Secondly, the radical polymer synthetic system needs to be extended. In addition to increase the study on the controlled / living radical polymerization, NP photoinitiator may also be applied in microemulsion or reverse-micelle polymerization, where more detailed study can be carried out in terms of the effect of surfactant and additives on the photoinitiation. Third, co-initiators, such as alkyl alcohol or amines, play an important role to increase the reaction efficiency, as they can react directly with the separated electrons and holes to form active species. Therefore, establishment of an optimal partnership between co-initiator and NP photoinitiating dynamics which can favor the reaction synergistically requires numerous attempts. Meanwhile, the influence of solvent on photopolymerization cannot be neglected. The last but not least, in the regard of the universality of radical polymerization in practical manufacturing, polymerization reactions using a larger variety of monomers are expected. In previous study, mainly acrylate chemicals (e.g., MMA) were used as the representative monomer only to display the feasibility of the polymerization; however, it is far away from the development of the application of the NP photopolymerization system. Therefore, in the future, this may be improved by using nano-photoinitiators to synthesize macromolecules, polymers / copolymers with more functionalities and more complex structures.

Acknowledgements

All authors would like to acknowledge research funding of National

Key R&D Program of China (2017YFE0102700) from the Ministry of Science and Technology (MOST). J.Z. is grateful for the support from National Natural Science Foundation of China (NSFC, No. 51872128) and Jiangsu University (17JDG008). H.L. thanks the support from NSFC (No. 51732007). H-N.L. thanks the NSFC (No. 21705085) and Jiangsu University (17JDG007).

References

- [1] K. Tanaka, F. Toda, Solvent-free organic synthesis, *Chem. Rev.* 100 (2000) 1025–1074, <https://doi.org/10.1021/cr940089p>.
- [2] L.F. Tietze, Domino reactions in organic synthesis, *Chem. Rev.* 96 (1996) 115–136, <https://doi.org/10.1021/cr950027e>.
- [3] R.A. Sheldon, Green solvents for sustainable organic synthesis: state of the art, *Green Chem.* 7 (2005) 267–278, <https://doi.org/10.1039/b418069k>.
- [4] W. Zhang, B.W. Cue (Eds.), *Green Techniques for Organic Synthesis and Medicinal Chemistry*, John Wiley & Sons, Ltd, Chichester, UK, 2012, <https://doi.org/10.1002/9780470711828>.
- [5] S. Dadashi-Silab, S. Doran, Y. Yagci, Photoinduced electron transfer reactions for macromolecular syntheses, *Chem. Rev.* 116 (2016) 10212–10275, <https://doi.org/10.1021/acs.chemrev.5b00586>.
- [6] A. Albini, M. Fagnoni, Green chemistry and photochemistry were born at the same time, *Green Chem.* 6 (2004) 1–6, <https://doi.org/10.1039/b309592d>.
- [7] S. Chatani, C.J. Kloxin, C.N. Bowman, The power of light in polymer science: photochemical processes to manipulate polymer formation, structure, and properties, *Polym. Chem.* 5 (2014) 2187–2201, <https://doi.org/10.1039/C3PY01334K>.
- [8] S. Protti, M. Fagnoni, The sunny side of chemistry: green synthesis by solar light, *Photochem. Photobiol. Sci.* 8 (2009) 1499–1516, <https://doi.org/10.1039/b909128a>.
- [9] T.P. Yoon, M.A. Ischay, J. Du, Visible light photocatalysis as a greener approach to photochemical synthesis, *Nat. Chem.* 2 (2010) 527–532, <https://doi.org/10.1038/nchem.687>.
- [10] D.M. Schultz, T.P. Yoon, Solar synthesis: prospects in visible light photocatalysis, *Science* 343 (2014) 1239176, <https://doi.org/10.1126/science.1239176>.
- [11] K. Mikami, *Green Reaction Media in Organic Synthesis*, Blackwell Pub, 2005.
- [12] M.-O. Simon, C.-J. Li, Green chemistry oriented organic synthesis in water, *Chem. Soc. Rev.* 41 (2012) 1415–1427, <https://doi.org/10.1039/C1CS15222J>.
- [13] J. Tian, Z. Zhao, A. Kumar, R.I. Boughton, H. Liu, Recent progress in design, synthesis, and applications of one-dimensional TiO_2 nanostructured surface heterostructures: a review, *Chem. Soc. Rev.* 43 (2014) 6920–6937, <https://doi.org/10.1039/C4CS00180J>.
- [14] T. Inoue, A. Fujishima, S. Konishi, K. Honda, Photoelectrocatalytic reduction of

- carbon dioxide in aqueous suspensions of semiconductor powders, *Nature* 277 (1979) 637–638, <https://doi.org/10.1038/277637a0>.
- [15] J. Zhang, X. Jin, P.I. Morales-Guzman, X. Yu, H. Liu, H. Zhang, L. Razzari, J.P. Claverie, Engineering the absorption and field enhancement properties of Au-TiO₂ nano-hybrid via whispering gallery mode resonances for photocatalytic water splitting, *ACS Nano* 10 (2016) 4496–4503, <https://doi.org/10.1021/acsnano.6b00263>.
 - [16] Y. Paz, Application of TiO₂ photocatalysis for air treatment: patents' overview, *Appl. Catal. B Environ.* 99 (2010) 448–460, <https://doi.org/10.1016/J.APCATB.2010.05.011>.
 - [17] D. Spasiano, R. Marotta, S. Malato, P. Fernandez-Ibanez, I. Di Somma, Solar photocatalysis: materials, reactors, some commercial, and pre-industrialized applications. A comprehensive approach, *Appl. Catal. B Environ.* 170–171 (2015) 90–123, <https://doi.org/10.1016/J.APCATB.2014.12.050>.
 - [18] S. Banerjee, D.D. Dionysiou, S.C. Pillai, Self-cleaning applications of TiO₂ by photo-induced hydrophilicity and photocatalysis, *Appl. Catal. B Environ.* 176–177 (2015) 396–428, <https://doi.org/10.1016/J.APCATB.2015.03.058>.
 - [19] X. Zhang, Y. Wang, B. Liu, Y. Sang, H. Liu, Heterostructures construction on TiO₂ nanobelts: a powerful tool for building high-performance photocatalysts, *Appl. Catal. B Environ.* 202 (2017) 620–641, <https://doi.org/10.1016/J.APCATB.2016.09.068>.
 - [20] Y. Wang, X. Wang, M. Antonietti, Polymeric graphitic carbon nitride as a heterogeneous organocatalyst: from photochemistry to multipurpose catalysis to sustainable chemistry, *Angew. Chem. Int. Ed.* 51 (2012) 68–89, <https://doi.org/10.1002/anie.201101182>.
 - [21] Q. Xiang, J. Yu, M. Jaroniec, Graphene-based semiconductor photocatalysts, *Chem. Soc. Rev.* 41 (2012) 782–796, <https://doi.org/10.1039/C1CS15172J>.
 - [22] J.L. White, M.F. Baruch, J.E. Pander, Y. Hu, I.C. Fortmeyer, J.E. Park, T. Zhang, K. Liao, J. Gu, Y. Yan, T.W. Shaw, E. Abelev, A.B. Bocarsly, Light-driven heterogeneous reduction of carbon dioxide: photocatalysts and photoelectrodes, *Chem. Rev.* 115 (2015) 12888–12935, <https://doi.org/10.1021/acs.chemrev.5b00370>.
 - [23] D. Friedmann, A. Hakki, H. Kim, W. Choi, D. Bahnemann, Heterogeneous photocatalytic organic synthesis: state-of-the-art and future perspectives, *Green Chem.* 18 (2016) 5391–5411, <https://doi.org/10.1039/C6GC01582D>.
 - [24] J. Chen, J. Cen, X. Xu, X. Li, The application of heterogeneous visible light photocatalysts in organic synthesis, *Catal. Sci. Technol.* 6 (2016) 349–362, <https://doi.org/10.1039/C5CY01289A>.
 - [25] X. Chang, T. Wang, J. Gong, CO₂ photo-reduction: insights into CO₂ activation and reaction on surfaces of photocatalysts, *Energy Environ. Sci.* 9 (2016) 2177–2196, <https://doi.org/10.1039/C6EE00383D>.
 - [26] X. Li, J. Yu, M. Jaroniec, Hierarchical photocatalysts, *Chem. Soc. Rev.* 45 (2016) 2603–2636, <https://doi.org/10.1039/C5CS00838G>.
 - [27] C. Wang, Z. Sun, Y. Zheng, Y.H. Hu, Recent progress in visible light photocatalytic conversion of carbon dioxide, *J. Mater. Chem. A* 7 (2019) 865–887, <https://doi.org/10.1039/C8TA09865D>.
 - [28] J. Ran, M. Jaroniec, S.Z. Qiao, Cocatalysts in semiconductor-based photocatalytic CO₂ reduction: achievements, challenges, and opportunities, *Adv. Mater.* 30 (2018) 1–31, <https://doi.org/10.1002/adma.201704649>.
 - [29] S. Zeng, P. Kar, U.K. Thakur, K. Shankar, A review on photocatalytic CO₂ reduction using perovskite oxide nanomaterials, *Nanotechnology* 29 (2018) 052001, <https://doi.org/10.1088/1361-6528/aa9fb1>.
 - [30] R. Shi, G.I.N. Waterhouse, T. Zhang, Recent progress in photocatalytic CO₂ reduction over perovskite oxides, *Sol. RRL* 1 (2017) 1700126, <https://doi.org/10.1002/solr.201700126>.
 - [31] J. Low, J. Yu, W. Ho, Graphene-based photocatalysts for CO₂ reduction to solar fuel, *J. Phys. Chem. Lett.* 6 (2015) 4244–4251, <https://doi.org/10.1021/acs.jpclett.5b01610>.
 - [32] S. Peiris, J. McMurtrie, H.-Y. Zhu, Metal nanoparticle photocatalysts: emerging processes for green organic synthesis, *Catal. Sci. Technol.* 6 (2016) 320–338, <https://doi.org/10.1039/C5CY02048D>.
 - [33] C. Wang, D. Astruc, Nanogold plasmonic photocatalysis for organic synthesis and clean energy conversion, *Chem. Soc. Rev.* 43 (2014) 7188–7216, <https://doi.org/10.1039/C4CS00145A>.
 - [34] G. Palmisano, V. Augugliaro, M. Pagliaro, L. Palmisano, Photocatalysis: a promising route for 21st century organic chemistry, *Chem. Commun.* 0 (2007) 3425, <https://doi.org/10.1039/b700395c>.
 - [35] Y. Shiraishi, T. Hirai, Selective organic transformations on titanium oxide-based photocatalysts, *J. Photochem. Photobiol. C Photochem. Rev.* 9 (2008) 157–170, <https://doi.org/10.1016/J.JPHOTOCHEMREV.2008.05.001>.
 - [36] G. Palmisano, E. García-López, G. Marci, V. Loddo, S. Yurdakal, V. Augugliaro, L. Palmisano, Advances in selective conversions by heterogeneous photocatalysis, *Chem. Commun.* 46 (2010) 7074–7089, <https://doi.org/10.1039/c0cc02087g>.
 - [37] H. Lu, J. Yao, Recent advances in liquid-phase heterogeneous photocatalysis for organic synthesis by selective oxidation, *Curr. Org. Chem.* 18 (2014) 1365–1372.
 - [38] J.C. Colmenares, R. Luque, Heterogeneous photocatalytic nanomaterials: prospects and challenges in selective transformations of biomass-derived compounds, *Chem. Soc. Rev.* 43 (2014) 765–778, <https://doi.org/10.1039/C3CS00262A>.
 - [39] S.-H. Li, S. Liu, J.C. Colmenares, Y.-J. Xu, A sustainable approach for lignin valorization by heterogeneous photocatalysis, *Green Chem.* 18 (2016) 594–607, <https://doi.org/10.1039/C5GC02109J>.
 - [40] T. Zhang, W. Lin, Metal-organic frameworks for artificial photosynthesis and photocatalysis, *Chem. Soc. Rev.* 43 (2014) 5982–5993, <https://doi.org/10.1039/C4CS00103F>.
 - [41] G. Palmisano, M. Addamo, V. Augugliaro, T. Caronna, A. Di Paola, E.G. López, V. Loddo, G. Marci, L. Palmisano, M. Schiavello, Selectivity of hydroxyl radical in the partial oxidation of aromatic compounds in heterogeneous photocatalysis, *Catal. Today* 122 (2007) 118–127, <https://doi.org/10.1016/J.CATTOD.2007.01.026>.
 - [42] M. Gattrell, N. Gupta, A. Co, A review of the aqueous electrochemical reduction of CO₂ to hydrocarbons at copper, *J. Electroanal. Chem.* 594 (2006) 1–19, <https://doi.org/10.1016/J.JELECHEM.2006.05.013>.
 - [43] Y. Izumi, Recent advances in the photocatalytic conversion of carbon dioxide to fuels with water and/or hydrogen using solar energy and beyond, *Coord. Chem. Rev.* 257 (2013) 171–186, <https://doi.org/10.1016/J.CCR.2012.04.018>.
 - [44] K. Li, X. An, K.H. Park, M. Khraisheh, J. Tang, A critical review of CO₂ photo-conversion: catalysts and reactors, *Catal. Today* 224 (2014) 3–12, <https://doi.org/10.1016/J.CATTOD.2013.12.006>.
 - [45] J.A. Brydson, *Plastics Materials*, Butterworth-Heinemann, 1999.
 - [46] N.M. Bikales, Present and future directions of basic research on polymeric materials, *Polym. J.* 19 (1987) 11–20, <https://doi.org/10.1016/J.POLYJM.19.11>.
 - [47] P.J. Flory, *Principles of Polymer Chemistry*, Cornell University Press, 1953.
 - [48] K.M. and, J. Xia, Atom transfer radical polymerization, *Chem. Rev.* 101 (2001) 2921–2990, <https://doi.org/10.1021/CR940534G>.
 - [49] P. Akhter, M. Hussain, G. Saracco, N. Russo, Novel nanostructured-TiO₂ materials for the photocatalytic reduction of CO₂ greenhouse gas to hydrocarbons and syngas, *Fuel* 149 (2015) 55–65, <https://doi.org/10.1016/J.FUEL.2014.09.079>.
 - [50] T. Ihara, M. Miyoshi, M. Ando, S. Sugihara, Y. Iriyama, Preparation of a visible-light-active TiO₂ photocatalyst by RF plasma treatment, *J. Mater. Sci.* 36 (2001) 4201–4207, <https://doi.org/10.1023/A:1017929207882>.
 - [51] J. Huo, Y. Hu, H. Jiang, C. Li, In situ surface hydrogenation synthesis of Ti³⁺ self-doped TiO₂ with enhanced visible light photocatalytic activity, *Nanoscale* 6 (2014) 9078–9084, <https://doi.org/10.1039/C4NR00972J>.
 - [52] J. Cai, Y. Wang, Y. Zhu, M. Wu, H. Zhang, X. Li, Z. Jiang, M. Meng, In situ formation of disorder-engineered TiO₂ (B)-anatase heterophase junction for enhanced photocatalytic hydrogen evolution, *ACS Appl. Mater. Interfaces* 7 (2015) 24987–24992, <https://doi.org/10.1021/acsami.5b07318>.
 - [53] J. Li, M. Zhang, Z. Guan, Q. Li, C. He, J. Yang, Synergistic effect of surface and bulk single-electron-trapped oxygen vacancy of TiO₂ in the photocatalytic reduction of CO₂, *Appl. Catal. B Environ.* 206 (2017) 300–307, <https://doi.org/10.1016/J.APCATB.2017.01.025>.
 - [54] V.P. Indrakanti, H.H. Schobert, J.D. Kubicki, Quantum mechanical modeling of CO₂ interactions with irradiated stoichiometric and oxygen-deficient anatase TiO₂ surfaces: implications for the photocatalytic reduction of CO₂, *Energy Fuels* 23 (2009) 5247–5256, <https://doi.org/10.1021/ef9003957>.
 - [55] V.P. Indrakanti, J.D. Kubicki, H.H. Schobert, Photoinduced activation of CO₂ on TiO₂ surfaces: quantum chemical modeling of CO₂ adsorption on oxygen vacancies, *Fuel Process. Technol.* 92 (2011) 805–811, <https://doi.org/10.1016/J.FUPROC.2010.09.007>.
 - [56] H. Yaghoubi, Z. Li, Y. Chen, H.T. Ngo, V.R. Bhethanabotla, B. Joseph, S. Ma, R. Schlaf, A. Takshi, Toward a visible light-driven photocatalyst: the effect of midgap-states-induced energy gap of undoped TiO₂ nanoparticles, *ACS Catal.* 5 (2015) 327–335, <https://doi.org/10.1021/cs501539q>.
 - [57] M. Hussain, P. Akhter, G. Saracco, N. Russo, Nanostructured TiO₂/KIT-6 catalysts for improved photocatalytic reduction of CO₂ to tunable energy products, *Appl. Catal. B Environ.* 170–171 (2015) 53–65, <https://doi.org/10.1016/J.APCATB.2015.01.007>.
 - [58] Y.Y. Lee, H.S. Jung, J.M. Kim, Y.T. Kang, Photocatalytic CO₂ conversion on highly ordered mesoporous materials: comparisons of metal oxides and compound semiconductors, *Appl. Catal. B Environ.* 224 (2018) 594–601, <https://doi.org/10.1016/J.APCATB.2017.10.068>.
 - [59] F. Galli, M. Compagnoni, D. Vitali, C. Pirola, C.L. Bianchi, A. Villa, L. Prati, I. Rossetti, CO₂ photoreduction at high pressure to both gas and liquid products over titanium dioxide, *Appl. Catal. B Environ.* 200 (2017) 386–391, <https://doi.org/10.1016/J.APCATB.2016.07.038>.
 - [60] Q. Xu, J. Yu, J. Zhang, J. Zhang, G. Liu, Cubic anatase TiO₂ nanocrystals with enhanced photocatalytic CO₂ reduction activity, *Chem. Commun.* 51 (2015) 7950–7953, <https://doi.org/10.1039/C5CC01087J>.
 - [61] P. Li, Y. Zhou, Z. Zhao, Q. Xu, X. Wang, M. Xiao, Z. Zou, Hexahedron prism-anchored octahedral CeO₂: crystal facet-based homojunction promoting efficient solar fuel synthesis, *J. Am. Chem. Soc.* 137 (2015) 9547–9550, <https://doi.org/10.1021/jacs.5b05926>.
 - [62] X. Cui, Z. Pan, L. Zhang, H. Peng, G. Zheng, Selective etching of nitrogen-doped carbon by steam for enhanced electrochemical CO₂ reduction, *Adv. Energy Mater.* 7 (2017) 1701456, <https://doi.org/10.1002/aenm.201701456>.
 - [63] H. Abdullah, M.M.R. Khan, H.R. Ong, Z. Yaakob, Modified TiO₂ photocatalyst for CO₂ photocatalytic reduction: an overview, *J. CO₂ Util.* 22 (2017) 15–32, <https://doi.org/10.1016/J.JCOU.2017.08.004>.
 - [64] G. Zhao, W. Zhou, Y. Sun, X. Wang, H. Liu, X. Meng, K. Chang, J. Ye, Efficient photocatalytic CO₂ reduction over Co(II) species modified CdS in aqueous solution, *Appl. Catal. B Environ.* 226 (2018) 252–257, <https://doi.org/10.1016/J.APCATB.2017.12.054>.
 - [65] J. Fu, J. Yu, C. Jiang, B. Cheng, g-C₃N₄-based heterostructured photocatalysts, *Adv. Energy Mater.* 8 (2018) 1701503, <https://doi.org/10.1002/aenm.201701503>.
 - [66] J. Low, B. Dai, T. Tong, C. Jiang, J. Yu, In situ irradiated X-Ray photoelectron spectroscopy investigation on a direct Z-scheme TiO₂/CdS composite film photocatalyst, *Adv. Mater.* (2018) 1802981, <https://doi.org/10.1002/adma.201802981>.
 - [67] M. Zhou, S. Wang, P. Yang, C. Huang, X. Wang, Boron carbon nitride semiconductors decorated with CdS nanoparticles for photocatalytic reduction of CO₂, *ACS Catal.* 8 (2018) 4928–4936, <https://doi.org/10.1021/acscatal.8b00104>.
 - [68] A. Roy, M. Chhetri, S. Prasad, U.V. Waghmare, C.N.R. Rao, Unique features of the

- photocatalytic reduction of H_2O and CO_2 by new catalysts based on the analogues of CdS , $\text{Cd}_4\text{P}_2\text{X}_3$ ($\text{X} = \text{Cl}, \text{Br}, \text{I}$). *ACS Appl. Mater. Interfaces* 10 (2018) 2526–2536, <https://doi.org/10.1021/acsaami.7b15992>.
- [69] L. Cheng, Q. Xiang, Y. Liao, H. Zhang, CdS -based photocatalysts, *Energy Environ. Sci.* 11 (2018) 1362–1391, <https://doi.org/10.1039/C7EE03640J>.
- [70] G. Xu, H. Zhang, J. Wei, H.-X. Zhang, X. Wu, Y. Li, C. Li, J. Zhang, J. Ye, Integrating the $\text{g-C}_3\text{N}_4$ Nanosheet with B–H bonding decorated metal–organic framework for CO_2 activation and photoreduction, *ACS Nano* 12 (2018) 5333–5340, <https://doi.org/10.1021/acsnano.8b00110>.
- [71] M. Ou, W. Tu, S. Yin, W. Xing, S. Wu, H. Wang, S. Wan, Q. Zhong, R. Xu, Amino-assisted anchoring of CsPbBr_3 perovskite quantum dots on porous $\text{g-C}_3\text{N}_4$ for enhanced photocatalytic CO_2 reduction, *Angew. Chemie* 130 (2018) 13758–13762, <https://doi.org/10.1002/ange.201808930>.
- [72] X. Liu, P. Wang, H. Zhai, Q. Zhang, B. Huang, Z. Wang, Y. Liu, Y. Dai, X. Qin, X. Zhang, Synthesis of synergetic phosphorus and cyano groups (CN) modified $\text{g-C}_3\text{N}_4$ for enhanced photocatalytic H_2 production and CO_2 reduction under visible light irradiation, *Appl. Catal. B Environ.* 232 (2018) 521–530, <https://doi.org/10.1016/J.APCATB.2018.03.094>.
- [73] J. Wang, T. Xia, L. Wang, X. Zheng, Z. Qi, C. Gao, J. Zhu, Z. Li, H. Xu, Y. Xiong, Enabling visible-light-driven selective CO_2 reduction by doping quantum dots: trapping electrons and suppressing H_2 evolution, *Angew. Chemie Int. Ed.* 57 (2018) 16447–16451, <https://doi.org/10.1002/anie.201810550>.
- [74] Y.-P. Yuan, S.-W. Cao, Y.-S. Liao, L.-S. Yin, C. Xue, Red phosphorus/ $\text{g-C}_3\text{N}_4$ heterojunction with enhanced photocatalytic activities for solar fuels production, *Appl. Catal. B Environ.* 140–141 (2013) 164–168, <https://doi.org/10.1016/J.APCATB.2013.04.006>.
- [75] H. Sheng, M.H. Oh, W.T. Osowiecki, W. Kim, A.P. Alivisatos, H. Frei, Carbon dioxide dimer radical anion as surface intermediate of photoinduced CO_2 reduction at aqueous Cu and CdSe nanoparticle catalysts by rapid-scan FT-IR spectroscopy, *J. Am. Chem. Soc.* 140 (2018) 4363–4371, <https://doi.org/10.1021/jacs.8b00271>.
- [76] R. Asahi, T. Morikawa, T. Ohwaki, K. Aoki, Y. Taga, Visible-light photocatalysis in nitrogen-doped titanium oxides, *Science* 293 (2001) 269–271, <https://doi.org/10.1126/science.1061051>.
- [77] J.C. Yu, W. Ho, J. Yu, H. Yip, P.K. Wong, J. Zhao, Efficient visible-light-induced photocatalytic disinfection on sulfur-doped nanocrystalline titania, *Environ. Sci. Technol.* 39 (2005) 1175–1179, <https://doi.org/10.1021/ES035374H>.
- [78] S. Mozia, M. Tomaszewska, B. Kosowska, B. Grzmil, A.W. Morawski, K. Kałucki, Decomposition of nonionic surfactant on a nitrogen-doped photocatalyst under visible-light irradiation, *Appl. Catal. B Environ.* 55 (2005) 195–200, <https://doi.org/10.1016/J.APCATB.2004.09.019>.
- [79] K. Wang, Q. Li, B. Liu, B. Cheng, W. Ho, J. Yu, Sulfur-doped $\text{g-C}_3\text{N}_4$ with enhanced photocatalytic CO_2 -reduction performance, *Appl. Catal. B Environ.* 176–177 (2015) 44–52, <https://doi.org/10.1016/J.APCATB.2015.03.045>.
- [80] J. Fu, B. Zhu, C. Jiang, B. Cheng, W. You, J. Yu, Hierarchical porous O-Doped $\text{g-C}_3\text{N}_4$ with enhanced photocatalytic CO_2 reduction activity, *Small* 13 (2017) 1603938, <https://doi.org/10.1002/smll.201603938>.
- [81] M. Tahir, N.S. Amin, Indium-doped TiO_2 nanoparticles for photocatalytic CO_2 reduction with H_2O vapors to CH_4 , *Appl. Catal. B Environ.* 162 (2015) 98–109, <https://doi.org/10.1016/J.APCATB.2014.06.037>.
- [82] O. Ola, M. Mercedes Maroto-Valer, Copper based TiO_2 honeycomb monoliths for CO_2 photoreduction, *Catal. Sci. Technol.* 4 (2014) 1631–1637, <https://doi.org/10.1039/C3CY00991B>.
- [83] F. Gonell, A.V. Puga, B. Julián-López, H. García, A. Corma, Copper-doped titania photocatalysts for simultaneous reduction of CO_2 and production of H_2 from aqueous sulfide, *Appl. Catal. B Environ.* 180 (2016) 263–270, <https://doi.org/10.1016/J.APCATB.2015.06.019>.
- [84] M. Park, B.S. Kwak, S.W. Jo, M. Kang, Effective CH_4 production from CO_2 photoreduction using $\text{TiO}_2/\text{x mol\% Cu-TiO}_2$ double-layered films, *Energy Convers. Manage.* 103 (2015) 431–438, <https://doi.org/10.1016/J.ENCONMAN.2015.06.029>.
- [85] J.Y. Do, Y. Im, B.S. Kwak, J.-Y. Kim, M. Kang, Dramatic CO_2 photoreduction with H_2O vapors for CH_4 production using the TiO_2 (bottom)/ Fe-TiO_2 (top) double-layered films, *Chem. Eng. J.* 275 (2015) 288–297, <https://doi.org/10.1016/J.CEJ.2015.03.066>.
- [86] T. Wang, X. Meng, G. Liu, K. Chang, P. Li, Q. Kang, L. Liu, M. Li, S. Ouyang, J. Ye, In situ synthesis of ordered mesoporous Co-doped TiO_2 and its enhanced photocatalytic activity and selectivity for the reduction of CO_2 , *J. Mater. Chem. A Mater. Energy Sustain.* 3 (2015) 9491–9501, <https://doi.org/10.1039/C4TA05892E>.
- [87] O. Ola, M.M. Maroto-Valer, Transition metal oxide based TiO_2 nanoparticles for visible light induced CO_2 photoreduction, *Appl. Catal. A Gen.* 502 (2015) 114–121, <https://doi.org/10.1016/J.APCATA.2015.06.007>.
- [88] B.S. Kwak, K. Vignesh, N.-K. Park, H.-J. Ryu, J.-I. Baek, M. Kang, Methane formation from photoreduction of CO_2 with water using TiO_2 including Ni ingredient, *Fuel* 143 (2015) 570–576, <https://doi.org/10.1016/J.FUEL.2014.11.066>.
- [89] Z. Xiong, Y. Zhao, J. Zhang, C. Zheng, Efficient photocatalytic reduction of CO_2 into liquid products over cerium doped titania nanoparticles synthesized by a sol-gel auto-ignited method, *Fuel Process. Technol.* 135 (2015) 6–13, <https://doi.org/10.1016/J.FUPROC.2014.09.017>.
- [90] L. Matějová, K. Kočí, M. Reli, L. Čapek, A. Hospodková, P. Peikertová, Z. Matěj, L. Obalová, A. Wach, P. Kuštrowski, A. Kotarba, Preparation, characterization and photocatalytic properties of cerium doped TiO_2 : on the effect of Ce loading on the photocatalytic reduction of carbon dioxide, *Appl. Catal. B Environ.* 152–153 (2014) 172–183, <https://doi.org/10.1016/J.APCATB.2014.01.015>.
- [91] H.-Y. Wu, N.H. Nguyen, H. Bai, S. Chang, J.C.S. Wu, Photocatalytic reduction of CO_2 using molybdenum-doped titanate nanotubes in a MEA solution, *RSC Adv.* 5 (2015) 63142–63151, <https://doi.org/10.1039/C5RA10408D>.
- [92] K. Sasan, F. Zuo, Y. Wang, P. Feng, Self-doped Ti^{3+} - TiO_2 as a photocatalyst for the reduction of CO_2 into a hydrocarbon fuel under visible light irradiation, *Nanoscale* 7 (2015) 13369–13372, <https://doi.org/10.1039/C5NR02974K>.
- [93] X. Zhang, T. Peng, S. Song, Recent advances in dye-sensitized semiconductor systems for photocatalytic hydrogen production, *J. Mater. Chem. A* 4 (2016) 2365–2402, <https://doi.org/10.1039/C5TA08939E>.
- [94] P. Kumar, C. Joshi, N. Labhsetwar, R. Boukherroub, S.L. Jain, A novel Ru/TiO_2 hybrid nanocomposite catalyzed photoreduction of CO_2 to methanol under visible light, *Nanoscale* 7 (2015) 15258–15267, <https://doi.org/10.1039/C5NR03712C>.
- [95] L. Wang, S. Duan, P. Jin, H. She, J. Huang, Z. Lei, T. Zhang, Q. Wang, Anchored Cu (II) tetra(4-carboxylphenyl)porphyrin to P25 (TiO_2) for efficient photocatalytic ability in CO_2 reduction, *Appl. Catal. B Environ.* 239 (2018) 599–608, <https://doi.org/10.1016/J.APCATB.2018.08.007>.
- [96] W. Yu, D. Xu, T. Peng, Enhanced photocatalytic activity of $\text{g-C}_3\text{N}_4$ for selective CO_2 reduction to CH_3OH via facile coupling of ZnO : a direct Z-scheme mechanism, *J. Mater. Chem. A* 3 (2015) 19936–19947, <https://doi.org/10.1039/C5TA05503B>.
- [97] N. Yazdanpour, S. Sharifnia, Photocatalytic conversion of greenhouse gases (CO_2 and CH_4) using copper phthalocyanine modified TiO_2 , *Sol. Energy Mater. Sol. Cells* 118 (2013) 1–8, <https://doi.org/10.1016/J.SOLMAT.2013.07.051>.
- [98] G. Gao, Y. Jiao, E.R. Wacławik, A. Du, Single atom (Pd/Pt) supported on graphitic carbon nitride as an efficient photocatalyst for visible-light reduction of carbon dioxide, *J. Am. Chem. Soc.* 138 (2016) 6292–6297, <https://doi.org/10.1021/jacs.6b02692>.
- [99] B. Pan, S. Luo, W. Su, X. Wang, Photocatalytic CO_2 reduction with H_2O over LaPO_4 nanorods deposited with Pt cocatalyst, *Appl. Catal. B Environ.* 168–169 (2015) 458–464, <https://doi.org/10.1016/J.APCATB.2014.12.046>.
- [100] S.-W. Cao, X.-F. Liu, Y.-P. Yuan, Z.-Y. Zhang, Y.-S. Liao, J. Fang, S.C.J. Loo, T.C. Sum, C. Xue, Solar-to-fuels conversion over $\text{In}_2\text{O}_3/\text{g-C}_3\text{N}_4$ hybrid photocatalysts, *Appl. Catal. B Environ.* 147 (2014) 940–946, <https://doi.org/10.1016/J.APCATB.2013.10.029>.
- [101] H. Shi, G. Chen, C. Zhang, Z. Zou, Polymeric $\text{g-C}_3\text{N}_4$ coupled with NaNbO_3 nanowires toward enhanced photocatalytic reduction of CO_2 into renewable fuel, *ACS Catal.* 4 (2014) 3637–3643, <https://doi.org/10.1021/cs500848f>.
- [102] M. Tasbihi, F. Fresno, U. Simon, I.J. Villar-García, V. Pérez-Dieste, C. Escudero, V.A. de la Peña O'Shea, On the selectivity of CO_2 photoreduction towards CH_4 using Pt/ TiO_2 catalysts supported on mesoporous silica, *Appl. Catal. B Environ.* 239 (2018) 68–76, <https://doi.org/10.1016/J.APCATB.2018.08.003>.
- [103] Z. Xiong, Z. Lei, C.-C. Kuang, X. Chen, B. Gong, Y. Zhao, J. Zhang, C. Zheng, J.C.S. Wu, Selective photocatalytic reduction of CO_2 into CH_4 over Pt- Cu_2O TiO_2 nanocrystals: the interaction between Pt and Cu_2O cocatalysts, *Appl. Catal. B Environ.* 202 (2017) 695–703, <https://doi.org/10.1016/J.APCATB.2016.10.001>.
- [104] Y. Wang, J. Zhao, Y. Li, C. Wang, Selective photocatalytic CO_2 reduction to CH_4 over Pt/ In_2O_3 : significant role of hydrogen adatom, *Appl. Catal. B Environ.* 226 (2018) 544–553, <https://doi.org/10.1016/J.APCATB.2018.01.005>.
- [105] S. Bai, X. Wang, C. Hu, M. Xie, J. Jiang, Y. Xiong, Two-dimensional $\text{g-C}_3\text{N}_4$: an ideal platform for examining facet selectivity of metal co-catalysts in photocatalysis, *Chem. Commun.* 50 (2014) 6094–6097, <https://doi.org/10.1039/C4CC00745J>.
- [106] W. Kim, T. Seok, W. Choi, Nafion layer-enhanced photosynthetic conversion of CO_2 into hydrocarbons on TiO_2 nanoparticles, *Energy Environ. Sci.* 5 (2012) 6066–6070, <https://doi.org/10.1039/c2ee03338k>.
- [107] K. Li, T. Peng, Z. Ying, S. Song, J. Zhang, Ag-loading on brookite TiO_2 quasi nanocubes with exposed {210} and {001} facets: activity and selectivity of CO_2 photoreduction to CO/CH_4 , *Appl. Catal. B Environ.* 180 (2016) 130–138, <https://doi.org/10.1016/J.APCATB.2015.06.022>.
- [108] Z. Wang, K. Teramura, S. Hosokawa, T. Tanaka, Photocatalytic conversion of CO_2 in water over Ag-modified $\text{La}_2\text{Ti}_2\text{O}_7$, *Appl. Catal. B Environ.* 163 (2015) 241–247, <https://doi.org/10.1016/J.APCATB.2014.07.052>.
- [109] Z. Wang, K. Teramura, Z. Huang, S. Hosokawa, Y. Sakata, T. Tanaka, Tuning the selectivity toward CO evolution in the photocatalytic conversion of CO_2 with H_2O through the modification of Ag-loaded Ga_2O_3 with a ZnGa_2O_4 layer, *Catal. Sci. Technol.* 6 (2016) 1025–1032, <https://doi.org/10.1039/C5CY01280E>.
- [110] M. Yamamoto, T. Yoshida, N. Yamamoto, T. Nomoto, Y. Yamamoto, S. Yagi, H. Yoshida, Photocatalytic reduction of CO_2 with water promoted by Ag clusters in Ag/ Ga_2O_3 photocatalysts, *J. Mater. Chem. A* 3 (2015) 16810–16816, <https://doi.org/10.1039/C5TA04815J>.
- [111] T. Baran, S. Wojtyła, A. Dibenedetto, M. Aresta, W. Macyk, Zinc sulfide functionalized with ruthenium nanoparticles for photocatalytic reduction of CO_2 , *Appl. Catal. B Environ.* 178 (2015) 170–176, <https://doi.org/10.1016/J.APCATB.2014.09.052>.
- [112] A. Kim, D.P. Debecker, F. Devred, V. Dubois, C. Sanchez, C. Sasse, CO_2 methanation on Ru/TiO_2 catalysts: On the effect of mixing anatase and rutile TiO_2 supports, *Appl. Catal. B Environ.* 220 (2018) 615–625, <https://doi.org/10.1016/J.APCATB.2017.08.058>.
- [113] I. Rossetti, A. Villa, M. Compagnoni, L. Prati, G. Ramis, C. Pirola, C.L. Bianchi, W. Wang, D. Wang, CO_2 photoconversion to fuels under high pressure: effect of TiO_2 phase and of unconventional reaction conditions, *Catal. Sci. Technol.* 5 (2015) 4481–4487, <https://doi.org/10.1039/C5CY00756A>.
- [114] Z. Xie, B. Yan, S. Kattel, J.H. Lee, S. Yao, Q. Wu, N. Rui, E. Gomez, Z. Liu, W. Xu, L. Zhang, J.G. Chen, Dry reforming of methane over CeO_2 -supported Pt-Co catalysts with enhanced activity, *Appl. Catal. B Environ.* 236 (2018) 280–293, <https://doi.org/10.1016/J.APCATB.2018.05.035>.
- [115] Y. Wei, X. Wu, Y. Zhao, L. Wang, Z. Zhao, X. Huang, J. Liu, J. Li, Efficient photocatalysts of TiO_2 nanocrystals-supported PtRu alloy nanoparticles for

- CO₂ reduction with H₂O: Synergistic effect of Pt-Ru, Appl. Catal. B Environ. 236 (2018) 445–457, <https://doi.org/10.1016/j.apcatb.2018.05.043>.
- [116] J. Jiao, Y. Wei, Y. Zhao, Z. Zhao, A. Duan, J. Liu, Y. Pang, J. Li, G. Jiang, Y. Wang, AuPd/3DOM-TiO₂ catalysts for photocatalytic reduction of CO₂: high efficient separation of photogenerated charge carriers, Appl. Catal. B Environ. 209 (2017) 228–239, <https://doi.org/10.1016/j.apcatb.2017.02.076>.
- [117] P.N. Paulino, V.M.M. Salim, N.S. Resende, Zn-Cu promoted TiO₂ photocatalyst for CO₂ reduction with H₂O under UV light, Appl. Catal. B Environ. 185 (2016) 362–370, <https://doi.org/10.1016/j.apcatb.2015.12.037>.
- [118] M. Tahir, B. Tahir, N.A.S. Amin, Synergistic effect in plasmonic Au/Ag alloy NPs co-coated TiO₂ NWs toward visible-light enhanced CO₂ photoreduction to fuels, Appl. Catal. B Environ. 204 (2017) 548–560, <https://doi.org/10.1016/j.apcatb.2016.11.062>.
- [119] A. García-Trenco, A. Regoutz, E.R. White, D.J. Payne, M.S.P. Shaffer, C.K. Williams, PdIn intermetallic nanoparticles for the hydrogenation of CO₂ to methanol, Appl. Catal. B Environ. 220 (2018) 9–18, <https://doi.org/10.1016/j.apcatb.2017.07.069>.
- [120] Q. Liu, Y. Zhou, J. Kou, X. Chen, Z. Tian, J. Gao, S. Yan, Z. Zou, High-yield synthesis of ultralong and ultrathin Zn₂GeO₄ nanoribbons toward improved photocatalytic reduction of CO₂ into renewable hydrocarbon fuel, J. Am. Chem. Soc. 132 (2010) 14385–14387, <https://doi.org/10.1021/ja1068596>.
- [121] C.-C. Yang, J. Vermimmen, V. Meynen, P. Cool, G. Mul, Mechanistic study of hydrocarbon formation in photocatalytic CO₂ reduction over Ti-SBA-15, J. Catal. 284 (2011) 1–8, <https://doi.org/10.1016/j.jcat.2011.08.005>.
- [122] X. Li, W. Li, Z. Zhuang, Y. Zhong, Q. Li, L. Wang, Photocatalytic reduction of carbon dioxide to methane over SiO₂-Pillared HNb₃O₈, J. Phys. Chem. C. 116 (2012) 16047–16053, <https://doi.org/10.1021/jp303365z>.
- [123] C. Wang, R.L. Thompson, J. Baltrus, C. Matrangola, Visible light photoreduction of CO₂ using CdSe/Pt/TiO₂ heterostructured catalysts, J. Phys. Chem. Lett. 1 (2010) 48–53, <https://doi.org/10.1021/jz9000032>.
- [124] J. Ye, C. Liu, D. Mei, Q. Ge, Active oxygen vacancy site for methanol synthesis from CO₂ hydrogenation on In₂O₃ (110): a DFT study, ACS Catal. 3 (2013) 1296–1306, <https://doi.org/10.1021/cs400132a>.
- [125] N. Rui, Z. Wang, K. Sun, J. Ye, Q. Ge, C. Liu, CO₂ hydrogenation to methanol over Pd/In₂O₃: effects of Pd and oxygen vacancy, Appl. Catal. B Environ. 218 (2017) 488–497, <https://doi.org/10.1016/j.apcatb.2017.06.069>.
- [126] L. Collado, A. Reynal, J.M. Coronado, D.P. Serrano, J.R. Durrant, V.A. de la Peña O'Shea, Effect of Au surface plasmon nanoparticles on the selective CO₂ photoreduction to CH₄, Appl. Catal. B Environ. 178 (2015) 177–185, <https://doi.org/10.1016/j.apcatb.2014.09.032>.
- [127] W. Tu, Y. Zhou, H. Li, P. Li, Z. Zou, Au@TiO₂ yolk-shell hollow spheres for plasmon-induced photocatalytic reduction of CO₂ to solar fuel via a local electromagnetic field, Nanoscale 7 (2015) 14232–14236, <https://doi.org/10.1039/C5NR02943K>.
- [128] E. Liu, L. Qi, J. Bian, Y. Chen, X. Hu, J. Fan, H. Liu, C. Zhu, Q. Wang, A facile strategy to fabricate plasmonic Cu modified TiO₂ nano-flower films for photocatalytic reduction of CO₂ to methanol, Mater. Res. Bull. 68 (2015) 203–209, <https://doi.org/10.1016/j.materresbull.2015.03.064>.
- [129] I.-H. Tseng, J.C. Wu, H.-Y. Chou, Effects of sol-gel procedures on the photocatalysis of Cu/TiO₂ in CO₂ photoreduction, J. Catal. 221 (2004) 432–440, <https://doi.org/10.1016/j.jcat.2003.09.002>.
- [130] Z. Wang, K. Teramura, S. Hosokawa, T. Tanaka, Highly efficient photocatalytic conversion of CO₂ into solid CO using H₂O as a reductant over Ag-modified ZnGa₂O₄, J. Mater. Chem. A. 3 (2015) 11313–11319, <https://doi.org/10.1039/C5TA01697E>.
- [131] R. Pang, K. Teramura, H. Asakura, S. Hosokawa, T. Tanaka, Highly selective photocatalytic conversion of CO₂ by water over Ag-loaded SrNb₂O₆ nanorods, Appl. Catal. B Environ. 218 (2017) 770–778, <https://doi.org/10.1016/j.apcatb.2017.06.052>.
- [132] S. Iguchi, K. Teramura, S. Hosokawa, T. Tanaka, A ZnTa₂O₆ photocatalyst synthesized via solid state reaction for conversion of CO₂ into CO in water, Catal. Sci. Technol. 6 (2016) 4978–4985, <https://doi.org/10.1039/C6CY00271D>.
- [133] A. Halder, M. Kilianová, B. Yang, E.C. Tyo, S. Seifert, R. Prucek, A. Panáček, P. Suchomel, O. Tomanec, D.J. Gosztola, D. Milde, H.-H. Wang, L. Kvítek, R. Zbořil, S. Vajda, Highly efficient Cu-decorated iron oxide nanocatalyst for low pressure CO₂ conversion, Appl. Catal. B Environ. 225 (2018) 128–138, <https://doi.org/10.1016/j.apcatb.2017.11.047>.
- [134] H. Li, S. Gan, H. Wang, D. Han, L. Niu, Interrelated superhybrid of AgBr supported on graphitic-C₃N₄-decorated nitrogen-doped graphene: high engineering photocatalytic activities for water purification and CO₂ reduction, Adv. Mater. 27 (2015) 6906–6913, <https://doi.org/10.1002/adma.201502755>.
- [135] J.A.H. Dreyer, P. Li, L. Zhang, G.K. Beh, R. Zhang, P.H.-L. Sit, W.Y. Teoh, Influence of the oxide support reducibility on the CO₂ methanation over Ru-based catalysts, Appl. Catal. B Environ. 219 (2017) 715–726, <https://doi.org/10.1016/j.apcatb.2017.08.011>.
- [136] J. Dou, Y. Sheng, C. Choong, L. Chen, H.C. Zeng, Silica nanowires encapsulated Ru nanoparticles as stable nanocatalysts for selective hydrogenation of CO₂ to CO, Appl. Catal. B Environ. 219 (2017) 580–591, <https://doi.org/10.1016/j.apcatb.2017.07.083>.
- [137] B. László, K. Báán, E. Varga, A. Oszkó, A. Erdőhelyi, Z. Kónya, J. Kiss, Photo-induced reactions in the CO₂-methane system on titanate nanotubes modified with Au and Rh nanoparticles, Appl. Catal. B Environ. 199 (2016) 473–484, <https://doi.org/10.1016/j.apcatb.2016.06.057>.
- [138] X. Jiang, N. Koizumi, X. Guo, C. Song, Bimetallic Pd-Cu catalysts for selective CO₂ hydrogenation to methanol, Appl. Catal. B Environ. 170–171 (2015) 173–185, <https://doi.org/10.1016/j.apcatb.2015.01.010>.
- [139] K. Sun, T. Cheng, L. Wu, Y. Hu, J. Zhou, A. MacLennan, Z. Jiang, Y. Gao, W.A. Goddard, Z. Wang, Ultrahigh mass activity for carbon dioxide reduction enabled by gold-iron core-shell nanoparticles, J. Am. Chem. Soc. 139 (2017) 15608–15611, <https://doi.org/10.1021/jacs.7b09251>.
- [140] J. Lin, C. Ma, Q. Wang, Y. Xu, G. Ma, J. Wang, H. Wang, C. Dong, C. Zhang, M. Ding, Enhanced low-temperature performance of CO₂ methanation over mesoporous Ni/Al₂O₃-ZrO₂ catalysts, Appl. Catal. B Environ. 243 (2019) 262–272, <https://doi.org/10.1016/j.apcatb.2018.10.059>.
- [141] X. Jia, X. Zhang, N. Rui, X. Hu, C. Liu, Structural effect of Ni/ZrO₂ catalyst on CO₂ methanation with enhanced activity, Appl. Catal. B Environ. 244 (2019) 159–169, <https://doi.org/10.1016/j.apcatb.2018.11.024>.
- [142] F. Wang, B. Han, L. Zhang, L. Xu, H. Yu, W. Shi, CO₂ reforming with methane over small-sized Ni/SiO₂ catalysts with unique features of sintering-free and low carbon, Appl. Catal. B Environ. 235 (2018) 26–35, <https://doi.org/10.1016/j.apcatb.2018.04.069>.
- [143] Y. Yan, Y. Dai, Y. Yang, A.A. Lapkin, Improved stability of Y₂O₃ supported Ni catalysts for CO₂ methanation by precursor-determined metal-support interaction, Appl. Catal. B Environ. 237 (2018) 504–512, <https://doi.org/10.1016/j.apcatb.2018.06.021>.
- [144] L. Lu, Z. Xin, X. Wang, S. Wang, H. Zhu, T. Li, Y. Gu, S. Yan, Z. Zou, KOH-modified Ni/LaTiO₂N Schottky junction efficiently reducing CO₂ to CH₄ under visible light irradiation, Appl. Catal. B Environ. 244 (2019) 786–794, <https://doi.org/10.1016/j.apcatb.2018.12.002>.
- [145] H. Inoue, H. Moriwaki, K. Maeda, H. Yoneyama, Photoreduction of carbon dioxide using chalcogenide semiconductor microcrystals, J. Photochem. Photobiol. A Chem. 86 (1995) 191–196, [https://doi.org/10.1016/1010-6030\(94\)03936-O](https://doi.org/10.1016/1010-6030(94)03936-O).
- [146] M. Liang, T. Borjigin, Y. Zhang, B. Liu, H. Liu, H. Guo, Controlled assemble of hollow heterostructured g-C₃N₄@CeO₂ with rich oxygen vacancies for enhanced photocatalytic CO₂ reduction, Appl. Catal. B Environ. 243 (2019) 566–575, <https://doi.org/10.1016/j.apcatb.2018.11.010>.
- [147] K. Kočí, V. Matějka, P. Kovář, Z. Lacný, L. Obalová, Comparison of the pure TiO₂ and kaolinite/TiO₂ composite as catalyst for CO₂ photocatalytic reduction, Catal. Today 161 (2011) 105–109, <https://doi.org/10.1016/j.cattod.2010.08.026>.
- [148] S. Bernadet, E. Tavernier, D.-M. Ta, R.A.L. Vallée, S. Ravaine, A. Fécant, R. Backov, Bulk photodriven CO₂ conversion through TiO₂@Si(HIPE) monolithic macrocellular foams, Adv. Funct. Mater. (2019) 1807767, <https://doi.org/10.1002/adfm.201807767>.
- [149] A. Olivo, V. Trevisan, E. Ghedini, F. Pinna, C.L. Bianchi, A. Naldoni, G. Cruciani, M. Signoretto, CO₂ photoreduction with water: Catalyst and process investigation, J. CO₂ Util. 12 (2015) 86–94, <https://doi.org/10.1016/j.jcou.2015.06.001>.
- [150] B. Fang, Y. Xing, A. Bonakdarpour, S. Zhang, D.P. Wilkinson, Hierarchical CuO-TiO₂ hollow microspheres for highly efficient photodriven reduction of CO₂ to CH₄, ACS Sustain. Chem. Eng. 3 (2015) 2381–2388, <https://doi.org/10.1021/acsschemeng.5b00724>.
- [151] W. Kim, H. Frei, Directed assembly of cuprous oxide nanocatalyst for CO₂ reduction coupled to heterobinuclear ZrOCo^{II} light absorber in mesoporous silica, ACS Catal. 5 (2015) 5627–5635, <https://doi.org/10.1021/acscatal.5b01306>.
- [152] H.-C. Hsu, I. Shown, H.-Y. Wei, Y.-C. Chang, H.-Y. Du, Y.-G. Lin, C.-A. Tseng, C.-H. Wang, L.-C. Chen, Y.-C. Lin, K.-H. Chen, Graphene oxide as a promising photocatalyst for CO₂ to methanol conversion, Nanoscale 5 (2013) 262–268, <https://doi.org/10.1039/C2NR31718D>.
- [153] W. Tu, Y. Zhou, Q. Liu, Z. Tian, J. Gao, X. Chen, H. Zhang, J. Liu, Z. Zou, Robust hollow spheres consisting of alternating titania nanosheets and graphene nanosheets with high photocatalytic activity for CO₂ conversion into renewable fuels, Adv. Funct. Mater. 22 (2012) 1215–1221, <https://doi.org/10.1002/adfm.201102566>.
- [154] W. Tu, Y. Zhou, Q. Liu, S. Yan, S. Bao, X. Wang, M. Xiao, Z. Zou, An in situ simultaneous reduction-hydrolysis technique for fabrication of TiO₂-Graphene 2D sandwich-like hybrid nanosheets: graphene-promoted selectivity of photocatalytic-driven hydrogenation and coupling of CO₂ into methane and ethane, Adv. Funct. Mater. 23 (2013) 1743–1749, <https://doi.org/10.1002/adfm.201202349>.
- [155] P.-Q. Wang, Y. Bai, P.-Y. Luo, J.-Y. Liu, Graphene-WO₃ nanobelt composite: elevated conduction band toward photocatalytic reduction of CO₂ into hydrocarbon fuels, Catal. Commun. 38 (2013) 82–85, <https://doi.org/10.1016/j.jcatcom.2013.04.020>.
- [156] P. Kumar, C. Joshi, A. Barras, B. Sieber, A. Addad, L. Boussekey, S. Szunerits, R. Boukherroub, S.L. Jain, Core-shell structured reduced graphene oxide wrapped magnetically separable rGO@CuZnO/Fe₃O₄ microspheres as superior photocatalyst for CO₂ reduction under visible light, Appl. Catal. B Environ. 205 (2017) 654–665, <https://doi.org/10.1016/j.apcatb.2016.11.060>.
- [157] Z. Li, X. Meng, Z. Zhang, Recent development on MoS₂-based photocatalysis: a review, J. Photochem. Photobiol. C Photochem. Rev. 35 (2018) 39–55, <https://doi.org/10.1016/j.jphotochemrev.2017.12.002>.
- [158] Y. Wang, Z. Zhang, L. Zhang, Z. Luo, J. Shen, H. Lin, J. Long, J.C.S. Wu, X. Fu, X. Wang, C. Li, Visible-light driven overall conversion of CO₂ and H₂O to CH₄ and O₂ on 3D-SiC@2D-MoS₂ heterostructure, J. Am. Chem. Soc. 140 (2018) 14595–14598, <https://doi.org/10.1021/jacs.8b09344>.
- [159] F. Xu, B. Zhu, B. Cheng, J. Yu, J. Xu, 1D/2D TiO₂/MoS₂ hybrid nanostructures for enhanced photocatalytic CO₂ reduction, Adv. Opt. Mater. 6 (2018) 1800911, <https://doi.org/10.1002/adom.201800911>.
- [160] F. Chen, H. Huang, L. Ye, T. Zhang, Y. Zhang, X. Han, T. Ma, Thickness-dependent facet junction control of layered BiOI₂ single crystals for highly efficient CO₂ photoreduction, Adv. Funct. Mater. 28 (2018) 1804284, <https://doi.org/10.1002/adfm.201804284>.
- [161] J. Jin, T. He, Facile synthesis of Bi₂S₃ nanoribbons for photocatalytic reduction of

- CO₂ into CH₃OH, *Appl. Surf. Sci.* 394 (2017) 364–370, <https://doi.org/10.1016/J.APSUSC.2016.10.118>.
- [162] S. Xie, Z. Shen, H. Zhang, J. Cheng, Q. Zhang, Y. Wang, Photocatalytic coupling of formaldehyde to ethylene glycol and glycolaldehyde over bismuth vanadate with controllable facets and cocatalysts, *Catal. Sci. Technol.* 7 (2017) 923–933, <https://doi.org/10.1039/C6CY02510B>.
- [163] Y. Bai, L. Ye, T. Chen, P. Wang, L. Wang, X. Shi, P.K. Wong, Synthesis of hierarchical bismuth-rich Bi₄O₅Br₃I_{2-x} solid solutions for enhanced photocatalytic activities of CO₂ conversion and Cr(VI) reduction under visible light, *Appl. Catal. B Environ.* 203 (2017) 633–640, <https://doi.org/10.1016/J.APCATB.2016.10.066>.
- [164] M. Gao, J. Yang, T. Sun, Z. Zhang, D. Zhang, H. Huang, H. Lin, Y. Fang, X. Wang, Persian buttercup-like BiOBr_xCl_{1-x} solid solution for photocatalytic overall CO₂ reduction to CO and O₂, *Appl. Catal. B Environ.* 243 (2019) 734–740, <https://doi.org/10.1016/J.APCATB.2018.11.020>.
- [165] S. Gao, B. Gu, X. Jiao, Y. Sun, X. Zu, F. Yang, W. Zhu, C. Wang, Z. Feng, B. Ye, Y. Xie, Highly efficient and exceptionally durable CO₂ photoreduction to methanol over freestanding defective single-unit-Cell bismuth vanadate layers, *J. Am. Chem. Soc.* 139 (2017) 3438–3445, <https://doi.org/10.1021/jacs.6b11263>.
- [166] L. Ye, X. Jin, C. Liu, C. Ding, H. Xie, K.H. Chu, P.K. Wong, Thickness-ultrathin and bismuth-rich strategies for BiOBr to enhance photoreduction of CO₂ into solar fuels, *Appl. Catal. B Environ.* 187 (2016) 281–290, <https://doi.org/10.1016/J.APCATB.2016.01.044>.
- [167] H. Yang, N. Han, J. Deng, J. Wu, Y. Wang, Y. Hu, P. Ding, Y. Li, Y. Li, J. Lu, Selective CO₂ reduction on 2D mesoporous Bi nanosheets, *Adv. Energy Mater.* 8 (2018) 1801536, <https://doi.org/10.1002/aenm.201801536>.
- [168] L. Yuan, K.-Q. Lu, F. Zhang, X. Fu, Y.-J. Xu, Unveiling the interplay between light-driven CO₂ photocatalytic reduction and carbonaceous residues decomposition: a case study of Bi₂WO₆/TiO₂ binanosheets, *Appl. Catal. B Environ.* 237 (2018) 424–431, <https://doi.org/10.1016/J.APCATB.2018.06.019>.
- [169] L. Ye, H. Wang, X. Jin, Y. Su, D. Wang, H. Xie, X. Liu, X. Liu, Synthesis of olive-green few-layered BiOI for efficient photoreduction of CO₂ into solar fuels under visible/near-infrared light, *Sol. Energy Mater. Sol. Cells* 144 (2016) 732–739, <https://doi.org/10.1016/J.SOLMAT.2015.10.022>.
- [170] S. Cao, B. Shen, T. Tong, J. Fu, J. Yu, 2D/2D heterojunction of ultrathin MXene/Bi₂WO₆ nanosheets for improved photocatalytic CO₂ reduction, *Adv. Funct. Mater.* 28 (2018) 1800136, <https://doi.org/10.1002/adfm.201800136>.
- [171] S. Ijaz, M.F. Ehsan, M.N. Ashiq, T. He, Synthesis of a Bi₂S₃/CeO₂ nanocatalyst and its visible light-driven conversion of CO₂ into CH₃OH and CH₄, *Catal. Sci. Technol.* 5 (2015) 5208–5215, <https://doi.org/10.1039/C5CY00955C>.
- [172] X. Li, J. Chen, H. Li, J. Li, Y. Xu, Y. Liu, J. Zhou, Photoreduction of CO₂ to methanol over Bi₂S₃/CdS photocatalyst under visible light irradiation, *J. Nat. Gas Chem.* 20 (2011) 413–417, [https://doi.org/10.1016/S1003-9953\(10\)60212-5](https://doi.org/10.1016/S1003-9953(10)60212-5).
- [173] H. Li, J. Li, Z. Ai, F. Jia, L. Zhang, Oxygen vacancy-mediated photocatalysis of BiOCl: reactivity, selectivity, and perspectives, *Angew. Chemie Int. Ed.* 57 (2018) 122–138, <https://doi.org/10.1002/anie.201705628>.
- [174] Z. Lei, Y. Xue, W. Chen, W. Qiu, Y. Zhang, S. Horike, L. Tang, MOFs-based heterogeneous catalysts: new opportunities for energy-related CO₂ conversion, *Adv. Energy Mater.* 8 (2018) 1801587, <https://doi.org/10.1002/aenm.201801587>.
- [175] S. Wang, X. Wang, Multifunctional metal-organic frameworks for photocatalysis, *Small* 11 (2015) 3097–3112, <https://doi.org/10.1002/smll.201500084>.
- [176] W. Yang, X. Li, Y. Li, R. Zhu, H. Pang, Applications of metal-organic-framework-derived carbon materials, *Adv. Mater.* (2018) 1804740, <https://doi.org/10.1002/adma.201804740>.
- [177] I.I. Alkhatib, C. Garlisi, M. Pagliaro, K. Al-Ali, G. Palmisano, Metal-organic frameworks for photocatalytic CO₂ reduction under visible radiation: a review of strategies and applications, *Catal. Today* (2018), <https://doi.org/10.1016/J.CATTOD.2018.09.032>.
- [178] A. Dhakshinamoorthy, A.M. Asiri, H. García, Metal-organic framework (MOF) compounds: photocatalysts for redox reactions and solar fuel production, *Angew. Chemie Int. Ed.* 55 (2016) 5414–5445, <https://doi.org/10.1002/anie.201505581>.
- [179] M. Liu, Y.-F. Mu, S. Yao, S. Guo, X.-W. Guo, Z.-M. Zhang, T.-B. Lu, Photosensitizing single-site metal-organic framework enabling visible-light-driven CO₂ reduction for syngas production, *Appl. Catal. B Environ.* 245 (2019) 496–501, <https://doi.org/10.1016/J.APCATB.2019.01.014>.
- [180] R. Li, W. Zhang, K. Zhou, Metal-organic-Framework-Based catalysts for photoreduction of CO₂, *Adv. Mater.* 30 (2018) 1705512, <https://doi.org/10.1002/adma.201705512>.
- [181] L. Jiao, Y. Wang, H.-L. Jiang, Q. Xu, Metal-organic frameworks as platforms for catalytic applications, *Adv. Mater.* 30 (2018) 1703663, <https://doi.org/10.1002/adma.201703663>.
- [182] S. Sato, T. Arai, T. Morikawa, K. Uemura, T.M. Suzuki, H. Tanaka, T. Kajino, Selective CO₂ conversion to formate conjugated with H₂O oxidation utilizing semiconductor/complex hybrid photocatalysts, *J. Am. Chem. Soc.* 133 (2011) 15240–15243, <https://doi.org/10.1021/ja204881d>.
- [183] W. Chen, B. Han, C. Tian, X. Liu, S. Liang, H. Deng, Z. Lin, MOFs-derived ultrathin holey Co₃O₄ nanosheets for enhanced visible light CO₂ reduction, *Appl. Catal. B Environ.* 244 (2019) 996–1003, <https://doi.org/10.1016/J.APCATB.2018.12.045>.
- [184] A. Crake, K.C. Christoforidis, A. Kafizas, S. Zafeirotas, C. Petit, CO₂ capture and photocatalytic reduction using bifunctional TiO₂/MOF nanocomposites under UV-vis irradiation, *Appl. Catal. B Environ.* 210 (2017) 131–140, <https://doi.org/10.1016/J.APCATB.2017.03.039>.
- [185] D. Sun, L. Ye, Z. Li, Visible-light-assisted aerobic photocatalytic oxidation of amines to imines over NH₂-MIL-125(Ti), *Appl. Catal. B Environ.* 164 (2015) 428–432, <https://doi.org/10.1016/J.APCATB.2014.09.054>.
- [186] H.-Q. Xu, J. Hu, D. Wang, Z. Li, Q. Zhang, Y. Luo, S.-H. Yu, H.-L. Jiang, Visible-light photoreduction of CO₂ in a metal-organic framework: boosting electron-hole separation via electron trap states, *J. Am. Chem. Soc.* 137 (2015) 13440–13443, <https://doi.org/10.1021/jacs.5b08773>.
- [187] X. Liu, S. Inagaki, J. Gong, Heterogeneous molecular systems for photocatalytic CO₂ reduction with water oxidation, *Angew. Chemie - Int. Ed.* 55 (2016) 14924–14950, <https://doi.org/10.1002/anie.201600395>.
- [188] K. Li, B. Peng, T. Peng, Recent advances in heterogeneous photocatalytic CO₂ conversion to solar fuels, *ACS Catal.* 6 (2016) 7485–7527, <https://doi.org/10.1021/acscatal.6b02089>.
- [189] R.K. Yadav, G.H. Oh, N.-J. Park, A. Kumar, K. Kong, J.-O. Baeg, Highly selective solar-driven methanol from CO₂ by a Photocatalyst/Biocatalyst integrated system, *J. Am. Chem. Soc.* 136 (2014) 16728–16731, <https://doi.org/10.1021/ja509650r>.
- [190] X. Ji, J. Wang, L. Mei, W. Tao, A. Barrett, Z. Su, S. Wang, G. Ma, J. Shi, S. Zhang, Porphyrin/SiO₂/Cp*⁺Rh(bpy)Cl hybrid nanoparticles mimicking chloroplast with enhanced electronic energy transfer for biocatalyzed artificial photosynthesis, *Adv. Funct. Mater.* 28 (2018) 1705083, <https://doi.org/10.1002/adfm.201705083>.
- [191] H.-J. Freund, M.W. Roberts, Surface chemistry of carbon dioxide, *Surf. Sci. Rep.* 25 (1996) 225–273, [https://doi.org/10.1016/S0167-5729\(96\)00007-6](https://doi.org/10.1016/S0167-5729(96)00007-6).
- [192] H.-J. Freund, R.P. Messmer, On the bonding and reactivity of CO₂ on metal surfaces, *Surf. Sci.* 172 (1986) 1–30, [https://doi.org/10.1016/0039-6028\(86\)90580-7](https://doi.org/10.1016/0039-6028(86)90580-7).
- [193] V.P. Indrakanti, J.D. Kubicki, H.H. Schobert, Photoinduced activation of CO₂ on Ti-based heterogeneous catalysts: Current state, chemical physics-based insights and outlook, *Energy Environ. Sci.* 2 (2009) 745–758, <https://doi.org/10.1039/b822176f>.
- [194] H. He, P. Zapol, L.A. Curtiss, Computational screening of dopants for photocatalytic two-electron reduction of CO₂ on anatase (101) surfaces, *Energy Environ. Sci.* 5 (2012) 6196–6205, <https://doi.org/10.1039/c2ee02665a>.
- [195] S. Neatu, J.A. Maciá-Agulló, P. Concepción, H. García, Gold-Copper nanoalloys supported on TiO₂ as photocatalysts for CO₂ reduction by water, *J. Am. Chem. Soc.* 136 (2014) 15969–15976, <https://doi.org/10.1021/ja506433k>.
- [196] S.S. Tan, L. Zou, E. Hu, Kinetic modelling for photosynthesis of hydrogen and methane through catalytic reduction of carbon dioxide with water vapour, *Catal. Today* 131 (2008) 125–129, <https://doi.org/10.1016/J.CATTOD.2007.10.011>.
- [197] Slamet, H.W. Nasution, E. Purnama, S. Kosela, J. Gunlazuardi, Photocatalytic reduction of CO₂ on copper-doped Titania catalysts prepared by improved-impregnation method, *Catal. Commun.* 6 (2005) 313–319, <https://doi.org/10.1016/J.CATCOM.2005.01.011>.
- [198] S.C. Yan, S.X. Ouyang, J. Gao, M. Yang, J.Y. Feng, X.X. Fan, L.J. Wan, Z.S. Li, J.H. Ye, Y. Zhou, Z.G. Zou, A room-temperature reactive-template route to mesoporous ZnGa₂O₄ with improved photocatalytic activity in reduction of CO₂, *Angew. Chemie Int. Ed.* 49 (2010) 6400–6404, <https://doi.org/10.1002/anie.201003270>.
- [199] Y. Hori, K. Kikuchi, S. Suzuki, Production of CO and CH₄ in electrochemical reduction of CO₂ at metal electrodes in aqueous hydrogencarbonate solution, *Chem. Lett.* 14 (1985) 1695–1698, <https://doi.org/10.1246/cl.1985.1695>.
- [200] Y. Hori, K. Kikuchi, A. Murata, S. Suzuki, Production of methane and ethylene in electrochemical reduction of carbon dioxide at copper electrode in aqueous hydrogencarbonate solution, *Chem. Lett.* 15 (1986) 897–898, <https://doi.org/10.1246/cl.1986.897>.
- [201] W.-N. Wang, W.-J. An, B. Ramalingam, S. Mukherjee, D.M. Niedzwiedzki, S. Gangopadhyay, P. Biswas, Size and structure matter: enhanced CO₂ photoreduction efficiency by size-resolved ultrafine Pt nanoparticles on TiO₂ single crystals, *J. Am. Chem. Soc.* 134 (2012) 11276–11281, <https://doi.org/10.1021/ja304075b>.
- [202] Keita Ikeue, A. Hiromi Yamashita, M. Anpo, T. Takekoshi, Photocatalytic reduction of CO₂ with H₂O on Ti-β zeolite photocatalysts: effect of the hydrophobic and hydrophilic properties, *J. Phys. Chem. B* 105 (2001) 8350–8355, <https://doi.org/10.1021/JP010885G>.
- [203] K. Mori, H. Yamashita, M. Anpo, Photocatalytic reduction of CO₂ with H₂O on various titanium oxide photocatalysts, *RSC Adv.* 2 (2012) 3165–3172, <https://doi.org/10.1039/c2ra01332k>.
- [204] Y. Liao, S.-W. Cao, Y. Yuan, Q. Gu, Z. Zhang, C. Xue, Efficient CO₂ capture and photoreduction by amine-functionalized TiO₂, *Chem. - A Eur. J.* 20 (2014) 10220–10222, <https://doi.org/10.1002/chem.201403321>.
- [205] Y. Hori, A. Murata, R. Takahashi, Formation of hydrocarbons in the electrochemical reduction of carbon dioxide at a copper electrode in aqueous solution, *J. Chem. Soc. Faraday Trans. 1 Phys. Chem. Condens. Phases* 85 (1989) 2309–2326, <https://doi.org/10.1039/f19898502309>.
- [206] P. Wardman, Reduction potentials of one-electron couples involving free radicals in aqueous solution, *J. Phys. Chem. Ref. Data* 18 (1989) 1637–1755, <https://doi.org/10.1063/1.555843>.
- [207] T. Hirakawa, C. Koga, N. Negishi, K. Takeuchi, S. Matsuzawa, An approach to elucidating photocatalytic reaction mechanisms by monitoring dissolved oxygen: effect of H₂O₂ on photocatalysis, *Appl. Catal. B Environ.* 87 (2009) 46–55, <https://doi.org/10.1016/J.APCATB.2008.08.027>.
- [208] T. Kawai, T. Sakata, Conversion of carbohydrate into hydrogen fuel by a photocatalytic process, *Nature* 286 (1980) 474–476, <https://doi.org/10.1038/286474a0>.
- [209] F.H. Hussein, G. Pattenden, R. Rudham, J.J. Russell, Photo-oxidation of alcohols catalysed by platinumised titanium dioxide, *Tetrahedron Lett.* 25 (1984) 3363–3364, [https://doi.org/10.1016/S0040-4039\(01\)81385-X](https://doi.org/10.1016/S0040-4039(01)81385-X).
- [210] F.H. Hussein, R. Rudham, Photocatalytic dehydrogenation of liquid propan-2-ol by platinumized anatase and other catalysts, *J. Chem. Soc. Faraday Trans. 1 Phys. Chem. Condens. Phases* 80 (1984) 2817–2825, <https://doi.org/10.1039/f19848002817>.
- [211] C. Wang, R. Pagel, D.W. Bahnemann, J.K. Dohrmann, Quantum yield of

- formaldehyde formation in the presence of colloidal TiO₂-based photocatalysts: effect of intermittent illumination, platinization, and deoxygenation, *J. Phys. Chem. B* 108 (2004) 14082–14092, <https://doi.org/10.1021/JP048046S>.
- [212] S. Furukawa, T. Shishido, K. Teramura, T. Tanaka, Photocatalytic Oxidation of Alcohols over TiO₂ Covered with Nb₂O₅, *ACS Catal.* 2 (2012) 175–179, <https://doi.org/10.1021/cs2005554>.
- [213] L.-M. Zhao, Q.-Y. Meng, X.-B. Fan, C. Ye, X.-B. Li, B. Chen, V. Ramamurthy, C.-H. Tung, L.-Z. Wu, Photocatalysis with quantum dots and visible light: selective and efficient oxidation of alcohols to carbonyl compounds through a radical relay process in water, *Angew. Chemie Int. Ed.* 56 (2017) 3020–3024, <https://doi.org/10.1002/anie.201700243>.
- [214] L. Chen, J. Tang, L.-N. Song, P. Chen, J. He, C.-T. Au, S.-F. Yin, Heterogeneous photocatalysis for selective oxidation of alcohols and hydrocarbons, *Appl. Catal. B Environ.* 242 (2019) 379–388, <https://doi.org/10.1016/j.apcatb.2018.10.025>.
- [215] M. Fujihira, Y. Satoh, T. Osa, Heterogeneous photocatalytic oxidation of aromatic compounds on TiO₂, *Nature* 293 (1981) 206–208, <https://doi.org/10.1038/293206a0>.
- [216] K.R. Phillips, S.C. Jensen, M. Baron, S.-C. Li, C.M. Friend, Sequential photo-oxidation of methanol to methyl formate on TiO₂ (110), *J. Am. Chem. Soc.* 135 (2013) 574–577, <https://doi.org/10.1021/ja3106797>.
- [217] A. Tanaka, K. Hashimoto, H. Kominami, Selective photocatalytic oxidation of aromatic alcohols to aldehydes in an aqueous suspension of gold nanoparticles supported on cerium(IV) oxide under irradiation of green light, *Chem. Commun.* 47 (2011) 10446–10448, <https://doi.org/10.1039/c1cc13801d>.
- [218] A. Tanaka, K. Hashimoto, H. Kominami, Preparation of Au/CeO₂ exhibiting strong surface plasmon resonance effective for selective or chemoselective oxidation of alcohols to aldehydes or ketones in aqueous suspensions under irradiation by green light, *J. Am. Chem. Soc.* 134 (2012) 14526–14533, <https://doi.org/10.1021/ja305225s>.
- [219] A. Maldotti, A. Molinari, R. Juárez, H. Garcia, Photoinduced reactivity of Au–H intermediates in alcohol oxidation by gold nanoparticles supported on ceria, *Chem. Sci.* 2 (2011) 1831–1834, <https://doi.org/10.1039/c1sc00283j>.
- [220] G.L. Hallett-Tapley, M.J. Silvero, M. González-Béjar, M. Grenier, J.C. Netto-Ferreira, J.C. Scaiano, Plasmon-mediated catalytic oxidation of *sec*-Phenethyl and benzyl alcohols, *J. Phys. Chem. C* 115 (2011) 10784–10790, <https://doi.org/10.1021/jp202769a>.
- [221] B. Li, B. Zhang, S. Nie, L. Shao, L. Hu, Optimization of plasmon-induced photocatalysis in electrospon Au/CeO₂ hybrid nanofibers for selective oxidation of benzyl alcohol, *J. Catal.* 348 (2017) 256–264, <https://doi.org/10.1016/j.jcat.2016.12.025>.
- [222] D. Tsukamoto, Y. Shiraishi, Y. Sugano, S. Ichikawa, S. Tanaka, T. Hirai, Gold Nanoparticles Located at the Interface of Anatase/Rutile TiO₂ Particles as Active Plasmonic Photocatalysts for Aerobic Oxidation, *J. Am. Chem. Soc.* 134 (2012) 6309–6315, <https://doi.org/10.1021/ja2120647>.
- [223] W. Zhang, E. Fernández-Fuero, Y. Ni, M. van Schie, J. Gacs, R. Renirie, R. Wever, F.G. Mutti, D. Rother, M. Alcalde, F. Hollmann, Selective aerobic oxidation reactions using a combination of photocatalytic water oxidation and enzymatic oxyfunctionalizations, *Nat. Catal.* 1 (2018) 55–62, <https://doi.org/10.1038/s41929-017-0001-5>.
- [224] Y. Ide, M. Matsuoka, M. Ogawa, Efficient visible-light-induced photocatalytic activity on gold-nanoparticle-supported layered titanate, *J. Am. Chem. Soc.* 132 (2010) 16762–16764, <https://doi.org/10.1021/ja1083514>.
- [225] Z. Zheng, B. Huang, X. Qin, X. Zhang, Y. Dai, M.-H. Whangbo, Facile in situ synthesis of visible-light plasmonic photocatalysts M@TiO₂ (M = Au, Pt, Ag) and evaluation of their photocatalytic oxidation of benzene to phenol, *J. Mater. Chem.* 21 (2011) 9079–9087, <https://doi.org/10.1039/c1jm10983a>.
- [226] S. Naya, A. Inoue, H. Tada, Self-assembled heterosupramolecular visible light photocatalyst consisting of gold nanoparticle-loaded titanium(IV) dioxide and surfactant, *J. Am. Chem. Soc.* 132 (2010) 6292–6293, <https://doi.org/10.1021/ja101711j>.
- [227] X. Cao, Z. Chen, R. Lin, W.-C. Cheong, S. Liu, J. Zhang, Q. Peng, C. Chen, T. Han, X. Tong, Y. Wang, R. Shen, W. Zhu, D. Wang, Y. Li, A photochromic composite with enhanced carrier separation for the photocatalytic activation of benzylic C–H bonds in toluene, *Nat. Catal.* 1 (2018) 704–710, <https://doi.org/10.1038/s41929-018-0128-z>.
- [228] S. Sarina, S. Bai, Y. Huang, C. Chen, J. Jia, E. Jaatinen, G.A. Ayoko, Z. Bao, H. Zhu, Visible light enhanced oxidant free dehydrogenation of aromatic alcohols using Au–Pd alloy nanoparticle catalysts, *Green Chem.* 16 (2014) 331–341, <https://doi.org/10.1039/C3GC41866A>.
- [229] S. Sarina, H. Zhu, E. Jaatinen, Q. Xiao, H. Liu, J. Jia, C. Chen, J. Zhao, Enhancing catalytic performance of palladium in gold and palladium alloy nanoparticles for organic synthesis reactions through visible light irradiation at ambient temperatures, *J. Am. Chem. Soc.* 135 (2013) 5793–5801, <https://doi.org/10.1021/ja400527a>.
- [230] J. Guiard, E. Paszkiewicz, J. Sadowska, D.R. Bundle, Design and synthesis of a universal antigen to detect brucellosis, *Angew. Chemie Int. Ed.* 52 (2013) 7181–7185, <https://doi.org/10.1002/anie.201302303>.
- [231] N. Zhang, M.-Q. Yang, Z.-R. Tang, Y.-J. Xu, CdS–graphene nanocomposites as visible light photocatalyst for redox reactions in water: a green route for selective transformation and environmental remediation, *J. Catal.* 303 (2013) 60–69, <https://doi.org/10.1016/j.jcat.2013.02.026>.
- [232] N. Zhang, M.-Q. Yang, Z.-R. Tang, Y.-J. Xu, Toward improving the graphene–semiconductor composite photoactivity by the addition of metal ions as generic interfacial mediator, *ACS Nano* 8 (2014) 623–633, <https://doi.org/10.1021/nn405242t>.
- [233] Y. Zhang, Z.-R. Tang, X. Fu, Y.-J. Xu, Engineering the unique 2D Mat of graphene to achieve graphene–TiO₂ nanocomposite for photocatalytic selective transformation: what advantage does graphene have over its forebear carbon nanotube? *ACS Nano* 5 (2011) 7426–7435, <https://doi.org/10.1021/nn202519j>.
- [234] N. Zhang, Y. Zhang, X. Pan, M.-Q. Yang, Y.-J. Xu, Constructing ternary CdS–graphene–TiO₂ hybrids on the flatland of graphene oxide with enhanced visible-light photoactivity for selective transformation, *J. Phys. Chem. C* 116 (2012) 18023–18031, <https://doi.org/10.1021/jp303503c>.
- [235] J. Xie, R. Jin, A. Li, Y. Bi, Q. Ruan, Y. Deng, Y. Zhang, S. Yao, G. Sankar, D. Ma, J. Tang, Highly selective oxidation of methane to methanol at ambient conditions by titanium dioxide-supported iron species, *Nat. Catal.* 1 (2018) 889–896, <https://doi.org/10.1038/s41929-018-0170-x>.
- [236] R. Rinaldi, R. Jastrzebski, M.T. Clough, J. Ralph, M. Kennema, P.C.A. Bruijninx, B.M. Weckhuysen, Paving the way for lignin valorisation: recent advances in bioengineering, biorefining and catalysis, *Angew. Chemie Int. Ed.* 55 (2016) 8164–8215, <https://doi.org/10.1002/anie.201510351>.
- [237] X. Wu, X. Pan, S. Xie, J. Lin, J. Cheng, Q. Zhang, L. Chen, Y. Wang, Solar energy-driven lignin-first approach to full utilization of lignocellulosic biomass under mild conditions, *Nat. Catal.* 1 (2018) 772–780, <https://doi.org/10.1038/s41929-018-0148-8>.
- [238] F. Raza, D. Yim, J.H. Park, H.-I. Kim, S.-J. Jeon, J.-H. Kim, Structuring Pd nanoparticles on 2H-WS₂ nanosheets induces excellent photocatalytic activity for cross-coupling reactions under visible light, *J. Am. Chem. Soc.* 139 (2017) 14767–14774, <https://doi.org/10.1021/jacs.7b08619>.
- [239] S. Xie, Z. Shen, J. Deng, P. Guo, Q. Zhang, H. Zhang, C. Ma, Z. Jiang, J. Cheng, D. Deng, Y. Wang, Visible light-driven C–H activation and C–C coupling of methanol into ethylene glycol, *Nat. Commun.* 9 (2018) 1–7, <https://doi.org/10.1038/s41467-018-03543-y>.
- [240] A. Micek-Ilnicka, E. Bielańska, L. Lityńska-Dobrzyńska, A. Bielański, Carbon nanotubes, silica and titania supported heteropolyacid H₃PW₁₂O₄₀ as the catalyst for ethanol conversion, *Appl. Catal. A Gen.* 421–422 (2012) 91–98, <https://doi.org/10.1016/j.apcatb.2012.02.001>.
- [241] Y. Huang, Z. Liu, G. Gao, G. Xiao, A. Du, S. Bottle, S. Sarina, H. Zhu, Stable copper nanoparticle photocatalysts for selective epoxidation of alkenes with visible light, *ACS Catal.* 7 (2017) 4975–4985, <https://doi.org/10.1021/acscatal.7b01180>.
- [242] P. Christopher, H. Xin, S. Linic, Visible-light-enhanced catalytic oxidation reactions on plasmonic silver nanostructures, *Nat. Chem.* 3 (2011) 467–472, <https://doi.org/10.1038/nchem.1032>.
- [243] Y. Zhang, N. Zhang, Z.-R. Tang, Y.-J. Xu, Graphene transforms wide band gap ZnS to a visible light photocatalyst. The new role of graphene as a macromolecular photosensitizer, *ACS Nano* 6 (2012) 9777–9789, <https://doi.org/10.1021/nn304154s>.
- [244] A. Marimuthu, J. Zhang, S. Linic, Tuning selectivity in propylene epoxidation by plasmon mediated photo-switching of Cu oxidation state, *Science* 339 (2013) 1590–1593, <https://doi.org/10.1126/science.1231631>.
- [245] B. Ohtani, H. Osaki, S. Nishimoto, T. Kagiya, A redox combined photocatalysis: new method of N-alkylation of ammonia by TiO₂/Pt suspended in alcohols, *Tetrahedron Lett.* 27 (1986) 2019–2022, [https://doi.org/10.1016/S0040-4039\(00\)84437-8](https://doi.org/10.1016/S0040-4039(00)84437-8).
- [246] H. Reiche, A.J. Bard, Heterogeneous photosynthetic production of amino acids from methane–ammonia–water at platinum/titanium dioxide. Implications in chemical evolution, *J. Am. Chem. Soc.* 101 (1979) 3127–3128, <https://doi.org/10.1021/ja00505a054>.
- [247] W.W. Dunn, Y. Aikawa, A.J. Bard, Heterogeneous photosynthetic production of amino acids at platinum/titanium dioxide suspensions by near ultraviolet light, *J. Am. Chem. Soc.* 103 (1981) 6893–6897, <https://doi.org/10.1021/ja00413a020>.
- [248] J. Onoe, T. Kawai, Photochemical formation of glycine and methylamine from glycolic acid and ammonia in the presence of particulate cadmium sulphide, *J. Chem. Soc. Chem. Commun.* 0 (1987) 1480–1481, <https://doi.org/10.1039/c39870001480>.
- [249] D. Štíbal, J. Sá, J.A. van Bokhoven, One-pot photo-reductive N-alkylation of aniline and nitroarene derivatives with primary alcohols over Au–TiO₂, *Catal. Sci. Technol.* 3 (2013) 94–98, <https://doi.org/10.1039/C2CY20511D>.
- [250] J.C. Colmenares, W. Ouyang, M. Ojeda, E. Kuna, O. Chernyayeva, D. Lisovyskiy, S. De, R. Luque, A.M. Balu, Mild ultrasound-assisted synthesis of TiO₂ supported on magnetic nanocomposites for selective photo-oxidation of benzyl alcohol, *Appl. Catal. B Environ.* 183 (2016) 107–112, <https://doi.org/10.1016/j.apcatb.2015.10.034>.
- [251] J. Zhang, D. Han, H. Zhang, M. Chaker, Y. Zhao, D. Ma, In situ recyclable gold nanoparticles using CO₂-switchable polymers for catalytic reduction of 4-nitrophenol, *Chem. Commun.* 48 (2012) 11510–11511, <https://doi.org/10.1039/c2cc35784d>.
- [252] J. Zhang, G. Chen, M. Chaker, F. Rosei, D. Ma, Gold nanoparticle decorated ceria nanotubes with significantly high catalytic activity for the reduction of nitrophenol and mechanism study, *Appl. Catal. B Environ.* 132–133 (2013) 107–115, <https://doi.org/10.1016/j.apcatb.2012.11.030>.
- [253] J. Zhang, G. Chen, D. Guay, M. Chaker, D. Ma, Highly active PtAu alloy nanoparticle catalysts for the reduction of 4-nitrophenol, *Nanoscale* 6 (2014) 2125–2130, <https://doi.org/10.1039/C3NR04715F>.
- [254] Q. Zhang, X. Jin, Z. Xu, J. Zhang, U.F. Rendón, L. Razzari, M. Chaker, D. Ma, Plasmonic Au-loaded hierarchical hollow porous TiO₂ spheres: synergistic catalysts for nitroaromatic reduction, *J. Phys. Chem. Lett.* 9 (2018) 5317–5326, <https://doi.org/10.1021/acs.jpclett.8b02393>.
- [255] L. Katsikas, J.S. Veličković, H. Weller, I.G. Popović, Thermogravimetric characterization of poly(methyl methacrylate) photopolymerised by colloidal cadmium sulphide, *J. Therm. Anal.* 49 (1997) 317–323, <https://doi.org/10.1007/BF01987453>.

- [256] A.J. Hoffman, H. Yee, G. Mills, M.R. Hoffmann, Photoinitiated polymerization of methyl methacrylate using Q-sized zinc oxide colloids, *J. Phys. Chem.* 96 (1992) 5540–5546, <https://doi.org/10.1021/j100192a066>.
- [257] H. Tada, M. Kubo, S. Ito, Y. Inubushi, N=N bond cleavage of azobenzene through Pt/TiO₂ photocatalytic reduction, *Chem. Commun.* 0 (2000) 977–978, <https://doi.org/10.1039/b001062f>.
- [258] X. Ke, S. Sarina, J. Zhao, X. Zhang, J. Chang, H. Zhu, Tuning the reduction power of supported gold nanoparticle photocatalysts for selective reductions by manipulating the wavelength of visible light irradiation, *Chem. Commun.* 48 (2012) 3509–3510, <https://doi.org/10.1039/c2cc17977f>.
- [259] X. Ke, X. Zhang, J. Zhao, S. Sarina, J. Barry, H. Zhu, Selective reductions using visible light photocatalysts of supported gold nanoparticles, *Green Chem.* 15 (2013) 236–244, <https://doi.org/10.1039/c2gc36542a>.
- [260] Y. Shiraishi, M. Katayama, M. Hashimoto, T. Hirai, Photocatalytic hydrogenation of azobenzene to hydrazobenzene on cadmium sulfide under visible light irradiation, *Chem. Commun.* 54 (2018) 452–455, <https://doi.org/10.1039/C7CC08428E>.
- [261] Y. Shiraishi, Y. Sugano, S. Tanaka, T. Hirai, One-pot synthesis of benzimidazoles by simultaneous photocatalytic and catalytic reactions on Pt@TiO₂ nanoparticles, *Angew. Chemie Int. Ed.* 49 (2010) 1656–1660, <https://doi.org/10.1002/anie.200906573>.
- [262] A. Hakkı, R. Dillert, D.W. Bahnemann, Arenesulfonic acid-functionalized mesoporous silica decorated with titania: a heterogeneous catalyst for the one-pot photocatalytic synthesis of quinolines from nitroaromatic compounds and alcohols, *ACS Catal.* 3 (2013) 565–572, <https://doi.org/10.1021/cs300736x>.
- [263] A. Pineda, L. Gomez, A.M. Balu, V. Sebastian, M. Ojeda, M. Arruebo, A.A. Romero, J. Santamaria, R. Luque, Laser-driven heterogeneous catalysis: efficient amide formation catalysed by Au/SiO₂ systems, *Green Chem.* 15 (2013) 2043–2049, <https://doi.org/10.1039/c3gc40166a>.
- [264] G. Liang, Y. Zhou, J. Zhao, A.Y. Khodakov, V.V. Ordonsky, Structure-sensitive and insensitive reactions in alcohol amination over nonsupported Ru nanoparticles, *ACS Catal.* 8 (2018) 11226–11234, <https://doi.org/10.1021/acscatal.8b02866>.
- [265] V. Brezová, A. Blažková, I. Šurina, B. Havlíková, Solvent effect on the photocatalytic reduction of 4-nitrophenol in titanium dioxide suspensions, *J. Photochem. Photobiol. A Chem.* 107 (1997) 233–237, [https://doi.org/10.1016/S1010-6030\(96\)04577-7](https://doi.org/10.1016/S1010-6030(96)04577-7).
- [266] K.D. Asmus, H. Moockel, A. Henglein, Pulse radiolytic study of the site of hydroxyl radical attack on aliphatic alcohols in aqueous solution, *J. Phys. Chem.* 77 (1973) 1218–1221, <https://doi.org/10.1021/j100629a007>.
- [267] M. Hecht, W.R. Fawcett, Solvent effects in the electroreduction of ethylenediaminetetraacetatocromium (III) at a mercury electrode, *J. Phys. Chem.* 99 (1995) 1311–1316, <https://doi.org/10.1021/j100004a035>.
- [268] C.B. Almquist, P. Biswas, The photo-oxidation of cyclohexane on titanium dioxide: an investigation of competitive adsorption and its effects on product formation and selectivity, *Appl. Catal. A Gen.* 214 (2001) 259–271, [https://doi.org/10.1016/S0926-860X\(01\)00495-1](https://doi.org/10.1016/S0926-860X(01)00495-1).
- [269] F. Soana, M. Sturini, L. Cermenati, A. Albini, Titanium dioxide photocatalyzed oxygenation of naphthalene and some of its derivatives, *J. Chem. Soc. Perkin Trans. 2* (2000) 699–704, <https://doi.org/10.1039/a908945d>.
- [270] V. Augugliaro, G. Camera-Roda, V. Loddo, G. Palmisano, L. Palmisano, J. Soria, S. Yurdakal, Heterogeneous photocatalysis and photoelectrocatalysis: from unselective abatement of noxious species to selective production of high-value chemicals, *J. Phys. Chem. Lett.* 6 (2015) 1968–1981, <https://doi.org/10.1021/acs.jpclett.5b00294>.
- [271] W. Mu, J.-M. Herrmann, P. Pichat, Room temperature photocatalytic oxidation of liquid cyclohexane into cyclohexanone over neat and modified TiO₂, *Catal. Letters* 3 (1989) 73–84, <https://doi.org/10.1007/BF00765057>.
- [272] T. Ohno, K. Tokieda, S. Higashida, M. Matsumura, Synergism between rutile and anatase TiO₂ particles in photocatalytic oxidation of naphthalene, *Appl. Catal. A Gen.* 244 (2003) 383–391, [https://doi.org/10.1016/S0926-860X\(02\)00610-5](https://doi.org/10.1016/S0926-860X(02)00610-5).
- [273] M.A. Fox, J.N. Yoonathan, Radical cation intermediates in the formation of Schiff bases on irradiated semiconductor powders, *Tetrahedron* 42 (1986) 6285–6291, [https://doi.org/10.1016/S0040-4020\(01\)88091-1](https://doi.org/10.1016/S0040-4020(01)88091-1).
- [274] S. Xu, P. Zhou, Z. Zhang, C. Yang, B. Zhang, K. Deng, S. Bottle, H. Zhu, Selective oxidation of 5-hydroxymethylfurfural to 2,5-furandicarboxylic acid using O₂ and a photocatalyst of Co-thiophopyrazine bonded to g-C₃N₄, *J. Am. Chem. Soc.* 139 (2017) 14775–14782, <https://doi.org/10.1021/jacs.7b08861>.
- [275] C.P. Canlas, J. Lu, N.A. Ray, N.A. Grosso-Giordano, S. Lee, J.W. Elam, R.E. Winans, R.P. Van Duyne, P.C. Stair, J.M. Notestein, Shape-selective sieving layers on an oxide catalyst surface, *Nat. Chem.* 4 (2012) 1030–1036, <https://doi.org/10.1038/nchem.1477>.
- [276] B. Ohtani, S. Tsuru, S. Nishimoto, T. Kagiya, K. Izawa, Photocatalytic one-step syntheses of cyclic imino acids by aqueous semiconductor suspensions, *J. Org. Chem.* 55 (1990) 5551–5553, <https://doi.org/10.1021/jo00308a005>.
- [277] B. Pal, S. Ikeda, H. Kominami, Y. Kera, B. Ohtani, Photocatalytic redox-combined synthesis of l-pipecolinic acid from l-lysine by suspended titania particles: effect of noble metal loading on the selectivity and optical purity of the product, *J. Catal.* 217 (2003) 152–159, [https://doi.org/10.1016/S0021-9517\(03\)00049-6](https://doi.org/10.1016/S0021-9517(03)00049-6).
- [278] Y. Shiraishi, H. Sakamoto, K. Fujiwara, S. Ichikawa, T. Hirai, Selective photocatalytic oxidation of aniline to nitrosobenzene by Pt nanoparticles supported on TiO₂ under visible light irradiation, *ACS Catal.* 4 (2014) 2418–2425, <https://doi.org/10.1021/cs500447n>.
- [279] H. Yoshida, H. Yuzawa, M. Aoki, K. Otake, H. Itoh, T. Hattori, Photocatalytic hydroxylation of aromatic ring by using water as an oxidant, *Chem. Commun.* 0 (2008) 4634–4635, <https://doi.org/10.1039/b811555a>.
- [280] J.C. Kuriacose, M.C. Markham, Mechanism of the photo-initiated polymerization of methyl methacrylate at Zinc Oxide surfaces, *J. Phys. Chem.* 65 (1961) 2232–2236, <https://doi.org/10.1021/j100829a032>.
- [281] M. Yamamoto, G. Oster, Zinc oxide-sensitized photopolymerization, *J. Polym. Sci. Part A-1 Polym. Chem.* 4 (1966) 1683–1688, <https://doi.org/10.1002/pol.1966.150040703>.
- [282] A.J. Hoffman, G. Mills, H. Yee, M.R. Hoffmann, Q-sized cadmium sulfide: synthesis, characterization, and efficiency of photoinitiation of polymerization of several vinyl monomers, *J. Phys. Chem.* 96 (1992) 5546–5552, <https://doi.org/10.1021/j100192a067>.
- [283] C.-W. Tsai, H.M. Chen, R.-S. Liu, K. Asakura, T.-S. Chan, Ni@NiO Core-Shell Structure-Modified Nitrogen-Doped InTaO₄ for Solar-Driven Highly Efficient CO₂ Reduction to Methanol, *J. Phys. Chem. C* 115 (2011) 10180–10186, <https://doi.org/10.1021/jp2020534>.
- [284] Z.-Y. Huang, T. Barber, G. Mills, M.-B. Morris, Heterogeneous photopolymerization of methyl methacrylate initiated by small ZnO particles, *J. Phys. Chem.* 98 (1994) 12746–12752, <https://doi.org/10.1021/j100099a044>.
- [285] A.L. Stroyuk, V.M. Granchak, S.Y. Kuchmii, Photopolymerization of butyl methacrylate initiated by hydrated ferric oxide nanoparticles, *Theor. Exp. Chem.* 37 (2001) 350–354, <https://doi.org/10.1023/A:1014752231171>.
- [286] I.G. Popović, L. Katsikas, H. Weller, The photopolymerization of methacrylic acid by colloidal semiconductors, *Polym. Bull.* 32 (1994) 597–603, <https://doi.org/10.1007/BF00973907>.
- [287] A.L. Stroyuk, V.M. Granchak, S.Y. Kuchmii, Polymerization of butylmethacrylate in isopropanol, photoinduced by quantum-sized CdS particles, *Theor. Exp. Chem.* 37 (2001) 174–179, <https://doi.org/10.1023/A:1011980321516>.
- [288] A.L. Stroyuk, S.Y. Kuchmii, V.M. Granchak, Photopolymerization of butyl methacrylate in the presence of nanoparticles of ZnO, sensitized to visible light with xanthene dyes, *Theor. Exp. Chem.* 38 (2002) 335–341, <https://doi.org/10.1023/A:1021757127331>.
- [289] A.L. Stroyuk, I.V. Sobran, A.V. Korzhak, A.E. Raevskaya, S.Y. Kuchmii, Photopolymerization of water-soluble acrylic monomers induced by colloidal CdS and Cd_{0.9}Zn_{0.1}S nanoparticles, *Colloid Polym. Sci.* 286 (2008) 489–498, <https://doi.org/10.1007/s00396-007-1824-4>.
- [290] A.L. Stroyuk, V.M. Granchak, A.V. Korzhak, S.Y. Kuchmii, Photoinitiation of butylmethacrylate polymerization by colloidal semiconductor nanoparticles, *J. Photochem. Photobiol. A Chem.* 162 (2004) 339–351, [https://doi.org/10.1016/S1010-6030\(03\)00371-X](https://doi.org/10.1016/S1010-6030(03)00371-X).
- [291] C. Dong, X. Ni, The photopolymerization and characterization of methyl methacrylate initiated by nanosized titanium dioxide, *J. Macromol. Sci. Part A* 41 (2004) 547–563, <https://doi.org/10.1081/MA-120030924>.
- [292] R. Ojha, S.K. Dolui, Photopolymerization of methyl methacrylate using dye-sensitized semiconductor based photocatalyst, *J. Photochem. Photobiol. A Chem.* 172 (2005) 121–125, <https://doi.org/10.1016/J.JPHOTOCHEM.2004.11.015>.
- [293] H. Kong, J. Song, J. Jang, Photocatalytic antibacterial capabilities of TiO₂–Biocidal polymer nanocomposites synthesized by a surface-initiated photopolymerization, *Environ. Sci. Technol.* 44 (2010) 5672–5676, <https://doi.org/10.1021/es1010779>.
- [294] A. Listorti, B. O'Regan, J.R. Durrant, Electron transfer dynamics in dye-sensitized solar cells, *Chem. Mater.* 23 (2011) 3381–3399, <https://doi.org/10.1021/cm200651e>.
- [295] J.A. Anta, E. Guillén, R. Tena-Zaera, ZnO-based dye-sensitized solar cells, *J. Phys. Chem. C* 116 (2012) 11413–11425, <https://doi.org/10.1021/jp3010025>.
- [296] X. Wang, X. Song, M. Lin, H. Wang, Y. Zhao, W. Zhong, Q. Du, Surface initiated graft polymerization from carbon-doped TiO₂ nanoparticles under sunlight illumination, *Polymer (Guildf.)* 48 (2007) 5834–5838, <https://doi.org/10.1016/J.POLYMER.2007.08.017>.
- [297] F. Ketting, B. Vonhören, J.A. Krings, S. Saito, B.J. Ravoo, One-step synthesis of patterned polymer brushes by photocatalytic microcontact printing, *Chem. Commun.* 51 (2015) 1027–1030, <https://doi.org/10.1039/C4CC08646E>.
- [298] N.C. Strandwitz, Y. Nonoguchi, S.W. Boettcher, G.D. Stucky, In situ photopolymerization of pyrrole in mesoporous TiO₂, *Langmuir* 26 (2010) 5319–5322, <https://doi.org/10.1021/la100913e>.
- [299] S. Dadashi-Silab, A.M. Asiri, S.B. Khan, K.A. Alamry, Y. Yagci, Semiconductor nanoparticles for photoinitiation of free radical polymerization in aqueous and organic media, *J. Polym. Sci. Part A Polym. Chem.* 52 (2014) 1500–1507, <https://doi.org/10.1002/pola.27145>.
- [300] R. Popielarz, O. Vogt, Effect of coinitiator type on initiation efficiency of two-component photoinitiator systems based on Eosin, *J. Polym. Sci. Part A Polym. Chem.* 46 (2008) 3519–3532, <https://doi.org/10.1002/pola.22688>.
- [301] S. Dadashi-Silab, Y. Yar, H. Yagci Acar, Y. Yagci, Magnetic iron oxide nanoparticles as long wavelength photoinitiators for free radical polymerization, *Polym. Chem.* 6 (2015) 1918–1922, <https://doi.org/10.1039/C4PY01658K>.
- [302] M. Dule, M. Biswas, Y. Biswas, T.K. Mandal, Redox-active poly(ionic liquid)-engineered Ag nanoparticle-decorated ZnO nanoflower heterostructure: A reusable composite catalyst for photopolymerization into high-molecular-weight polymers, *Polymer (Guildf.)* 133 (2017) 223–231, <https://doi.org/10.1016/J.POLYMER.2017.11.033>.
- [303] K. Chen, X. Deng, G. Dodekatos, H. Tüysüz, Photocatalytic polymerization of 3,4-ethylenedioxythiophene over cesium lead iodide perovskite quantum dots, *J. Am. Chem. Soc.* 139 (2017) 12267–12273, <https://doi.org/10.1021/jacs.7b06413>.
- [304] Z. Weng, X. Ni, D. Yang, J. Wang, W. Chen, Novel photopolymerizations initiated by alkyl radicals generated from photocatalyzed decarboxylation of carboxylic acids over oxide semiconductor nanoparticles: extended photo-Kolbe reactions, *J. Photochem. Photobiol. A Chem.* 201 (2009) 151–156, <https://doi.org/10.1016/J.JPHOTOCHEM.2008.10.013>.
- [305] B. Kiskan, J. Zhang, X. Wang, M. Antonietti, Y. Yagci, Mesoporous graphitic

- carbon nitride as a heterogenous visible light photoinitiator for radical polymerization, *ACS Macro Lett.* 1 (2012) 546–549, <https://doi.org/10.1021/mz300116w>.
- [306] S. Yamago, Y. Nakamura, Recent progress in the use of photoirradiation in living radical polymerization, *Polymer (Guildf)* 54 (2013) 981–994, <https://doi.org/10.1016/J.POLYMER.2012.11.046>.
- [307] W.H. Binder, R. Sachsenhofer, ‘Click’ chemistry in polymer and material science: an update, *Macromol. Rapid Commun.* 29 (2008) 952–981, <https://doi.org/10.1002/marc.200800089>.
- [308] K. Matyjaszewski, N.V. Tsarevsky, Macromolecular engineering by atom transfer radical polymerization, *J. Am. Chem. Soc.* 136 (2014) 6513–6533, <https://doi.org/10.1021/ja408069v>.
- [309] J. Yan, B. Li, F. Zhou, W. Liu, Ultraviolet light-induced surface-initiated atom-transfer radical polymerization, *ACS Macro Lett.* 2 (2013) 592–596, <https://doi.org/10.1021/mz400237w>.
- [310] S. Dadashi-Silab, M. Atilla Tasdelen, A. Mohamed Asiri, S. Bahadar Khan, Y. Yagci, Photoinduced atom transfer radical polymerization using semiconductor nanoparticles, *Macromol. Rapid Commun.* 35 (2014) 454–459, <https://doi.org/10.1002/marc.201300704>.
- [311] A. Anastasaki, V. Nikolaou, Q. Zhang, J. Burns, S.R. Samanta, C. Waldron, A.J. Haddleton, R. McHale, D. Fox, V. Percec, P. Wilson, D.M. Haddleton, Copper (II)/tertiary amine synergy in photoinduced living radical polymerization: accelerated synthesis of ω -Functional and α,ω -Heterofunctional poly(acrylates), *J. Am. Chem. Soc.* 136 (2014) 1141–1149, <https://doi.org/10.1021/ja411780m>.
- [312] S. Dadashi-Silab, M.A. Tasdelen, B. Kiskan, X. Wang, M. Antonietti, Y. Yagci, Photochemically mediated atom transfer radical polymerization using polymeric semiconductor mesoporous graphitic carbon nitride, *Macromol. Chem. Phys.* 215 (2014) 675–681, <https://doi.org/10.1002/macp.201400063>.
- [313] A. Bansal, A. Kumar, P. Kumar, S. Bojja, A.K. Chatterjee, S.S. Ray, S.L. Jain, Visible light-induced surface initiated atom transfer radical polymerization of methyl methacrylate on titania/reduced graphene oxide nanocomposite, *RSC Adv.* 5 (2015) 21189–21196, <https://doi.org/10.1039/C4RA15615C>.
- [314] B. Li, B. Yu, F. Zhou, Spatial control over brush growth through sunlight-induced atom transfer radical polymerization using dye-sensitized TiO_2 as a photocatalyst, *Macromol. Rapid Commun.* 35 (2014) 1287–1292, <https://doi.org/10.1002/marc.201400121>.
- [315] Y. Cao, Y. Xu, J. Zhang, D. Yang, J. Liu, Well-controlled atom transfer radical polymerizations of acrylates using recyclable niobium complex nanoparticle as photocatalyst under visible light irradiation, *Polymer (Guildf)* 61 (2015) 198–203, <https://doi.org/10.1016/J.POLYMER.2015.02.010>.
- [316] J. Zhang, A. Li, H. Liu, D. Yang, J. Liu, Well-controlled RAFT polymerization initiated by recyclable surface-modified $\text{Nb}(\text{OH})_5$ nanoparticles under visible light irradiation, *J. Polym. Sci. Part A Polym. Chem.* 52 (2014) 2715–2724, <https://doi.org/10.1002/pola.27288>.
- [317] J. Zhou, Q. Liu, W. Feng, Y. Sun, F. Li, Upconversion luminescent materials: advances and applications, *Chem. Rev.* 115 (2015) 395–465, <https://doi.org/10.1021/cr400478f>.
- [318] B.P. Fors, C.J. Hawker, Control of a living radical polymerization of methacrylates by light, *Angew. Chemie.* 124 (2012) 8980–8983, <https://doi.org/10.1002/ange.201203639>.
- [319] G. Zhang, I.Y. Song, T. Park, W. Choi, Recyclable and stable ruthenium catalyst for free radical polymerization at ambient temperature initiated by visible light photocatalysis, *Green Chem.* 14 (2012) 618–621, <https://doi.org/10.1039/c2gc16409d>.
- [320] M. Sahin, K.K. Krawczyk, P. Roszkowski, J. Wang, B. Kaynak, W. Kern, S. Schlögl, H. Grützmacher, Photoactive silica nanoparticles: influence of surface functionalization on migration and kinetics of radical-induced photopolymerization reactions, *Eur. Polym. J.* 98 (2018) 430–438, <https://doi.org/10.1016/J.EURPOLYMJ.2017.11.046>.
- [321] A.C. Balazs, T. Emrick, T.P. Russell, Nanoparticle polymer composites: where two small worlds meet, *Science.* 314 (2006) 1107–1110, <https://doi.org/10.1126/science.1130557>.
- [322] L. Nicolais, G. Carotenuto, *Metal-polymer Nanocomposites*, Wiley-Interscience, 2005.
- [323] Y. Zhang, X. Cui, F. Shi, Y. Deng, Nano-gold catalysis in fine chemical synthesis, *Chem. Rev.* 112 (2012) 2467–2505, <https://doi.org/10.1021/cr200260m>.
- [324] L.A. Dykman, N.G. Khlebtsov, Uptake of engineered gold nanoparticles into mammalian cells, *Chem. Rev.* 114 (2014) 1258–1288, <https://doi.org/10.1021/cr300441a>.
- [325] K. Saha, S.S. Agasti, C. Kim, X. Li, V.M. Rotello, Gold nanoparticles in chemical and biological sensing, *Chem. Rev.* 112 (2012) 2739–2779, <https://doi.org/10.1021/cr2001178>.
- [326] K.C. Anyaogu, X. Cai, D.C. Neckers, Gold nanoparticle photosensitized radical photopolymerization, *Photochem. Photobiol. Sci.* 7 (2008) 1469–1472, <https://doi.org/10.1039/b812328d>.
- [327] K.C. Anyaogu, X. Cai, D.C. Neckers, Gold nanoparticle photopolymerization of acrylates, *Macromolecules* 41 (2008) 9000–9003, <https://doi.org/10.1021/ma801391p>.
- [328] T. Ding, J. Mertens, A. Lombardi, O.A. Scherman, J.J. Baumberg, Light-directed tuning of plasmon resonances via plasmon-induced polymerization using hot electrons, *ACS Photonics* 4 (2017) 1453–1458, <https://doi.org/10.1021/acsp Photonics.7b00206>.
- [329] N.C. Strandwitz, A. Khan, S.W. Boettcher, A.A. Mikhailovsky, C.J. Hawker, T.-Q. Nguyen, G.D. Stucky, One- and two-photon induced polymerization of methylmethacrylate using colloidal CdS semiconductor quantum dots, *J. Am. Chem. Soc.* 130 (2008) 8280–8288, <https://doi.org/10.1021/ja711295k>.